

2010

## Differential GPS as a monitoring tool on Volcano Santa Ana (Illamatepec) and the Coatepeque Caldera, El Salvador

Hans N. Lechner  
*Michigan Technological University*

Follow this and additional works at: <https://digitalcommons.mtu.edu/etds>



Part of the [Geology Commons](#)

Copyright 2010 Hans N. Lechner

---

### Recommended Citation

Lechner, Hans N., "Differential GPS as a monitoring tool on Volcano Santa Ana (Illamatepec) and the Coatepeque Caldera, El Salvador", Master's Thesis, Michigan Technological University, 2010.  
<https://doi.org/10.37099/mtu.dc.etds/329>

Follow this and additional works at: <https://digitalcommons.mtu.edu/etds>



Part of the [Geology Commons](#)

Differential GPS as a Monitoring Tool on Volcano Santa  
Ana (Illamatepec) and the Coatepeque Caldera, El Salvador

By

Hans N. Lechner

A THESIS

Submitted in partial fulfillment of the requirements for the  
degree of

MASTER OF SCIENCE IN GEOLOGY

MICHIGAN TECHNOLOGICAL UNIVERSITY

2010

This thesis, "Differential GPS as a Monitoring Tool on Volcano Santa Ana (Illumatepec) and the Coatepeque Caldera, El Salvador," is hereby approved in partial fulfillment of the requirements for the Degree of MASTER OF SCIENCE IN GEOLOGY.

Department of Geological and Mining Engineering and Sciences

Signatures:

Thesis Advisor

\_\_\_\_\_  
William I. Rose

Thesis Co-Advisor

\_\_\_\_\_  
Charles DeMets

Department Chair

\_\_\_\_\_  
Wayne D. Pennington

# TABLE OF CONTENTS

TABLE OF FIGURES .....	5
LIST OF TABLES .....	6
ACKNOWLEDGEMENTS .....	7
ABSTRACT .....	8
1. INTRODUCTION .....	9
1.1. Tectonic Setting.....	9
1.2. Eruptive History .....	10
1.3. Deformation Monitoring with GPS.....	10
2. METHODS .....	13
2.1. Network and Field Measurements .....	13
2.2. Data Processing and Reduction.....	13
2.3. Measurements of Achievable Accuracy.....	16
2.3.1. Continuous GPS station – SNJE.....	16
2.3.2 Repeatability of interstation baselines .....	20
3. RESULTS .....	24
3.1. Repeatability.....	24
3.2. Scatter relative to Linear Fit.....	24
3.3. Hourly vs. 20-Minute Observations .....	29

3.4. Tropospheric Water Vapor Delay .....	32
3.5. Evidence of Surface Deformation .....	40
4. DISCUSSION.....	44
5. FUTURE WORK.....	49
6. CONCLUSIONS.....	50
7. REFERENCE LIST .....	52
APPENDIX A: NETWORK DEVELOPMENT .....	56
APPENDIX B: FIELD MEASUREMENTS .....	58
APPENDIX C: BASELINE PROCESSING .....	60
C.1. Project Setup .....	60
C.2. L1 vs. Iono-Free Fixed.....	63
C.3. Baseline Solution Improvements .....	70
APPENDIX D: STATISTICAL REDUCTION .....	75
Appendix D.1. Excel Statistics .....	76
APPENDIX E: REGRESSION PLOTS .....	79
APPENDIX F: BEST FIT RESIDUALS.....	90

# TABLE OF FIGURES

Figure 1. Map of El Salvador and the study area.....	11
Figure 2. GPS equipment.....	15
Figure 3. Daily and monthly position averages for SNJE. ....	17
Figure 4. 20-minute averages about the 24-hour mean and associated histograms.....	21
Figure 5. Positional scatter about the best fit line.....	26
Figure 6. RMS error versus baseline length and height.....	31
Figure 7. Total precipitable water vapor (PWV). ....	33
Figure 8. The difference in tropospheric delay versus the positional scatter.....	35
Figure 9. 2009 precipitation totals, PWV and positional scatter. ....	37
Figure 10. Vertical velocities.....	43
Figure 11. Horizontal velocity vectors.....	43
Figure 12. Daily RSAM averages for 2009. ....	46

## **LIST OF TABLES**

Table 1. GPS station information and occupation history.	14
Table 2. Misfit of the RMS and standard deviations over baseline distance.	30
Table 3. Misfit of the RMS and standard deviation over station elevation	30
Table 4. Station velocities and observed displacements.	41

## **ACKNOWLEDGEMENTS**

This research was supported by funding provided by the US National Science Foundation through grant number: 0530109. Technical guidance and GPS equipment was provided by Professor Charles DeMets and Neal Lord at the University of Wisconsin. Thanks to Eugene Levin at MTU for supplying the processing software. Great thanks especially to Demetrio Escobar and Douglas Hernandez for their input and guidance. RSAM, micro seismic, rainfall data, and excellent field support was provided by SNET (Servicio Nacional de Estudios Territoriales) El Salvador. Special thanks to Professor Bill Rose, Rüdiger Escobar-Wolf, Luke Bowman and Wendell Doman for their support in the field and in the lab. The United States Peace Corps supported living costs during the planning, testing and execution of this project.

I especially want to thank my wife Emily for all of her support, encouragement and patience through the duration of this project.



## ABSTRACT

We used differential GPS measurements from a 13 station GPS network spanning the Santa Ana Volcano and Coatepeque Caldera to characterize the inter-eruptive activity and tectonic movements near these two active and potentially hazardous features.

Caldera-forming events occurred from 70-40 ka and at Santa Ana/Izalco volcanoes eruptive activity occurred as recently as 2005. Twelve differential stations were surveyed for 1 to 2 hours on a monthly basis from February through September 2009 and tied to a centrally located continuous GPS station, which serves as the reference site for this volcanic network. Repeatabilities of the averages from 20-minute sessions taken over 20 hours or longer range from 2-11 mm in the horizontal (north and east) components of the inter-station baselines, suggesting a lower detection limit for the horizontal components of any short-term tectonic or volcanic deformation.

Repeatabilities of the vertical baseline component range from 12-34 mm. Analysis of the precipitable water vapor in the troposphere suggests that tropospheric decorrelation as a function of baseline lengths and variable site elevations are the most likely sources of vertical error. Differential motions of the 12 sites relative to the continuous reference site reveal inflation from February through July at several sites surrounding the caldera with vertical displacements that range from 61 mm to 139 mm followed by a lower magnitude deflation event on 1.8-7.4 km-long baselines. Uplift rates for the inflationary period reach 300 mm/yr with  $1\sigma$  uncertainties of  $\pm 26 - 119$  mm. Only one other station outside the caldera exhibits a similar deformation trend, suggesting a localized source. The results suggest that the use of differential GPS measurements from short duration occupations over short baselines can be a useful monitoring tool at sub-tropical volcanoes and calderas.

# 1. INTRODUCTION

## 1.1. Tectonic Setting

The Santa Ana Volcanic Complex (SAVC) is located in western El Salvador (figure 1) along the southern edge of the Median Trough, or Central Graben, which is an extension of the Nicaraguan Depression. The Median Trough could be defined as a series of bookshelf and transtensional faults formed by the right-lateral motion of the Central American Forearc sliver (Funk et al. 2009). It is postulated that the 14 +/- 2 mm/yr, counter clockwise, northwest motion of the forearc sliver is driven by transpressional forces caused by oblique subduction of the Cocos Plate under the Caribbean Plate along a concave subduction zone offshore of Nicaragua (DeMets 2001, Funk et al. 2009, Alvarado et al. 2010). The Santa Ana Volcanic Complex is comprised of the composite volcano Santa Ana – locally known as Illamatepec – Izalco volcano, Coatepeque Caldera as well as a NW-SE, linear system of parasitic vents and cinder cones (Pullinger 1998). It is likely that this NW-SE trend is the manifestation of a series of extensional, normal faults that dissect Santa Ana volcano, which is likely a pull-apart zone due to the right-lateral motion of the forearc sliver/Caribbean plate interaction (Stoiber and Carr 1977, Carr and Feigenson 2003, Funk et al. 2009).

## **1.2. Eruptive History**

Coatepeque Caldera is a 7 x 8 km collapse caldera and contains a lake of the same name. It is one of several large, active, collapse calderas in El Salvador and has produced approximately 24 km<sup>3</sup> of pyroclastic materials in three events between 40-70 ka (Pullinger 1998, Rose et al. 1999). Izalco volcano erupted almost continuously for nearly 200 years until 1966 (Rose and Stoiber 1969), while Santa Ana experienced a small eruption (VEI 3) in 2005. Debate exists over the mechanism of the 2005 eruption; Olmos et al. (2007) consider the eruption to have been strictly phreatic due to hydrothermal/gas interaction while Scolamacchia (2010) and Colvin (2010 et al. in review) suggests that it was phreato-magmatic driven by a small, shallow rhyolitic intrusion. Petrologic studies of volcanic complex by Carr and Pointier 1981 and Halsor and Rose 1988 suggest the presence of a substantial magma body below the volcanic complex. Currently, all three volcanoes demonstrate fumarolic or hydrothermal activity, suggesting a still present heat source. While this eruptive history is brief it demonstrates the nature of activity at the SAVC and illustrates the need for instrumentation and continuous monitoring.

## **1.3. Deformation Monitoring with GPS**

The application of GPS to volcano monitoring offers unique capabilities that allow us to track and monitor deformation (Dzurisin, 2000). Differential GPS is a technique based on the employment of two or more receivers where one receiver functions as a base station and is fixed at a location of known coordinates while the position of the remote-receiver, or rover, is determined from measurements relative to the base (Hoffmann-Wellenhof et al. 2001). With this type of GPS survey it is possible to eliminate or reduce multiple sources of error over short baselines and yield precise relative position estimates with short occupation durations. It is therefore feasible to establish and occupy multiple sites within a short time span. Furthermore, the data processing strategy is much less difficult using commercially available software than for high-precision absolute positioning.

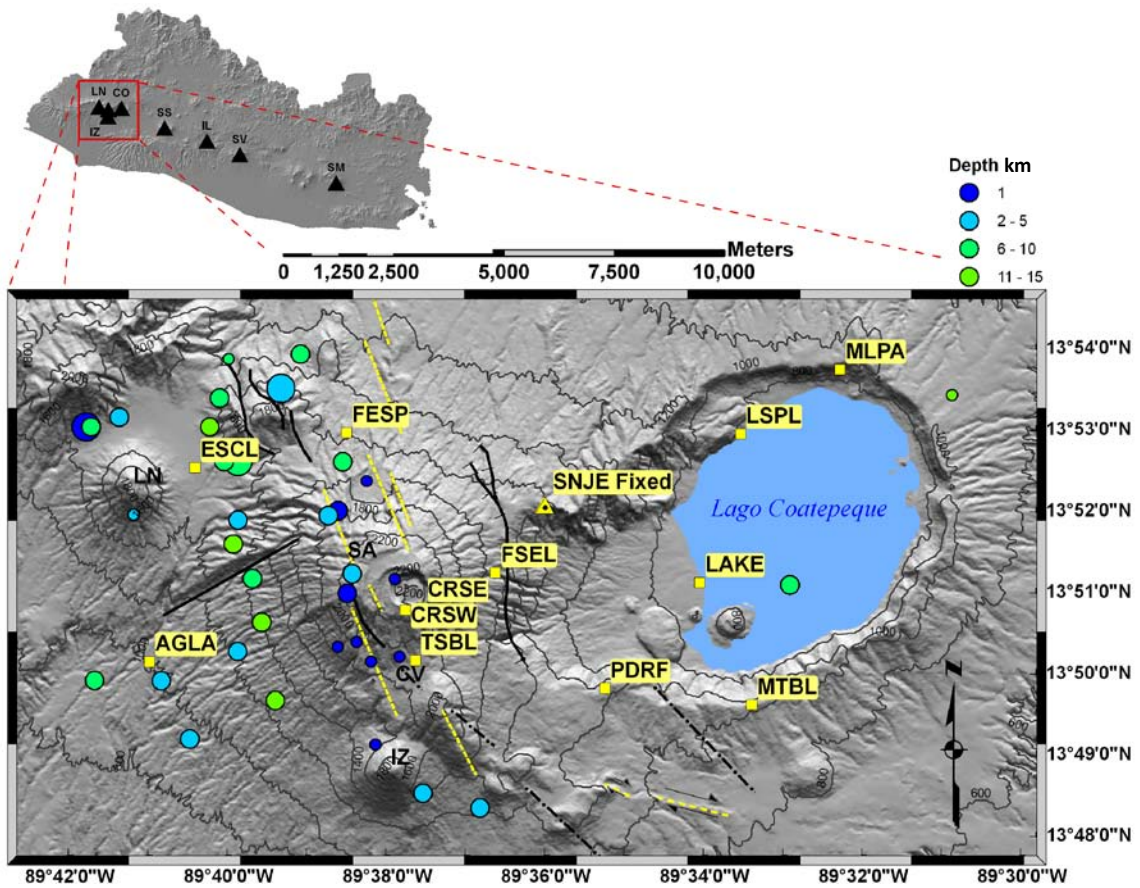


**Figure 1. Map of El Salvador and the study area.**

(SM) San Miguel, (SV) San Vicente, (IL) Ilopango, (SS) San Salvador, (CO) Coatepeque, (LN) Los Naranjos, (IZ) Izalco. Inset is the Santa Ana Volcanic Complex and the Coatepeque Caldera. Solid black lines show faults while black dotted lines show assumed faults identified and mapped by Weber and Wiesemann (1977) Yellow dotted lines represent regional tectonics identified by the author as distinct lineaments on the 25 m DEM with the exception of valleys radiating outward from the peaks of volcanoes. Circles represent micro-seismic events during the time period of this investigation. Diameters smallest to largest represent magnitudes < 1, 1-2, 2-3 respectively. Color gradient represents depths in km. Seismic data provided by SNET.

This initial investigation was designed as a pilot project for the Servicio Nacional de Estudios Territoriales (SNET) of El Salvador, to augment their monitoring capabilities at SAVC and to explore new strategies for monitoring active strato-volcanoes in subtropical regions. The goals of this study are to determine the feasibility of short occupation times in a dense GPS network (~ 100 km<sup>2</sup> footprint) on a sub-tropical composite volcano, to determine the achievable measurement precision and accuracy, and to monitor the inter-eruptive characteristics of the volcanic complex and caldera system at Santa Ana and Coatepeque Caldera. Our approach for the design of this network was to take advantage of a conveniently located continuously operating GPS (CGPS) station on the flanks of Santa Ana and utilize it as our fixed-position base station.

In section 2 we describe the methodologies of the network development and field measurements. In section 3 the results of our repeatability experiments, uncertainty versus baseline-distance, the possible error caused by tropospheric delay and evidence for a deformation event around the caldera are discussed. The possible deformation at the caldera is examined in section 4. In section 5 we make recommendations for the advancement of this project. We make our conclusions about this study in section 6 .

## **2. METHODS**

### **2.1. Network and Field Measurements**

During the spring and summer of 2008 a 13-stations GPS network was established on and around Santa Ana volcano and Coatepeque Caldera. Twelve of the stations are tied to the continuously operating GPS base-station SNJE in the center of the network and were surveyed using differential GPS (dGPS). Data were collected during monthly campaigns, which usually occurred during the last week of each month from February through September, 2009 (table 2). During data collection campaigns, the rover antenna was positioned and leveled on a spike mount tripod with a fixed height of 55 cm (figure 2).

We used a Trimble 5700 as our roving receiver and Trimble NetRS as our continuous GPS, base receiver. Both are 24-channel, dual frequency receivers with a Trimble Zephyr Geodetic choke ring antenna. During monthly campaigns we occupied each station from one to two hours and collected data at a 30-second sample rate.

### **2.2. Data Processing and Reduction**

We initially began our data processing strategy using Trimble GPSurvey and then examined whether other software options would produce significant differences in our results. A comparison was made between Trimble GPSurvey and Trimble Geomatics Office 1.6 (TGO). Both processing software packages were available to us and both produced results in close agreement with one another – we found the standard deviations of the 20-minute averages calculated by GPSurvey to be slightly less than those calculated by TGO by a maximum of 5mm in the vertical – however, we opted for the most current software, TGO as we found the user interface optimized and more convenient when resolving questionable baselines.

**Table 1. GPS station information and occupation history.**

AGLA and FSEL columns are shaded as the two end member baseline distances. Darker shaded cells indicate the long duration occupations in 2008 and 2009. Because the data files from the base-station, SNJE, come in 24-hour files beginning at 00:00:00 UTC we were required to divide our long occupations into two separate files for each day. Measurement campaigns are distinguished by thick black lines.

Baseline distances are relative to the fixed base station SNJE at 13.8682 N, 89.6007 E, 1660.191 m.

Standard deviation is the misfit about the best fit line for all occupations.

	AGLA	ESCL	MLPA	MTBL	LSPL	FESP	TSBL	PDRF	LAKE	CRSW	CRSE	FSEL
<b>Baseline dist. (m)</b>	9656.809	7974.08	7437.288	6581.848	4834.812	4772.375	4591.005	4408.605	4063.393	4001.219	3674.222	1888.905
<b>N Latitude</b>	13.8359	13.8757	13.8962	13.8273	13.8829	13.883	13.8362	13.8306	13.8524	13.8467	13.8471	13.8543
<b>E Longitude</b>	89.6834	89.674	89.5385	89.5569	89.5594	89.6422	89.6276	89.5878	89.5679	89.6298	89.6262	89.6108
<b>Elevation (m)</b>	1022.517	1449.291	919.041	1043.675	770.553	1592.912	1870.077	1259.262	742.859	2293.387	2288.74	1717.99
<b>Stand dev. N (mm)</b>	6	9	19	4	14	4	4	8	5	2	4	4
<b>Stand dev. E (mm)</b>	8	14	6	6	16	6	3	2	17	5	7	4
<b>Stand dev. U (mm)</b>	40	31	40	21	39	21	15	21	35	8	20	9
<b>Date</b>	<b>Occupation Duration - hours and minutes</b>											
9/18/2008												6:03
9/19/2008												16:23
9/22/2008	5:06											
9/23/2008	16:42											
2/23/2009	1:04	1:03										
2/24/2009							1:00	1:02				1:05
2/25/2009										1:01	1:00	
2/26/2009			1:00	1:05	1:00							
3/12/2009						1:03						
3/21/2009	1:00	1:01				1:00						
3/22/2009				1:00			1:03	1:01				0:51
3/23/2009			1:06		1:01				1:01			
3/27/2009										0:59	1:01	
4/30/2009										0:58	1:02	
5/3/2009	1:01	1:05		1:00		1:06		1:05				
5/4/2009			1:03		1:01		1:02		1:00			1:01
5/29/2009											1:00	
5/30/2009	1:02	1:07				1:01	1:12	0:56				
5/31/2009			0:36	1:01	1:01				1:03			1:00
6/26/2009										1:00	1:00	
6/27/2009	1:19	1:31				1:34						
6/28/2009			1:01		1:04		0:46		1:03			1:02
6/29/2009				1:06				1:01				
7/25/2009							1:04	1:01	1:04			1:00
7/26/2009	2:16	2:07				2:07						
8/27/2009										1:00	1:01	
8/30/2009	2:02	2:00				2:00						
8/31/2009					1:01		1:02		1:02			1:01
9/1/2009				1:01				1:00				
9/10/2009	6:21											
9/11/2009	15:45											
9/19/2009												6:22
9/20/2009												17:38
9/24/2009										1:01	1:01	
9/27/2009	2:02	2:01				2:15						
9/28/2009			1:01	1:02			1:08	1:03	1:02			1:01
<b>Total Occupations</b>	<b>10</b>	<b>8</b>	<b>7</b>	<b>7</b>	<b>6</b>	<b>8</b>	<b>8</b>	<b>8</b>	<b>7</b>	<b>6</b>	<b>7</b>	<b>10</b>



**a.**



**b.**

**Figure 2. GPS equipment.**

(a) Spike mount tripod with Trimble Zephyr Geodetic antenna. Tripod has a fixed height of 55 cm from pin to bottom of antenna mount. The spike on the tripod was placed in a 0.5 mm dimple on an anchored bench mark. (b) Trimble 5700, choke ring antenna and associated equipment. Photo by author.



All TGO baseline solutions were determined by a single-site-pair calculation from base to rover with a minimally constrained network adjustment. The 3-D – vector components – estimates in baseline difference between the fixed base-station and the rover along with the calculated 1- $\sigma$  uncertainties for each coordinate component were taken from TGO and statistically reduced to find the weighted mean. The weighted mean is determined by:

$$\bar{X} = \frac{\sum_{i=1}^n (X_i / \sigma_i^2)}{\sum_{i=1}^n (1 / \sigma_i^2)}$$

Where X is the difference in positional component (NEV) between rover and reference station for each baseline observation and  $\sigma$  is the standard error of each positional component calculated by TGO. Various efforts were employed to improve questionable baselines – those flagged by TGO. However, if the flags remained they were noted but not removed.

## **2.3. Measurements of Achievable Accuracy**

### **2.3.1. Continuous GPS station – SNJE**

The daily coordinates of our fixed continuous GPS station SNJE were determined in the International Terrestrial Reference Frame 2005 using GIPSY processing software. The repeatability of the daily and monthly average positions of the CGPS station SNJE (figure3 a-c) demonstrates that our base exhibited very stable behavior, with a standard deviation in the horizontal of 2 mm and 4 mm for the north and east components respectively, and 8 mm standard deviation in the vertical during the time period of this investigation.

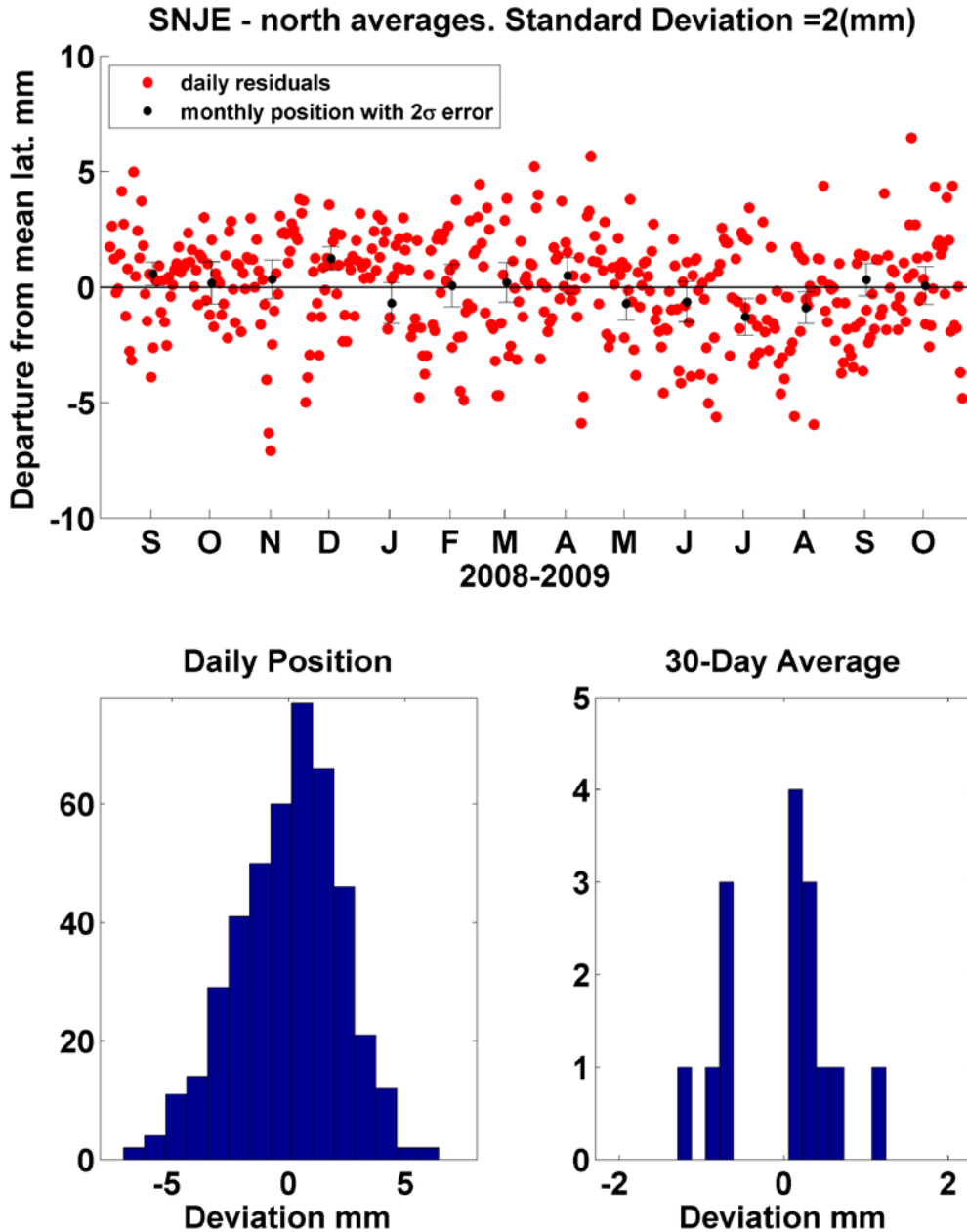
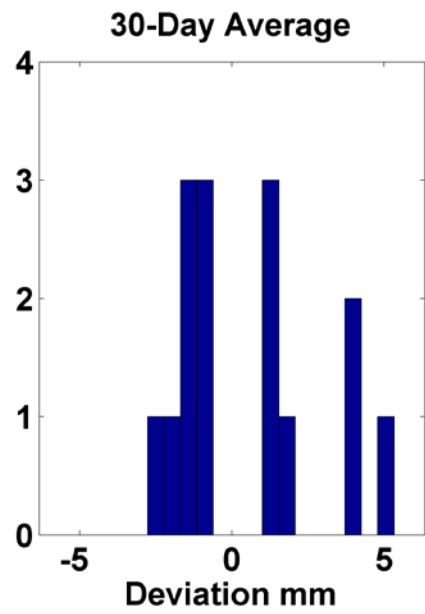
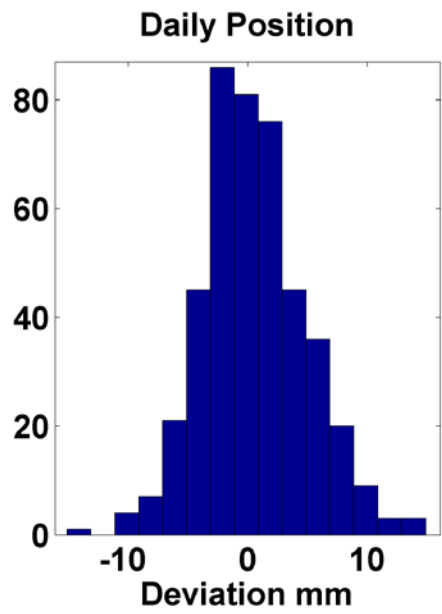
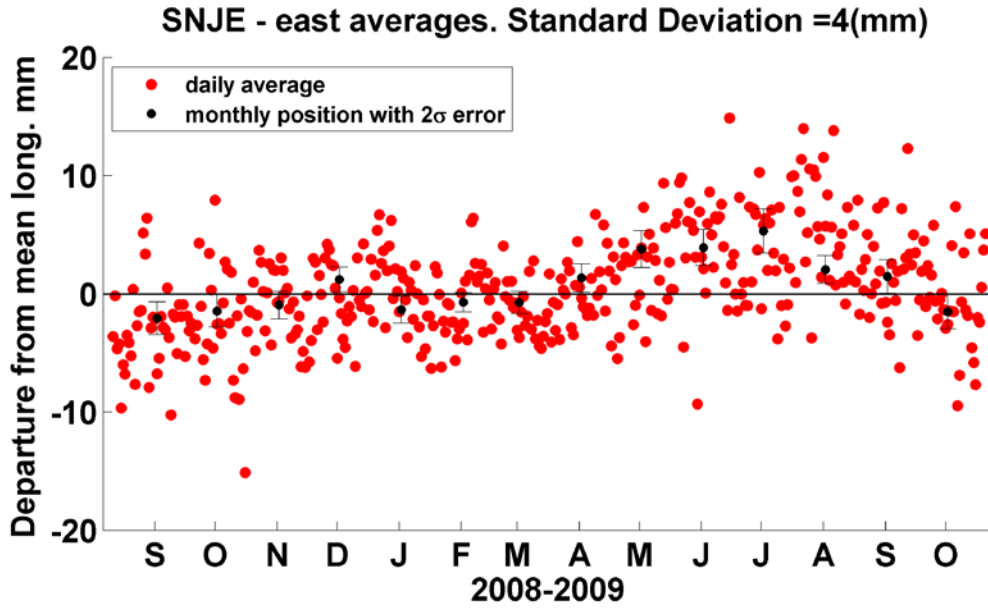
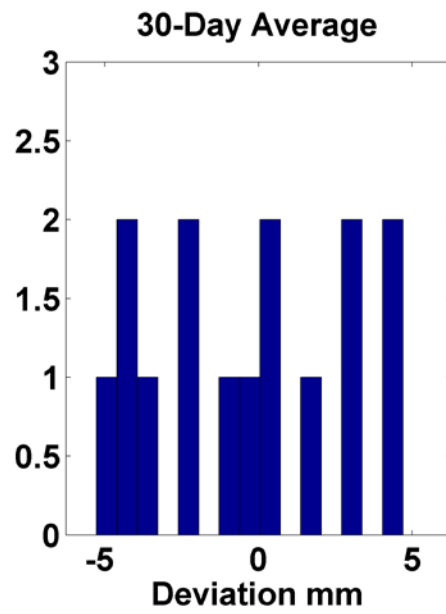
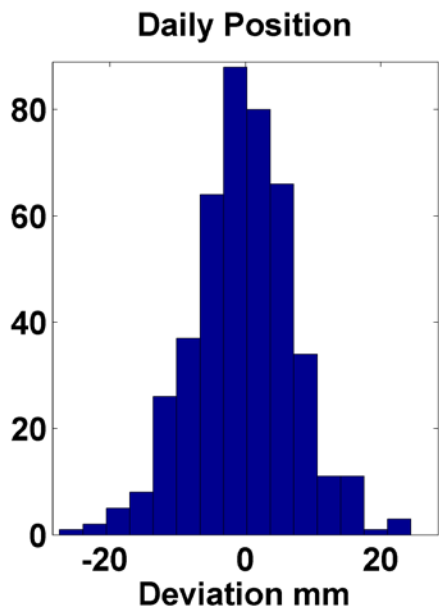
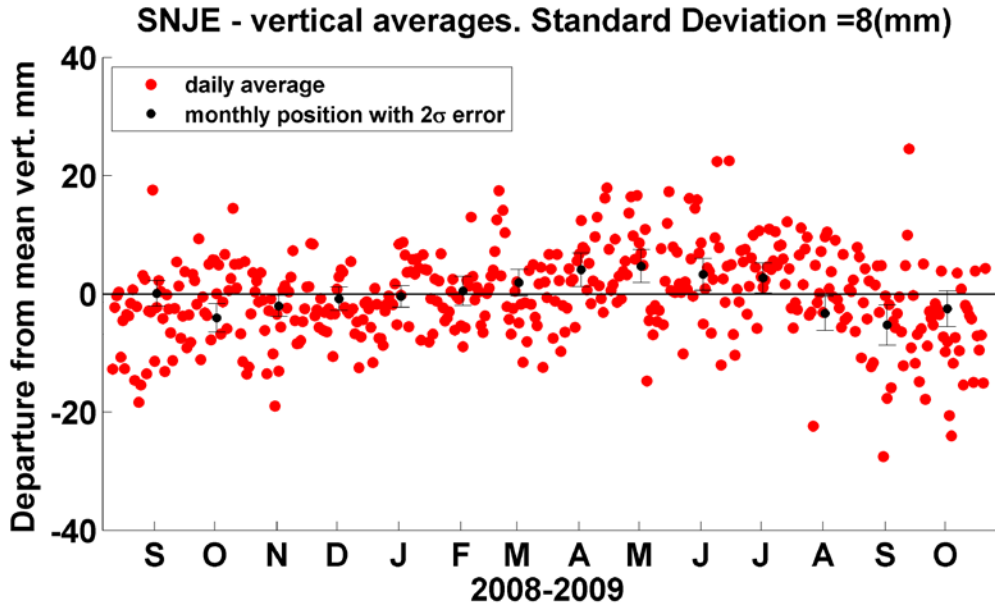


**Figure 3. Daily and monthly position averages for SNJE.**

Above, (a) north component at the SNJE fixed base station. East (b) and vertical (c), components on the following two pages. Daily averages (red) and monthly averages (black) with a 2- $\sigma$  error were determined with GIPSY processing software and reduced from a best fitting slope. Standard deviations of daily position averages are 2mm in the north, 4mm in the east and 8mm in the vertical.



(b).



(c).

### 2.3.2 Repeatability of interstation baselines

Our measure of repeatability for baseline accuracy is the scatter of residuals about a mean value from long duration (overnight) occupations (20-24 hours). In September 2008, we occupied the sites FSEL and AGLA for 22.43 hours and 21.8 hours respectively. Relative to SNJE, these two sites represent the shortest and longest baselines within the network at distances of 1888 m and 9656 m. The data were divided into 20-minute-long segments, and each 20-minute segment was used to estimate a baseline to the reference site SNJE. The standard deviations from the 22.43-hour mean for our closest site, FSEL, are 3 mm in the horizontal and 7 mm in the vertical, while at AGLA, the farthest station, the standard deviations relative to the 21.8 hour mean are 8 mm horizontal and 27 mm vertical. Based on these results we determine that one or two-hour occupation times would allow us to achieve a measure of accuracy that should be sufficient to capture any volcanic signal and possibly tectonic signal in excess of 10 mm horizontal and 30 mm vertical. We repeated this experiment in September, 2009 with 24-hour and 22.1-hour occupations and post processed using (TGO). We also reprocessed the original 2008 data with TGO to maintain continuity and ensure that the results were repeatable from one software package to another. The scatter about the 24-hour mean for the 2008 and 2009 overnight occupations (figure 4 a-c) was calculated by differencing the average position from each session from the weighted mean. From these residuals, and using built-in MATLAB tools, we calculated the standard deviation by

$$s = \left( \frac{1}{n-1} \sum_{i=1}^n (X_n - \bar{X})^2 \right)^{\frac{1}{2}}$$

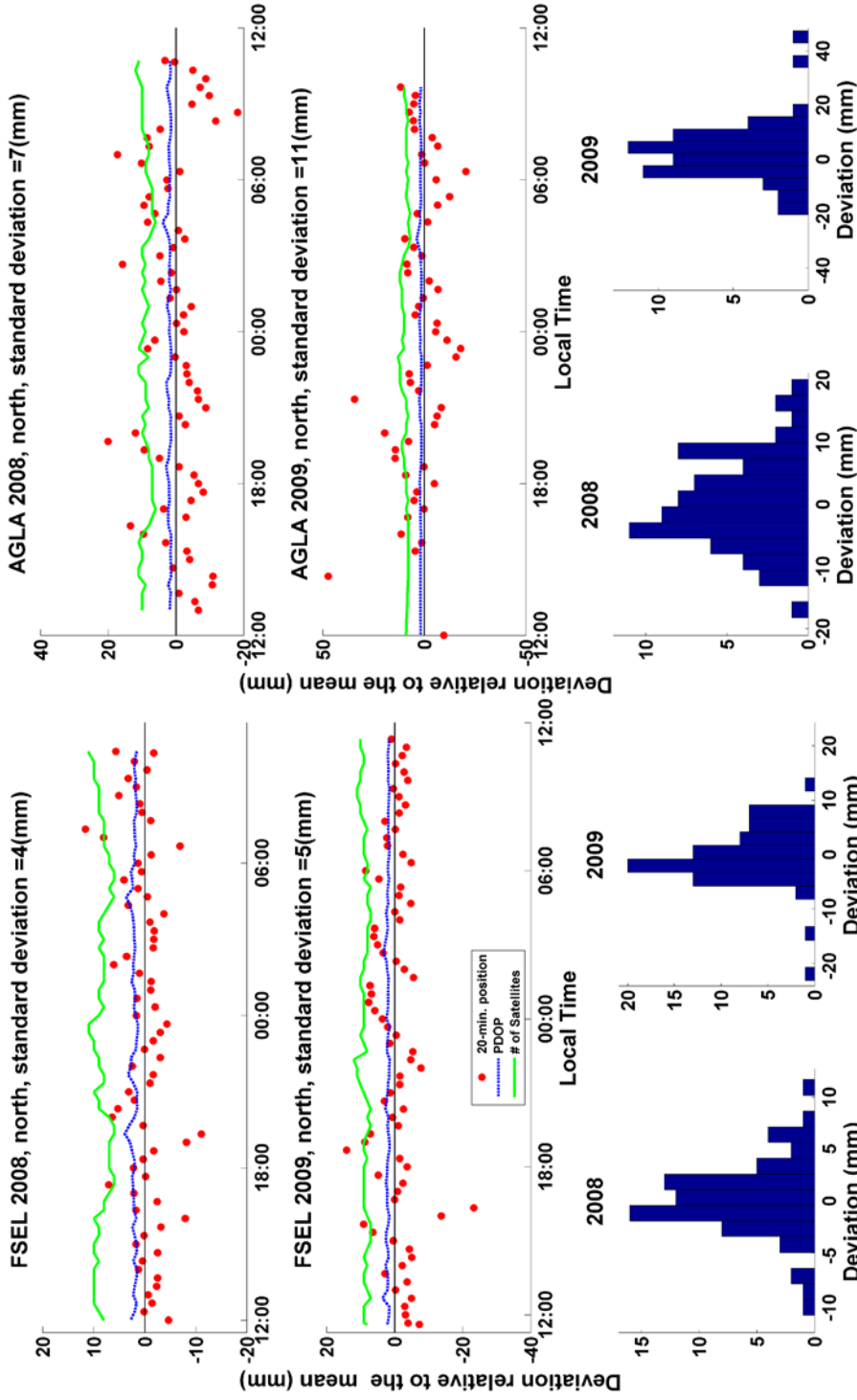
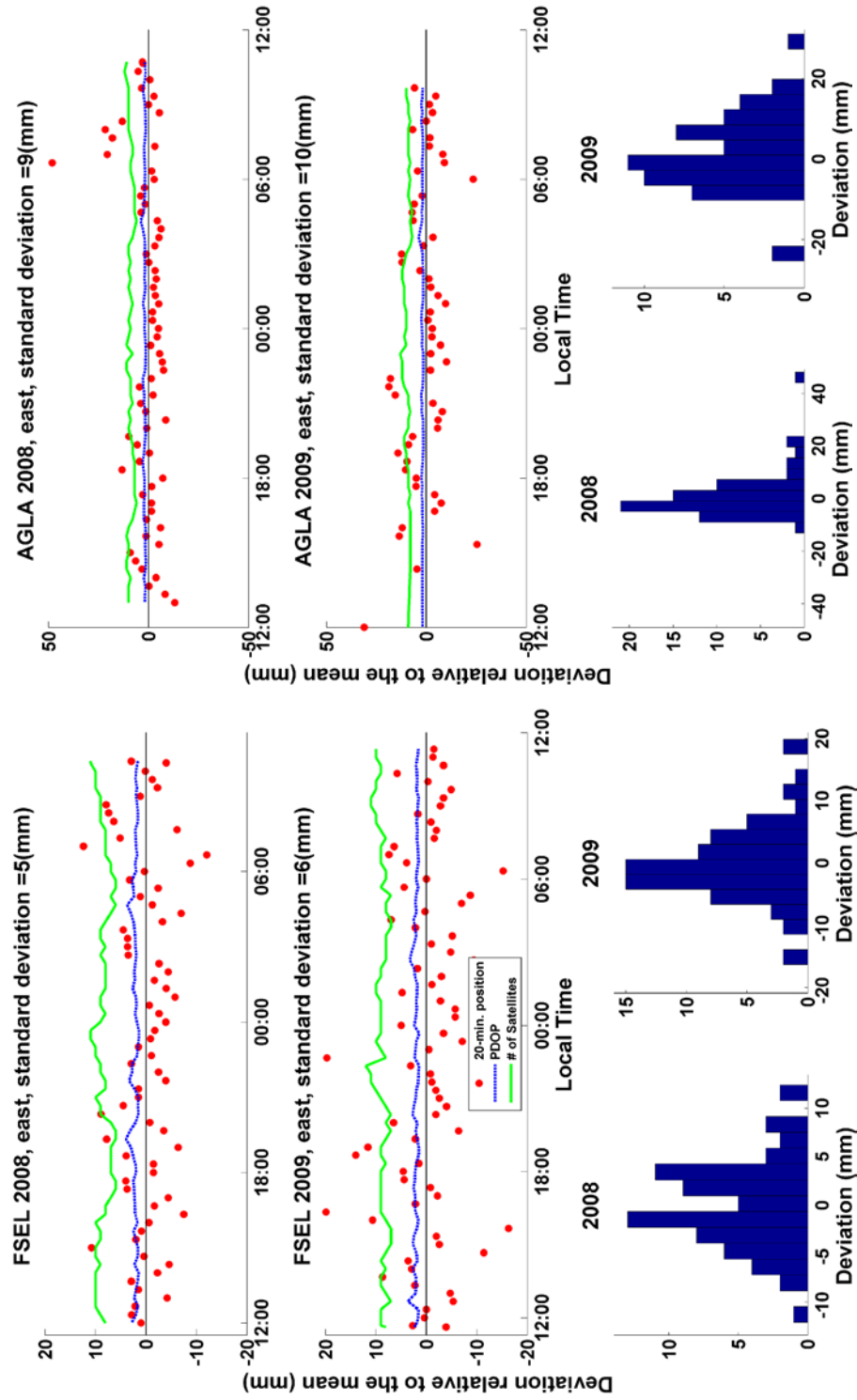
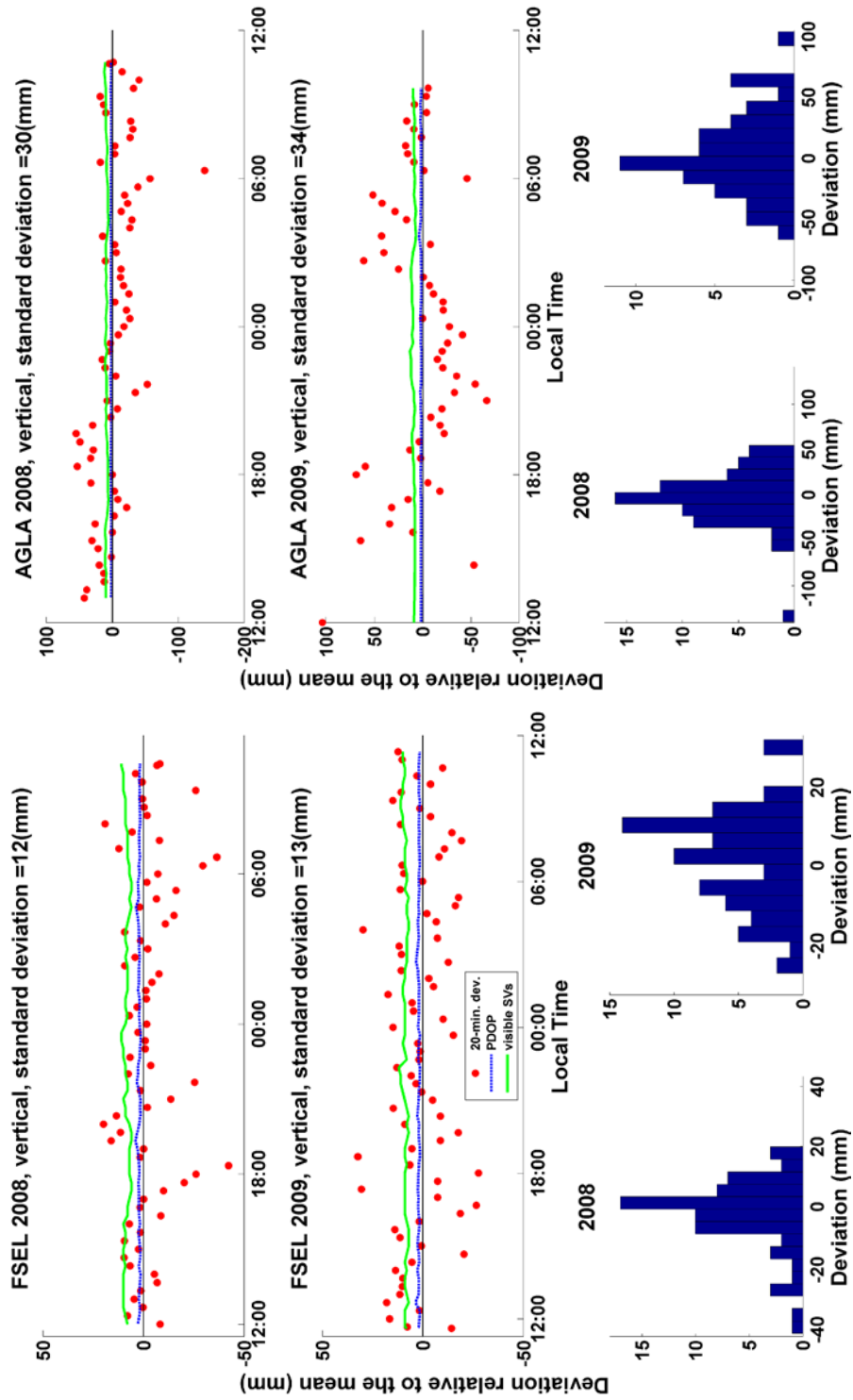


**Figure 4. 20-minute averages about the 24-hour mean and associated histograms.** Above (a) shows the results of the north component FSEL (left) and AGLA (right). East (b) and vertical (c) components are on the following pages. Red points are the 20-minute position averages, blue line is the position dilution of precision (PDOP) which is a function of satellite constellation geometry. PDOP values in the range of 4-5 are considered very good. Higher values indicate poor geometry and the possibility of a poor baseline solution for that time. Green line shows the number of satellites visible to the rover receiver.



(b).



(c).



## **3. RESULTS**

### **3.1. Repeatability**

After dividing the 2008 and 2009 20+ hour RINEX files into 20-min segments and then processing with TGO, we found that for the shortest baseline the 20-min repeatabilities are 4 mm and 5mm in the north, 5 mm and 6 mm in the east and 12 mm to 13 mm in the vertical. Conversely, for our longest baseline, we were able to repeat the baseline components to component to 7 mm and 11 mm in the north 9 mm to 10 mm in the east and 30 mm to 34 mm in the vertical. The standard deviations at FSEL data increased in 2009 by 1mm in NEV components, while at AGLA they are 4 mm, 1 mm and 4 mm greater in the NEV than those from 2008. Having produced results from two separate experiments which are consistent with each other we are confident that our measure of accuracy is repeatable under 5 mm in the vertical component. Furthermore, the repeatability of the 2008 and 2009 averages provides evidence that the above accuracies can be achieved with a minimal observation time of 20-minutes.

We also assessed the repeatability of baselines estimated from one-hour observation sessions, which was the typical duration of most of our differential measurements. At FSEL standard deviations are 3 mm, 3 mm and 5 mm, while at AGLA they are 6 mm, 8 mm and 23 mm for the NEV respectively. These results further enforce our measure of accuracy and justify our decision to observe sites for one to two hours by confirming that positional errors do average down over longer sessions.

### **3.2. Scatter relative to Linear Fit**

Each observation for each baseline was processed independently and further reduced using the statistics described above. A weighted least-squares regression from built-in MATLAB tools was used to find a best fit trend line for the difference from the weighted mean of each observation. From the linear regression we plotted the scatter

about the best-fit line (figure 5). The slopes of the lines in figure 5 (a-c) show the signal of deformation in each directional component. A notable feature appears to be an outlier, or misfit data point with significant error, in the north and east components (figure 5 a,b) for proximally located stations MLPA, LSPL and LAKE on 5/4/09. This is interesting not only because of their proximity to one another but because these stations were always observed in sequential order, when accessible, on the same day during each campaign.

Examination of the time series reveals several possible overall trends: 1) a positive slope in the east for CRSW, CRSE, FESP, MLPA, MTBL, LSPL and PDRF ; 2) a negative north slope for CRSW, CRSE, FESP, TSBL, MLPA, MTBL, PDRF and LAKE suggest that these sites are moving south and east relative to SNJE; 3) the most obvious trend is seen in the vertical component for stations surrounding the Coatepeque caldera: MLPA, MTBL, LSPL, PDRF and LAKE. In no other data set or cluster of stations is the vertical signal so pronounced, however, station AGLA – the most distal site – also exhibits a substantial vertical signal. While the overall vertical trend of the five caldera stations is a positive slope through the entire time series, looking at the scatter of the data points there also appears to be negative trend that occurs after July.

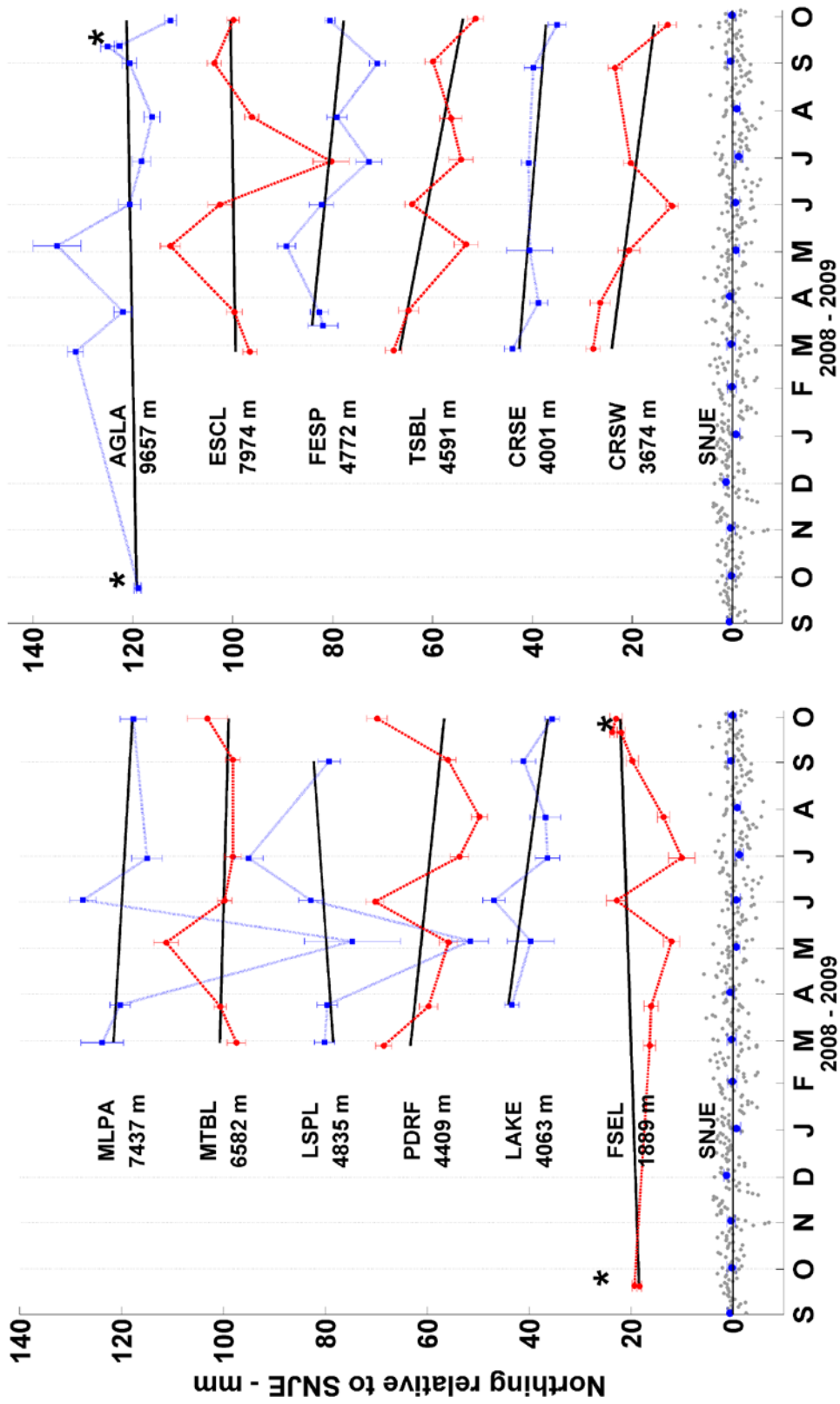
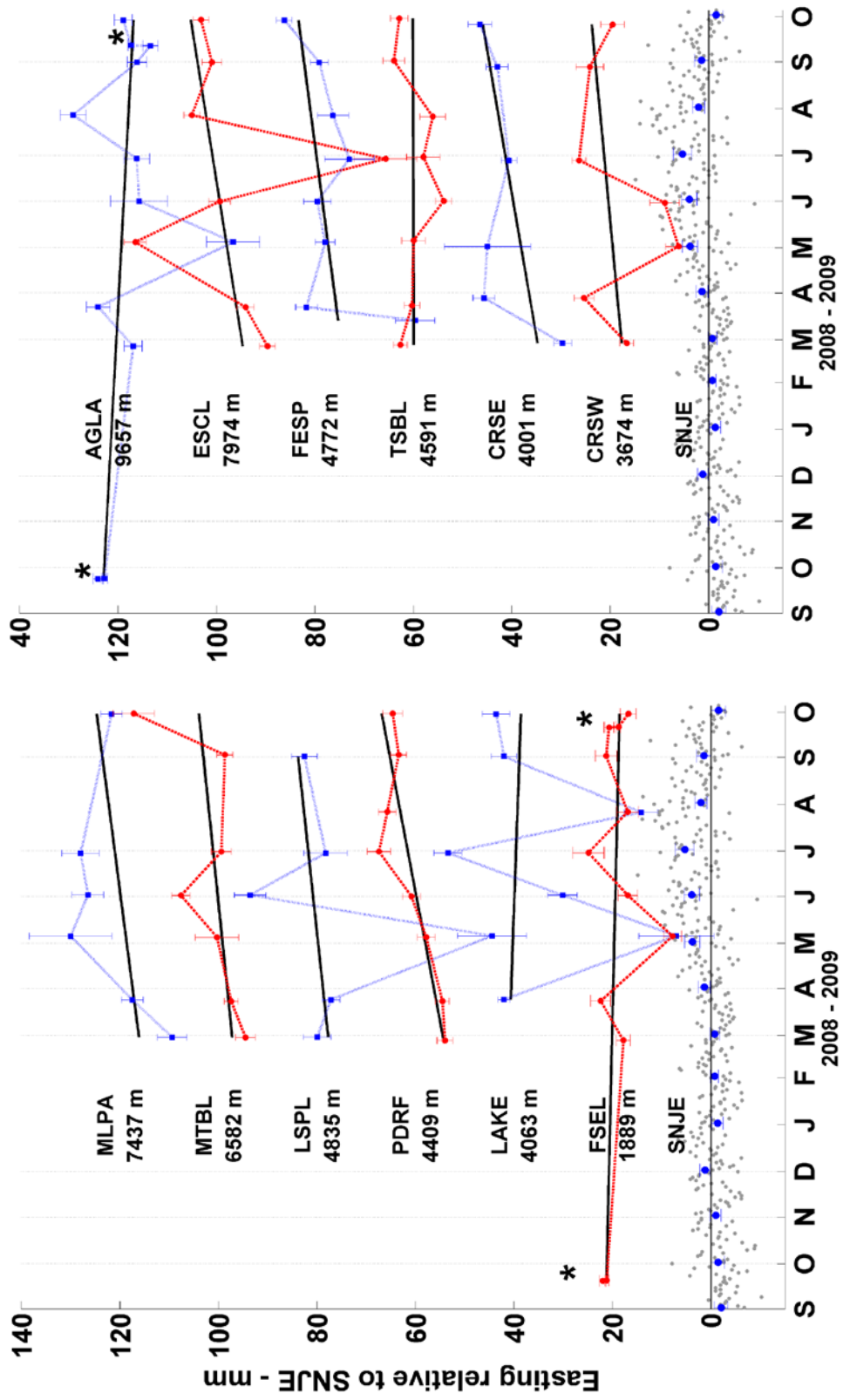
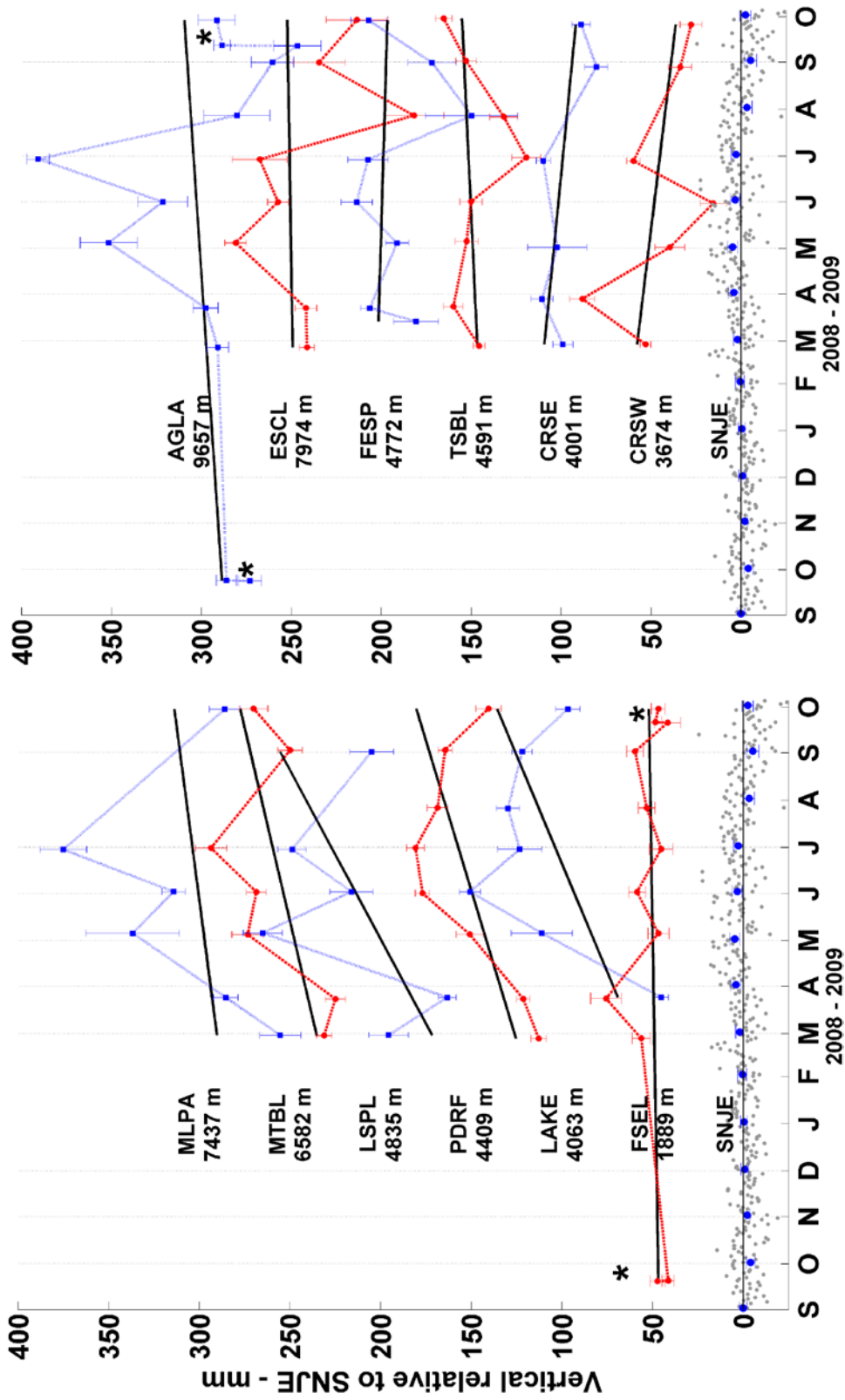


**Figure 5. Positional scatter about the best fit line.**

Above (a) the north component for stations near the caldera (left) and other stations around the volcano (right). East b, and vertical c, are found on the following pages. Error bars represent  $2\sigma$  error. Grey data points for the fixed base Station SNJE show the daily averages processed by GIPSY relative to ITRF 2005 and reduced by a best-fit line. Blue data points represent the monthly averages. Station identifications include distance from SNJE.



(b)



(c)

### 3.3. Hourly vs. 20-Minute Observations

We calculated the Root Mean Square (RMS) of the best-fit residuals from the total occupations from each station and compared it to the standard deviation about the mean from a sample of 20-minute sessions for each station (figure 6). We observe a decrease of accuracy as a function of both baseline length and site elevation. We make this comparison in an effort to determine whether baseline distance or site elevation plays a greater role in positional error. We also look for a distance or elevation threshold where the signal error exceeds our desired accuracy. In both plots, in all three components, we see the RMS of the total observations has a greater deviation from the mean compared to the standard deviation from 20-minute samples. However the magnitude from the trend lines in both horizontal components is of equivalent magnitude. We also see in the vertical for baseline distances under 5000 m, the standard deviation from the 20-minute sessions stays between 10 mm and 30 mm for distances under 10000 m, with the exception of one outlier. We also see the same pattern in the vertical component of plot (b). The 20-minute sessions exhibit a standard deviation between 10 mm and 30 mm with the exception of one outlier. We tabulated the magnitude of the misfit from the trend line for both RMS and standard deviations for baseline length (table 2) and site elevation (table 3). In the table we can see that the large outlier mentioned above in both vertical plots can be identified as station FESP. We see that in both vertical plots (a and b) and tables 1 and 2 the 20-minute sessions do not exhibit large magnitude scatter about the trend line and the standard deviation rarely exceeds 30 mm. This suggests to us the cause of our vertical uncertainty is possibly related to the decorrelation of the tropospheric zenith delay between base station and rover.

**Table 2. Misfit of the RMS and standard deviations over baseline distance.**

Absolute magnitude of the data points about the trend lines from figure 6 (a). Data is arranged by greatest distance at top and shortest distance at the bottom. The average differences in the north and east from the RMS line (left) are slightly greater than those of the standard deviations of the 20-minute sessions. Which suggests that both our month-to-month and 20-minute sessions are equally repeatable. The magnitude of station FESP in the vertical component of the 20-min. plots is highlighted to show the large outlier.

Station	Distance	Residuals differences RMS			Residuals differences 20-min		
		N	E	V	N	E	V
AGLA	9656.81	4.8	2.4	0.8	1.5	0.4	3.5
ESCL	7974.08	0.6	5.4	3.4	0.2	2	1.8
MLPA	7437.29	10.2	2.4	7.7	1.5	0.5	8.2
MTBL	6581.85	3.6	2.5	8.9	3.6	2.3	6.8
LSPL	4834.81	7.2	8.2	15.3	3.1	0.4	6.2
FESP	4772.38	1.9	1.3	1.7	1.7	10.5	33.1
TSBL	4591.01	2.2	4.5	7.8	0.2	5.8	9.2
PDRF	4408.61	1.5	5.2	0.6	0.3	5	6.6
LAKE	4063.39	1.1	9.3	14.4	8.3	4.1	8.1
CRSW	4001.22	4.1	2.3	12	0.7	0.9	2.4
CRSE	3674.22	0.9	0.2	1.2	3.5	0.4	5.6
FSEL	1888.91	0.2	2.5	3.5	1.7	1.6	2.3
average	5323.71	3.19167	3.85	6.44167	2.19167	2.825	7.81667

**Table 3. Misfit of the RMS and standard deviation over station elevation**

Absolute magnitude of the data points about the trend lines from figure 6 (b). Data is arranged with greatest elevation difference on top and lowest elevation difference on bottom. The average differences in the north and east from the RMS line (left) are slightly greater than those of the standard deviations of the 20-minute sessions. Which suggests that both our month-to-month and 20-minute sessions are equally repeatable. The magnitude of station FESP in the vertical component of the 20-min. plots is highlighted to show the large outlier.

Station	$\Delta$ height	Residuals differences RMS			Residuals differences 20-min		
		N	E	V	N	E	V
LAKE	918	4.6	5.4	0.8	6.1	3.2	5.2
LSPL	891	4.5	4.8	5.1	1	1	10.4
MLPA	742	10.7	3.4	10.1	2.6	0.1	0.3
AGLA	638	1.7	1.6	11.8	1.1	1.1	14.7
CRSW	633	6	3.9	19.6	1.5	1.6	3.4
CRSE	629	3.1	1.6	7.5	4.3	1.1	7.4
MTBL	617	3.1	2.9	6.9	4.1	2.7	2.5
PDRF	401	1.3	4.8	1.7	0.7	5.2	9.9
ESCL	211	3.5	8.9	12.5	1.5	0.6	3.6
TSBL	210	1.2	2.4	4.1	1.3	5.8	14.8
FESP	68	0.1	1.9	5.7	0.5	10.7	26
FSEL	58	0.4	0.4	6.2	0.4	2.5	11.1
average	501.333	3.35	3.5	7.66667	2.09167	2.96667	9.10833

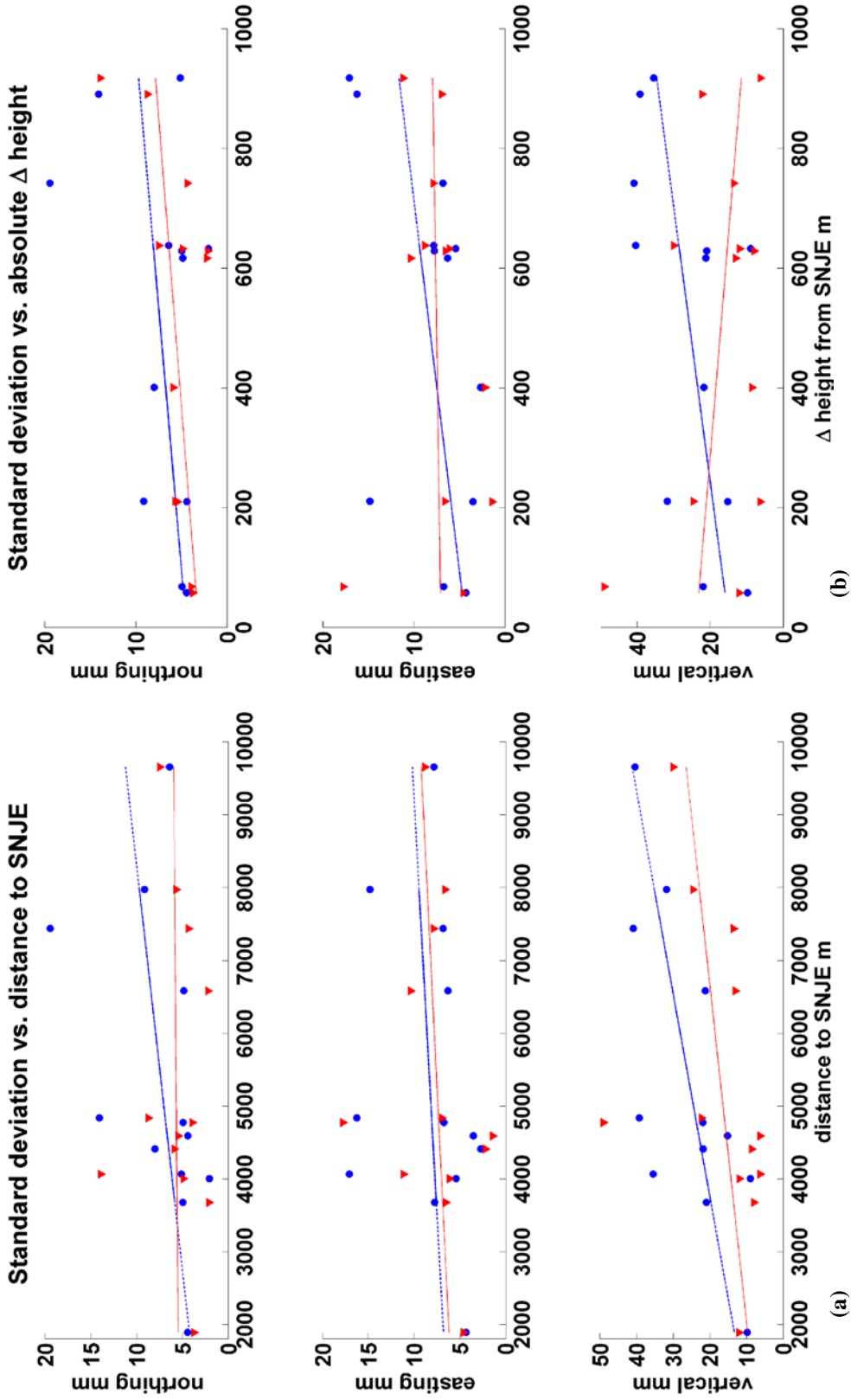


**Figure 6. RMS error versus baseline length and height.**

Red triangles represent the standard deviations from the mean of a sample of 20-minute segments from each station. Blue circles show the RMS of the residuals from the best-fitting line of total observations from each station. Standard deviations and RMS versus baseline distance (a) are shown on the left. Standard deviations and RMS versus site elevation (b) are shown on the right.



### 3.4. Tropospheric Water Vapor Delay

Using a linear carrier-code combination we have effectively eliminated the error caused by the total electron content in the ionosphere. The delay caused by the neutral troposphere and to a lesser degree the stratosphere, on the other hand, cannot be eliminated as easily. Tropospheric delay is the result of refraction of the signal as it passes through water vapor and other gas species in the lower atmosphere. During data processing we employed the Hopfield tropospheric model to eliminate the signal bias caused by the hydrostatic or “dry” troposphere and reduce error to sub-centimeter accuracy (Cove et al. 2004, Satirapod and Chalermawattanachai 2005). TGO software assumes that both base and rover antennas are sampling an equivalent column of the troposphere and that variations in signal propagation are equal. Base-station SNJE sits at an elevation of 1660.191 m. The elevations for FSEL and AGLA are found in table 1. The absolute  $\Delta$  elevation for FSEL is 57 m and 637 m  $\Delta$  elevation for AGLA. This type of antenna height difference can introduce a signal bias as high as 2-5 mm per 100 m of elevation difference (Satirapod and Chalermawattanachai 2005). Assuming the maximum bias of 5 mm per 100 m of elevation, AGLA could demonstrate 32 mm of vertical error and FSEL would demonstrate less than 3 mm. This is in strong agreement with the results from our repeatability experiments. Lawrence (2006) has shown that atmospheric errors for a differential network increase over baseline length due to “spatial decorrelation of the atmospheric delay.” We also know that variations in the “wet” troposphere, precipitable water vapor (PWV), will have a more pronounced effect on vertical position as the PWV is more difficult to model, especially in tropical environments with variable topography (Mendes 1998, Satirapod and Chalermawattanachai 2005, Collins & Langley 1997).

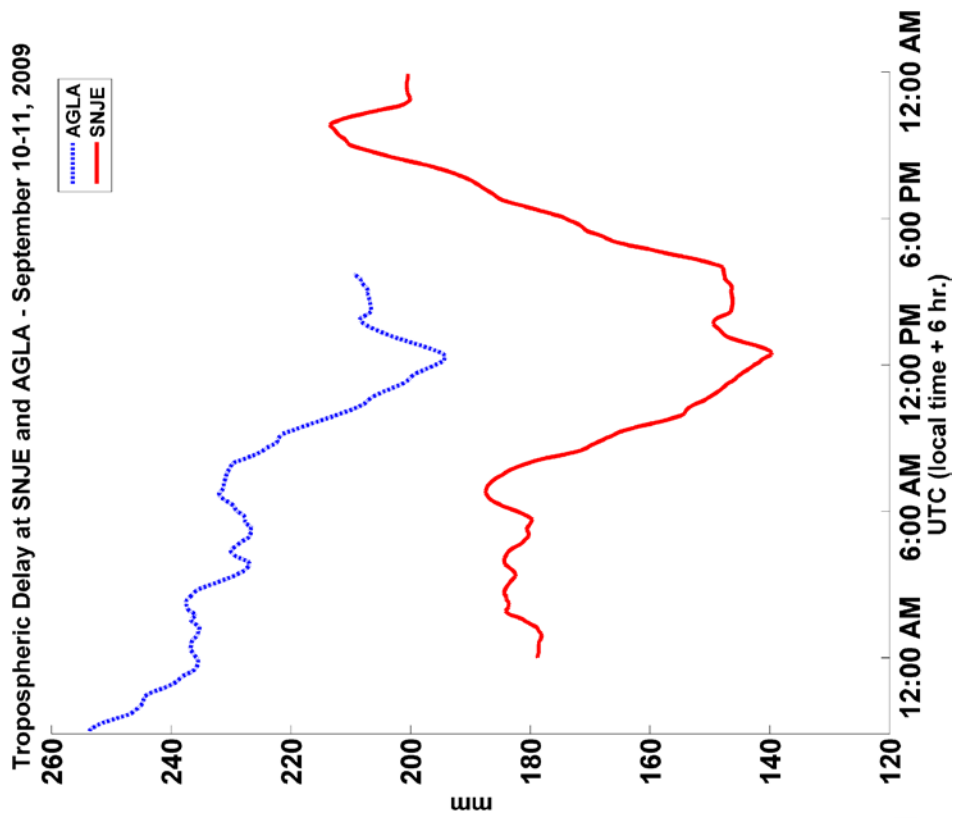
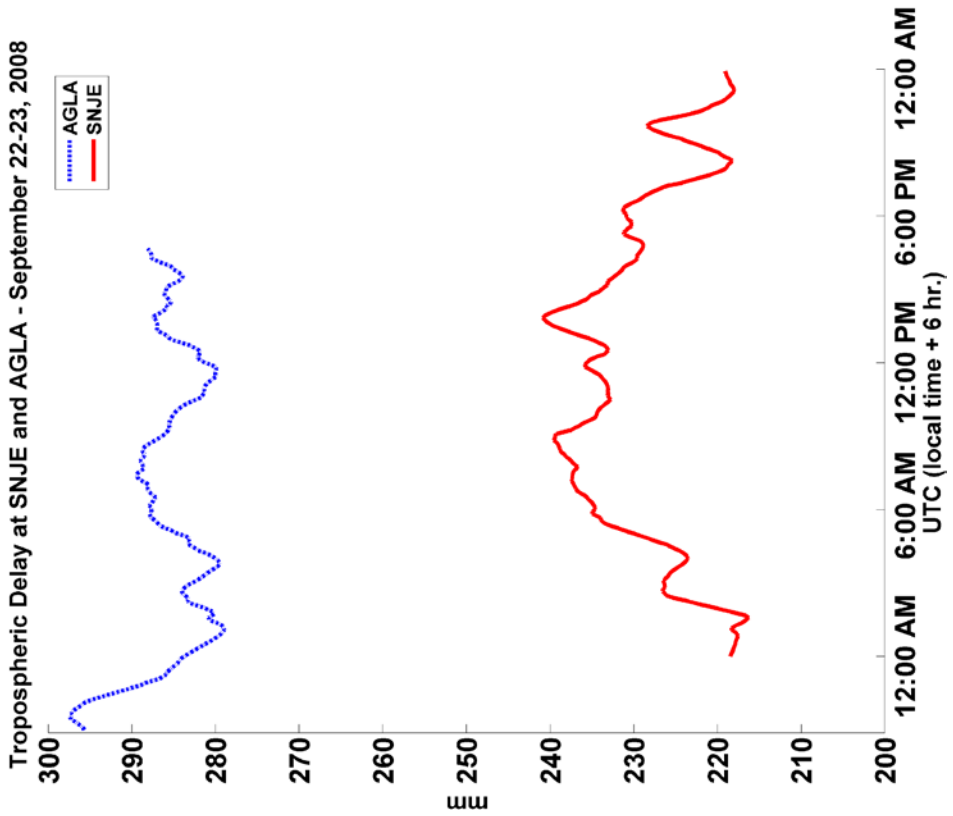
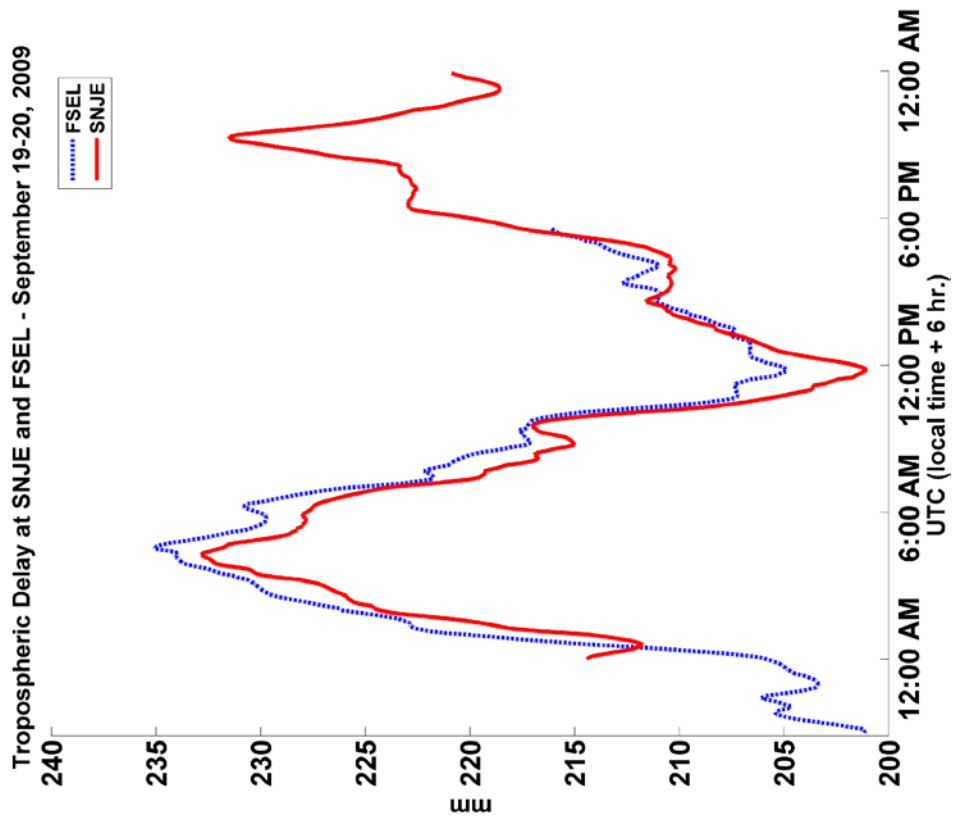
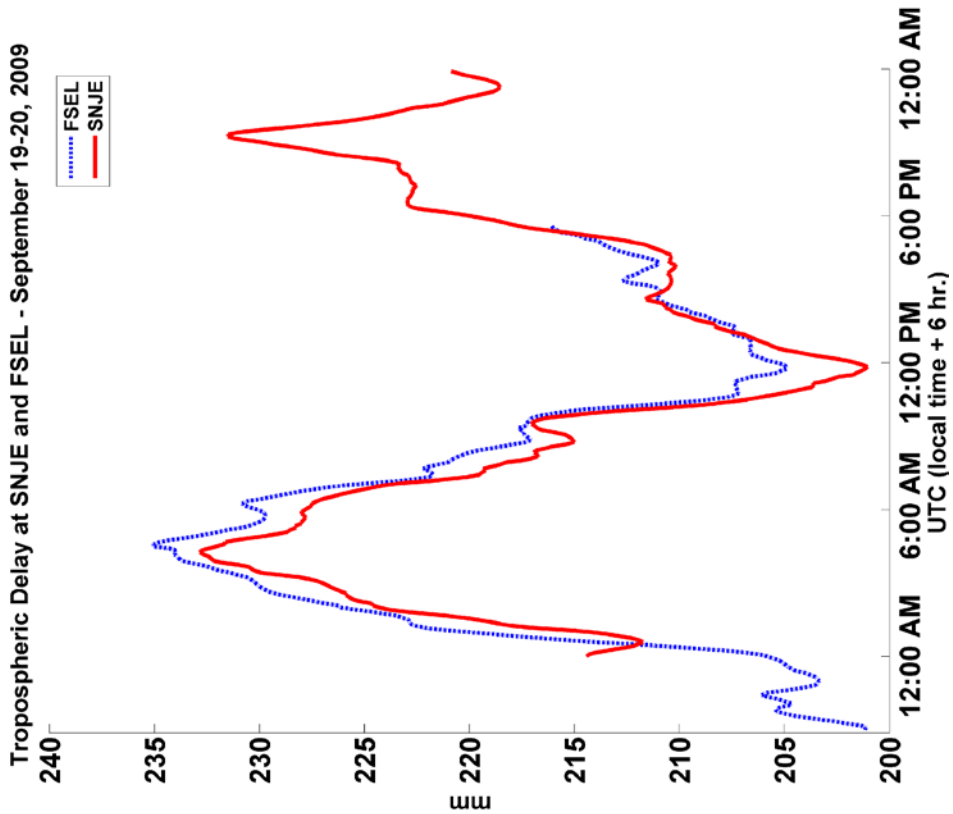


**Figure 7. Total precipitable water vapor (PWV).**

The signal delay (estimated by GPSY and expressed in millimeters) induced by the wet component of the troposphere. Above, (a) at rover-station AGLA and base-station SNJE during the overnight campaigns in 2008 (left) and 2009 (right). (b) FSEL to SNJE on the following page.



(b)

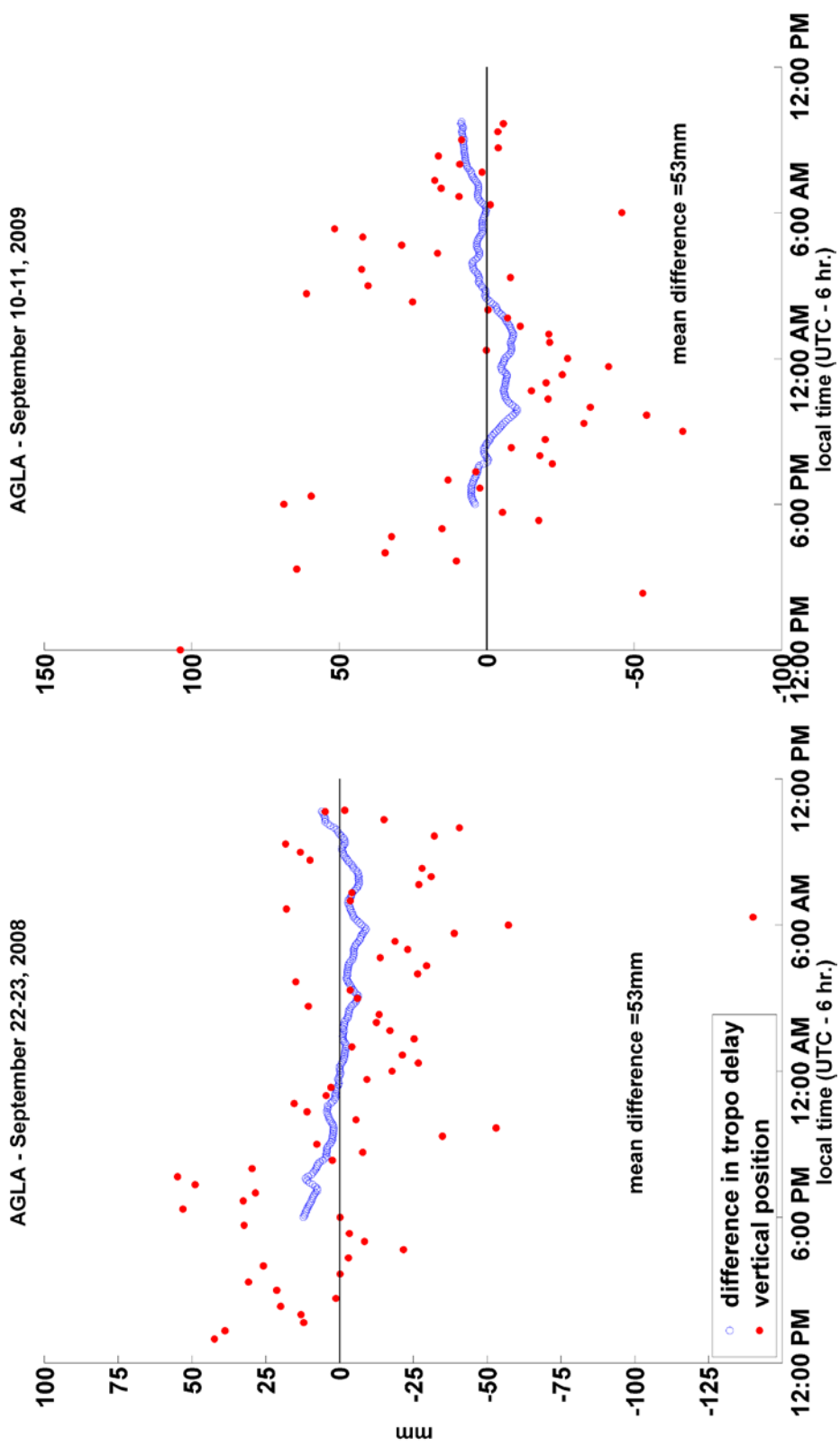
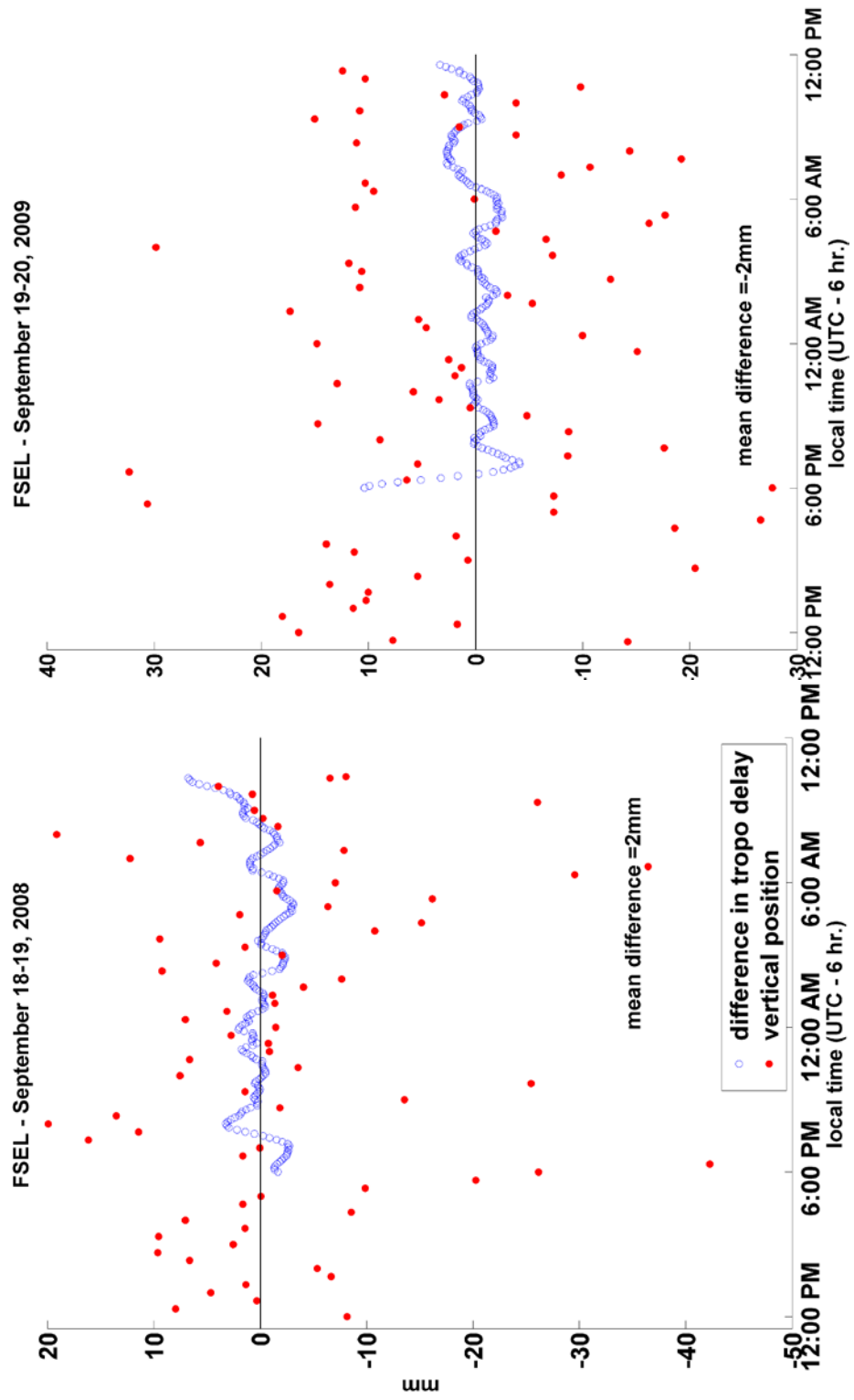


**Figure 8. The difference in tropospheric delay versus the positional scatter.**

Above, (a) The difference in signal delay between SNJE and rover station AGLA for the overnight occupations in September 2008 (left) and 2009 (right). Blue circles represent the difference in tropospheric delay between base and rover in 5-minute segments scattered about the mean difference (labeled on the plot). Red points are the 20-minute average deviations from the mean of vertical position delay. The scale is in mm and the time is local UTC-6. (b) SNJE and FSEL on the following page.



(b)

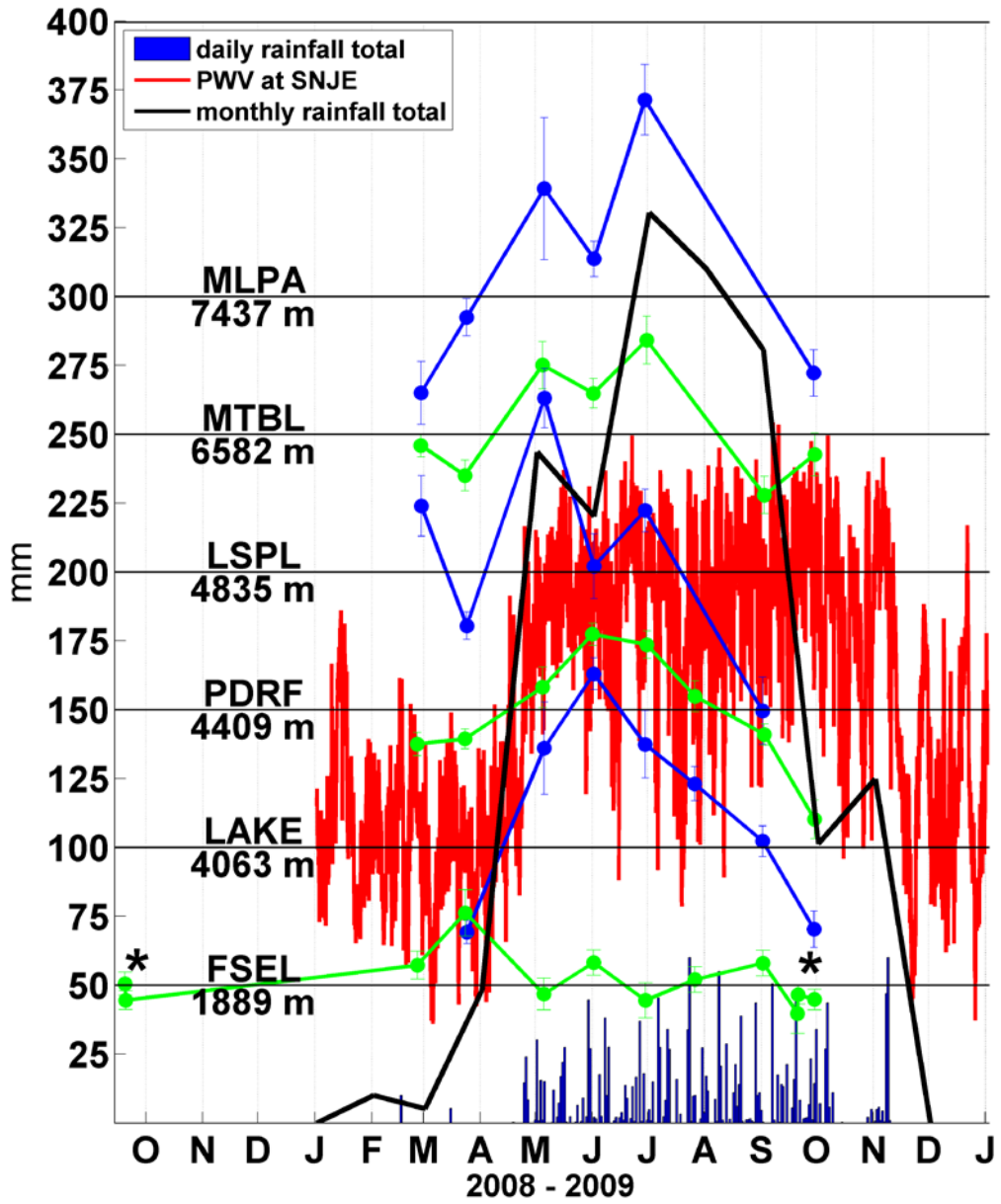


**Figure 9. 2009 precipitation totals, PWV and positional scatter.**

The red line shows the daily variation in signal delay in millimeters propagated by the precipitable water vapor (PWV) estimated by GIPSY through a vertical column of troposphere above the base station SNJE. Also plotted is total monthly rainfall (black line), and total daily rainfall in the black histogram at Santa Ana. Misfits about the best-fit of the vertical position for stations around the caldera are shown in blue and green lines.

Using GIPSY processing software, we were able to estimate the delay, in millimeters, caused by the PWV at rover stations AGLA and FSEL as well as the reference station SNJE for the dates of the overnight occupations in 2008 and 2009 (figure 7). We can see how the PWV not only varies through time of day, but appears very well correlated at FSEL and SNJE and quite decorrelated at AGLA and SNJE.

While the vertical water column varies over time, the average difference between base and rover remains fairly constant. We calculated the difference from SNJE to each rover station and plotted the variance about the mean and the vertical scatter about the 24-hour mean (figure 8). It should be noted that because SNJE data is collected in 24 hour files starting at 00:00 UTC each day and are processed independently, and the rover station data collection began at late-morning (local) and ended at late-morning the following day, we are unable to correlate a complete 24-hour file. Figure 8 shows us the deviation in tropospheric delay from the mean at AGLA is roughly +/- 20mm, while at FSEL the deviation rarely exceeds +/- 5mm for only brief intervals of time. This is in agreement with Satirapod and Chalermawattanachai (2005) and Lawrence (2006) and further demonstrates more tropospheric induced noise at AGLA than FSEL and thus longer baselines, or greater differences in site elevation, are more susceptible to wet, tropospheric delay and thus greater uncertainty in positional accuracy. The correlation coefficients between tropospheric delay and deviation of vertical position for FSEL are -0.0065 in 2008 and -0.1245 in 2009, whereas for AGLA they are 0.6976 and 0.6123. During the 2009 observation at FSEL the records indicate there were scattered showers during the first several hours and cloud cover through the night. We know from direct observation that there overcast conditions but no showers during the 2008, FSEL occupation. FSEL and SNJE undoubtedly experienced the same climatic conditions during the two overnight observations, which reinforces the lack of correlation between tropospheric delay and positional error for those two sites. At AGLA we know there was heavy cloud cover for the duration of the 2009 observation unfortunately we have no record of the weather conditions at the base-station, but it is possible that SNJE was experiencing different conditions due to distance and variable topography.

There appears to be a causal correlation between seasonal changes in PWV and vertical signal (figure 9). The rainy season in El Salvador typically begins in May and lasts through October and often into November with the highest levels of precipitation coming in June through September. In figure 9, the daily and monthly totals can be seen increasing seasonally in step with the increase of PWV at SNJE. This follows closely with the changes in vertical positions seen in the differential stations surrounding the caldera. We must point out that the bulk of our data set begins in February and we see consistent vertical change from the start at MLPA and PDRF followed by change at the remaining caldera sites beginning in March which precedes the onset of the large PWV increase. Furthermore, the stations in figure 9 begin a negative vertical trend roughly four months before the decrease in PWV. This suggests that the observed vertical signal is more than just an artifact of tropospheric delay.

While there is undoubtedly a correlation between tropospheric delay and vertical error, between 10 mm and 30 mm, at the longer baselines, we are still convinced that this dGPS technique has captured a large vertical signal – which exceeds the possible error – at sites around the volcano and the Coatepeque Caldera.



### **3.5. Evidence of Surface Deformation**

We observed a significant vertical signal at stations LAKE, LSPL, MLPA, MTBL and PDRF – around the caldera – from the initiation of data collection in February through June after which a deflationary trend through the end of data collection in October can be seen in the data (figure 5c). The two end members from the caldera sites, LAKE and MTBL exhibit a maximum and minimum vertical signal of 139 mm and 61 mm respectively (table 4). It should also be noted that stations AGLA and ESCL, while a considerable distance outside of the caldera, exhibit a similar vertical trend with a magnitude of vertical inflation (99 mm and 34 mm respectively) on the same order as those sites around the caldera. Because the large vertical signal at sites around the caldera can be more than an order of magnitude greater than the maximum apparent error we take this as measurable evidence that we have captured true vertical displacement around the caldera and as well as some sites around the volcano.

The symmetry and consistency of the vertical signal at these sites, especially at sites LAKE PDRF and MTBL is another compelling indicator that a real inflation/deflation event was measured using dGPS. It is also interesting to note a possible connection between magnitudes of deformation as a function of the spatial relationship relative to Volcano Santa Ana. All above mentioned stations are situated off the flanks of the volcano at more than 5 km from the crater and exhibit an inflationary trend of same order of magnitude. Conversely, FSEL, CRSE, and TSBL, situated within 2 km of the crater, show a very small magnitude negative vertical signal for the same time period. FESP and CRSW represent an inconsistency in this trend and exhibit a small magnitude positive vertical signal during the same time period.

**Table 4. Station velocities and observed displacements.**

Station velocities and observed displacement from February 27 through June 29, 2009. Velocities north (n), east (e) and up (u) are relative to the fixed base-station SNJE and were determined using a weighted least-squares linear regression. Error was calculated by multiplying the weighted error by the number of days in the observation period.

Observed Station Velocities and total vertical displacement								error +/- mm	# of days/ obs.
Station	Vn mm/yr	Ve mm/yr	Vu mm/yr	$\sigma_n$	$\sigma_e$	$\sigma_v$	$\Delta v$ (mm)		
AGLA	-32	-10	291	15	24	49	99	16	124/5
CRSE	-37	19	8	19	26	62	-3	20	121/5
CRSW	-6	22	23	9	25	17	8	6	125/4
ESCL	10	45	99	39	52	55	34	19	124/5
FESP	-20	9	20	27	39	58	6	19	121/5
FSEL	-4	-7	-28	17	26	36	-9	12	124/5
LAKE	-12	10	466	20	52	109	139	29	97/4
LSPL	25	23	277	46	45	119	92	40	122/5
MLPA	-5	54	248	37	11	69	83	23	122/5
MTBL	-1	25	181	16	15	40	61	14	125/5
PDRF	-23	34	228	27	7	26	78	9	125/5
TSBL	-26	-26	-28	19	8	45	-9	15	124/5

A linear regression for the time period July through September shows that almost all stations exhibit a reverse in vertical direction after July (appendix E). Unfortunately, due to seasonal agriculture, which would increase the likelihood of multipath error, the following stations were not measured during these campaigns: MLPA in July and August, MTBL in July, LSPL in July and September. Therefore, we are forced to make assumptions about the observed deflationary velocities for MLPA and LSPL.

The slope of the regression line for the north and east components allowed us to determine the horizontal velocity vectors for the time periods coinciding with the inflation event. The horizontal vectors reveal outward movement of the stations inside the caldera. Stations LSPL and MLPA on the north and southeast side appear to moving northeast and southwest, while LAKE, PDRF and MTBL, located on the southwest side of the caldera, all show south easterly horizontal trend. The horizontal vectors at PDRF and MTBL do conform to the inferred right lateral faults seen in figure 1.

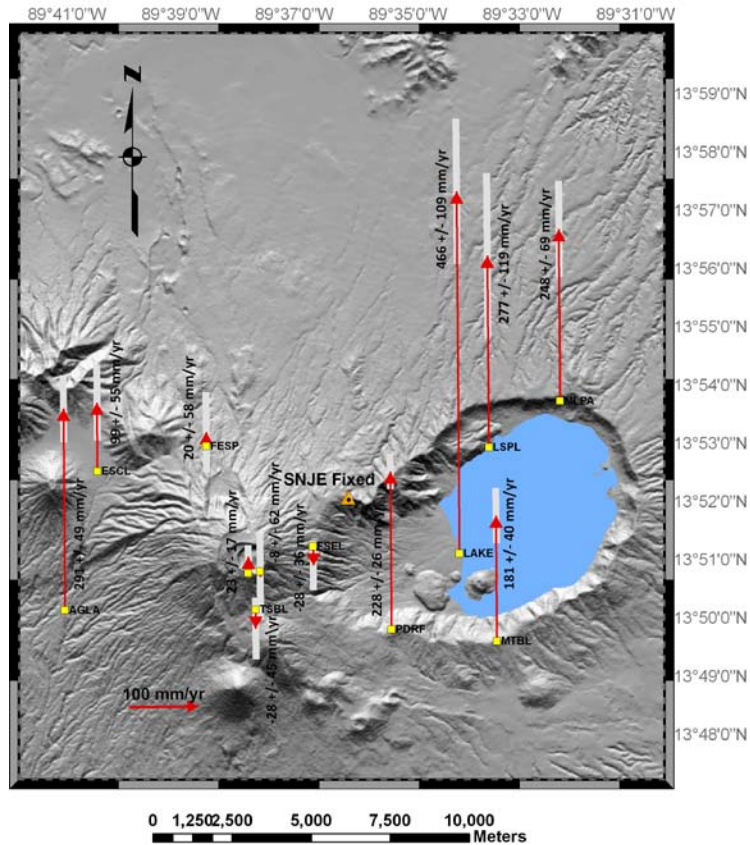


**Figure 10. Vertical velocities.**

Velocities for the GPS networks during the time period of February 27 through June 29, 2009 relative to SNJE. Error bars in grey represent 1- $\sigma$  error. Sites around the caldera showed a large inflationary trend during this time period.

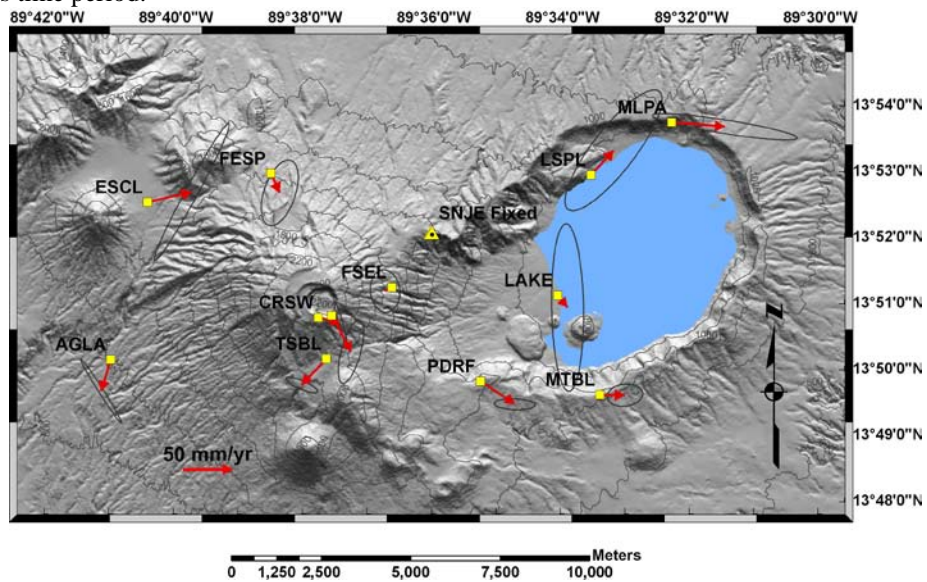


**Figure 11. Horizontal velocity vectors.**

Velocities for the time period of February 27 through June 29, 2009 relative to SNJE. Ellipses represent 1- $\sigma$  error.

## 4. DISCUSSION

Unrest at calderas is often a composite of multiple causes – tectonic, magmatic and hydrothermal - and they often exhibit subtle uplift and subsidence (Newhall and Dzurisin 1988). Another possible source of the observed deformation is the expansion of clay rich strata under the observed sites. There are likely some lacustrine deposits at lower elevations near the lake, however; we consider this an unlikely scenario, as very few expansive clays have been observed in the study area (D. Escobar, 2010 personal communication). Furthermore, site PDRF is located on a recent lava flow (most likely from the San Marcelino eruption in 1722) and would not likely demonstrate deformation due to soil expansion. Figure 1 shows station locations, the mapped and inferred regional tectonic features of that area, shallow micro-seismicity ( $>$  magnitude 3.0 and  $>$  15km depth) and figure 12 shows the daily RSAM averages for the study period. From the two figures we can see that very few seismic events occurred in or near the caldera, suggesting that the observed deformation is not likely tectonic.

The regional tectonic setting, of the Santa Ana complex is in an area of graben formation, or a pull-apart zone (Williams and Meyer-Abich 1955, Funk et al. 2009, Burkart and Self 1985, Stoiber and Carr 1973). It is not known with certainty if the faults identified in figure 1 are normal but it is a likely assumption. Pullinger (1998) suggests that the NW-SE trending volcanic features are the fissure eruptions which further imply a transtensional, or pull apart setting. This then presents the possibility that the base station SNJE experienced subsidence independent of, or relative to, the other stations in the network thereby producing an artificial inflationary signal. This scenario could explain the significant vertical signal seen at AGLA and to a lesser extent ESCL (figure 10). If we consider that the stations with considerable inflationary signal are situated either east (AGLA and ESCL) or west (caldera stations) of the cross-cutting fault zone and those stations with a small negative vertical signal (TSBL, CRSE, CRSW, FESP, FSEL) are found within the fault zone we can envision the movement relative to

SNJE that could produce our deformation signal. Of course, this also seems unlikely as we have demonstrated the stability of our base relative to ITRF2005 as well as the low frequency of seismic activity within the study area.

This leaves us with three alternative possibilities: seasonal barometric pressure changes, path delay induced error caused by the PWV or volcanic deformation. Rabbel and Zschau (1985) have shown that a relationship between surface deformation, +/- 5 mm in the vertical, and variations in atmospheric pressure exist. It may be possible that the floor of the caldera is more sensitive to atmospheric pressure changes and produces variable vertical velocities relative to sites outside the caldera. However, isolating this possibility to the caldera would not explain the deformation seen at AGLA and ESCL and especially PDRF. Also, the deflationary event begins before the middle of the rainy season, which is clearly linked to the highest rainfall and PWV and would likely correspond with the greater number of low pressure atmospheric perturbations. Furthermore the magnitudes of deformation related to atmospheric pressure do not correspond with the magnitude of observed deformation. The PWV could certainly be an influential factor on the degree of vertical signal actually measured in this study. Based on the bias estimates from Satirapod and Chalermawattanachai (2005), our sites with the greatest antenna height differences, could exhibit up to 45mm vertical signal error propagated by the wet zenith delay. However, as previously noted the vertical signal does not fully move in lock step with seasonal variability of the PWV and the deformation signal is up to an order of magnitude greater than the potential error. This leaves us with the likelihood of a volcanic signal.

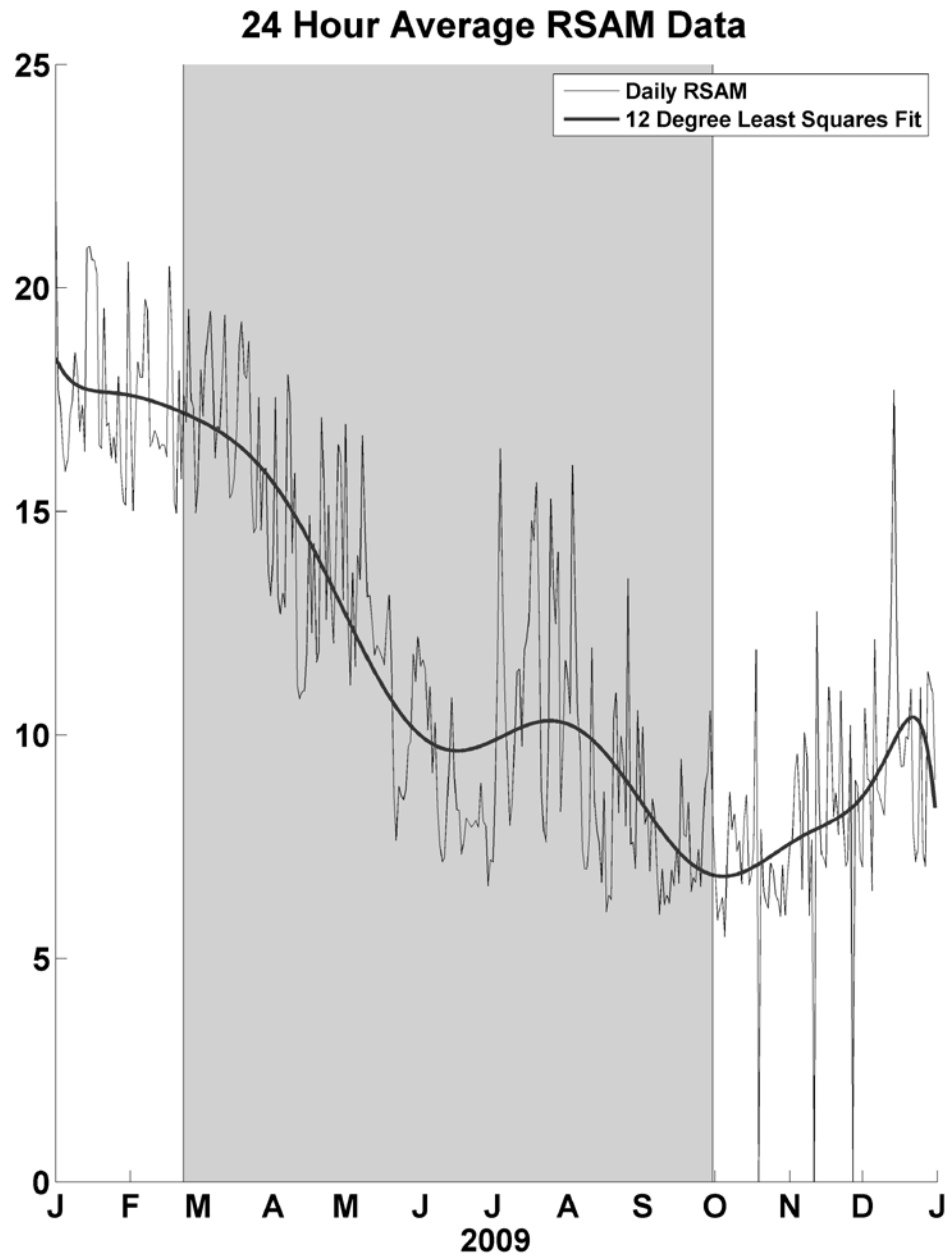


**Figure 12. Daily RSAM averages for 2009.**

The shaded area is the study period February 27 – September 29. Amplitude is on the y-axis, months of 2009 are on the x-axis. RSAM is the measured seismic amplitude from a seismometer located near station TSBL. Data provided by SNET.

Magma influx and volatile build up would almost certainly be accompanied by surface deformation (Van der Laat 1996, Dzurisin 2000) and it this type of behavior occurs at many calderas during non-eruptive phases (Newhall and Dzurisin, 1988). We know with almost absolute certainty that at one point there was a similarly sized magma body beneath the location of the Coatepeque Caldera. The existence of domes and cones within the caldera demonstrates that volcanic activity continued after the caldera forming event and the current hydrothermal activity in the southwest quadrant of the caldera confirms the presence of an existing heat source. A correlation between the hydrothermal vents and the vertical signal should not be ruled out. It has been shown that hydrothermal activity at Campi Flegri and at Yellowstone calderas is associated with ground surface deformation (Battaglia 2006, Hurwitz et al. 2007, Waite and Smith 2002). We also know that as recently as 1966 volcano Izalco was extruding lava, which clearly indicates an active magma body beneath that particular vent. Lastly, we know that in 2005 Santa Ana produced a phreatic or phreatomagmatic eruption. Colvin (in review) has outlined two eruption mechanism scenarios for the 2005 event at Santa Ana: 1) overpressure of the hydrothermal system caused by a crystallizing magma body, 2) overpressure caused by a magmatic intrusion. Olmos et al (2007) observed increased SO<sub>2</sub> emissions prior to the 2005 Santa Ana eruption, and believes it to be a combination of volatile accumulation at shallow levels and convective circulation within the magma conduit.

We cannot assume that a magmatic intrusion at Santa Ana volcano would have an influence on deformation at Coatepeque caldera unless we assume that there is a shared plumbing system or magma chamber. Carr and Pointier 1981 suggest there may be three separate magma bodies beneath the Santa Ana complex while Halsor and Rose (1988) postulate that closely spaced volcanoes can share a common parental magma chamber with separate plumbing systems and point to Izalco/Santa Ana as an example. Either stance would allow us to assume that a magma body currently exists beneath part or all of the SAVC and may or may not have influence on the behavior the caldera.



Obviously, a more time expansive data set is required to further investigate the true nature of this deformation. By increasing the frequency of observations and thus increasing the number of observations we could eliminate noise and glean clearer picture of the true signal. However, it seems evident that this type of GPS survey can be effectively used to measure large deformation (greater than 35mm vertical) on volcanoes with short occupation times on sub-10km baselines. This type of study is also an important tool to the monitoring and characterization efforts of quiescent or dormant composite volcanoes but should require monthly or bi-monthly measurements.

## 5. FUTURE WORK

The current study discusses the use of differential GPS as monitoring tool on Volcano Santa Ana and the Coatepeque Caldera. However, the short term of this study and the small number of observations has not permitted us to fully realize the potential of our GPS network. The following are suggestions to future students and scientists who are willing and able to reoccupy our differential sites and use the GPS observations to gain greater insight into the behavior of the Santa Ana Volcanic Complex.

1. Correlate lake level measurements with observed deformation. A study of vertical deformation around Lake Coatepeque correlated with lake level monitoring could provide insight into the nature of the deformation within the caldera. Is there differential uplift from one side to the other and how is the shore line affected?
2. Correlate deformation observations with hydrothermal and gas fluctuations. This would require frequent and long term GPS monitoring as well as DOAS, COSPEC or remote sensing techniques that capture gas flux. We could investigate whether increases in gas flux produce measureable deformation at sites on the volcano.
3. Three dimensional forward modeling such as Mogi. Deformation modeling provides a unique insight into the character of the source of deformation and is an excellent compliment to any GPS or deformation study.
4. Install a second continuous GPS station on the western flanks of the volcano. A strategically located CGPS station would not only improve our monitoring efforts on the volcano by reducing many baseline lengths but could also prove useful in monitoring the regional tectonics as well as tectonic plate movements.

## 6. CONCLUSIONS

During the course of this investigation we have established the achievable accuracy of differential GPS as a function of baseline distance, determined a repeatable level of accuracy as a function of observation time, developed an appropriate data processing and reduction strategy and identified a major source of error. Furthermore, we believe that we have captured a significant inflationary signal at sites around the Coatepeque Caldera.

Repeated differential GPS surveys at the Santa Ana Volcanic Complex from September 2008 to September 2009 reveal horizontal accuracy of roughly 10mm at a 10km and 5mm at baseline lengths under 2km. The achievable vertical accuracy is 30-35mm at 10km and 12-13mm under 2km. A likely cause of error is the decorrelation of the tropospheric delay over baseline distance caused by PWV. Based on these accuracies, an inflationary and deflationary trend was observed at sites within the Coatepeque Caldera from February through September 2009. This type of deformation is not uncommon at calderas and could indicate an accumulation of volatiles and magma convection at depth or gas-rich hydrothermal-fluid over-pressurization. Regional tectonics may also be responsible for the vertical signal and may indicate subsidence of the reference station relative to the differential stations. A strategically placed second reference station on the western side of the volcano would reduce most baseline distances to under 5km and almost guarantee sub-centimeter accuracy as well as reduce the ambiguity related to the regional tectonics. A more time expansive data set would be useful to determine the nature of the deformation, whether or not it is cyclical, and potentially to infer if it is an artifact of atmospheric noise, volcanic activity, or tectonically induced.

This type of GPS network can serve as an effective tool at sub-tropical volcanoes to monitor inter-eruptive activity. It may not be entirely suitable during a volcanic crisis due to the risk of operator's presence for equipment installation and management, but it can provide an inexpensive and accurate means to augment monitoring efforts for agencies and researchers with limited financial resources. The data obtained from GPS observations could be correlated with other data and modeled (e. g. with Mogi deformation model) to infer some characteristics of the source causing the deformation. As GPS equipment continues to become less expensive and data reduction methods improve it is likely that more and more volcanoes will be observed using these or similar techniques.

## 7. REFERENCE LIST

- Alvarado D, DeMets C, Tikoff B, Hernandez D, Wawrzyniec TF, Pullinger C, Mattioli G, Turner HL, Rodriguez M, Correa-Mora F. 2010. Forearc motion and deformation between El Salvador and Nicaragua: GPS, seismic, structural, and paleomagnetic observations. In press: *Lithosphere*.
- Battaglia M. 2006. Evidence for fluid migration as the source of deformation at Campi Flegrei caldera (Italy). *Geo Physical Research Letters*. 33 L01307
- Burkart B, Self S. 1985. Extension and rotation of crustal blocks in northern Central America and effect on the volcanic arc. *Geology*. 13:22-26.
- Carr MJ, Pointier NK. 1981. Evolution of a young parasitic cone towards a mature central vent; Izalco and Santa Ana volcanoes in El Salvador, Central America. *Journal of Volcanology and Geothermal Research*. 11(2-4): 277-292.
- Carr MJ, Feigenson MD, Patino LC, Walker JA. 2003. Volcanism and geochemistry in Central America: progress and problems. In: Eiler J. *Inside the Subduction Factory*. American Geophysical Union Monograph. 138:153-174.
- Carr MJ, Stoiber MD. 1972. Geologic setting of some destructive earthquakes in Central America. *Geological Society of America Bulletin*. 88(1): 151-156.
- Collins PJ, Langley RB. 1997. Estimating the Residual Tropospheric Delay for Airborne Differential GPS Positioning. In: *Proceedings of the 10<sup>th</sup> International Technical Meeting of the Satellite Division of the Institute of Navigation*. Kansas City, Missouri. p. 1197-1206.
- Colvin A, Escobar D, Gutierrez E, Montalvo F, Rose WI, Bowman L. 2010. The phreatomagmatic eruption of Santa Ana Volcano (El Salvador) in 2005: History and consequences. *Bulletin of Volcanology*. In review.

- Cove KM, Santos M, Wells D, Bisnath S. 2004. Improved Tropospheric Delay Estimation for Long Baseline, Carrier-Phase Differential GPS Positioning in a coastal Environment. In: Proceedings of ION GNSS 2004. Long Beach, CA. p. 925-932.
- DeMets C. 2001. A new estimate for present-day Cocos-Caribbean plate motion: Implications for slip along the Central American volcanic arc. *Geophysical Research Letters*. 28:4043-4046.
- Dodson AH, Shardlow PJ, Hubbard LCM, Elgered G, Jarlemark POJ. 1996. Wet tropospheric effects on precise relative GPS height determination. *Journal of Geodesy*. 70:188-202.
- Dzurisin D. 2000. Volcano geodesy: challenges and opportunities for the 21<sup>st</sup> century. *Philosophical Transactions of the Royal Society* . (358):1547-1566.
- Funk J, Mann P, McIntosh K, Stephens J. 2009. Cenozoic tectonics of the Nicaraguan depression, Nicaragua, and Median Trough, El Salvador, based on seismic-reflection profiling and remote-sensing data. *Geologic Society of America Bulletin*. 121(11-12):1491-1521.
- Halsor SP, Rose WI. 1988. Common characteristics of paired volcanoes in northern Central America. *Journal of Geophysical Research*. 93(B5): 4467-4476
- Hoffman-Wellenhof B, Lichtenegger H, Collins J. 2001. *Global Positioning System Theory and Practice*. 5<sup>th</sup> ed. New York, NY. Springer-Verlag/Wien.
- Hurwitz S, Christiansen LB, Hsieh P. 2007. Hydrothermal fluid flow and deformation in large calderas: Inferences from numerical simulations. *Journal of Geophysical Research*. 112 B02206
- Lawrence D, Langley RB, Kim D, Chan FC, Pervan B. 2006. Decorrelation of Troposphere Across Short Baselines. *IEEE/ION PLANS*. San Diego, California, U.S.A.

- Mendes VB, Langley RB. 1998. Tropospheric Zenith Delay Prediction Accuracy for Airborne GPS High-Precision Positioning. In: Proceedings of 54th Annual Meeting of the ION. p. 337-347.
- Newhall CG, Dzurisin D. 1988. Historical unrest at large calderas of the world. U.S. Geological Survey. Professional paper 1855
- Olmos R, Barrancos J, Rivera C, Barahona F, Lopez DL, Henriquez B, Hernandez A, Benitez E, Hernandez PA, Nemesio PM, Galle B. 2007. Anomalous emissions of SO<sub>2</sub> during the recent eruption of Santa Ana Volcano, El Salvador, Central America. *Pure and Applied Geophysics*. 164:2489-2506.
- Rabbel W, Zschau J. 1985. Static deformations and gravity changes at the earth's surface due to atmospheric loading. *Journal of Geophysics*. 56:81-89
- Rose WI, Stoiber RE. 1969. The 1966 eruption of Izalco, El Salvador. *Journal of Geophysical Research*. 74(12):3119-3130.
- Rose WI, Conway FM, Pullinger CR, Deino A, McIntosh WC. 1999. An improved age framework for late Quaternary silicic eruptions in northern Central America. *Bulletin of Volcanology*. 61:106-120.
- Pullinger C. 1998. Evolution of the Santa Ana Volcanic Complex, El Salvador; [MS Thesis], Houghton, Michigan Technological University, 151p.
- Satirapod C, Chalermawattanachai P. 2005. Impact of different tropospheric models on GPS baseline accuracy: case study in Thailand. *Journal of Global Positioning Systems*. 4(1-2):36-40.
- Scolamacchia T, Pullinger C, Caballero L, Montalvo F, Orosco LEB, Hernandez GC. 2010. The 2005 eruption of Ilamatepec (Santa Ana) volcano, El Salvador. *Journal of Volcanology and Geothermal Research*. 189:291-318.

Stoiber RE, Carr MJ. 1973. Quaternary volcanic and tectonic segmentation of Central America. *Bulletin of Volcanology*.37(3):304-325.

Van der Laat R. 1996. Ground-Deformation Methods and Results. In: Scarpa R, Tilling RI. *Monitoring and Mitigation of Volcano Hazards*.1<sup>st</sup> ed. Berlin, Germany: Springer-Verlag Berlin Heidelberg. P. 147-168.

Waite GP, Smith RB. 2002. Seismic evidence for fluid migration accompanying subsidence of the Yellowstone caldera. *Journal of Geophysical Research*. 107(B9):2177.

Weber HS, Wieseemann G. 1977. *Geologic Map of the Republic of El Salvador/Central America*. Hannover, Germany. Bundesanstalt für Geowissenschaften und Rohstoffe.

Williams H, Meyer-Abich H. 1955. Volcanism in the Southern Part of El Salvador with Particular Reference to the Collapse Basins of Lakes Coatepeque and Ilopango. *Geological Sciences*. 32:1-64



## **APPENDIX A: NETWORK DEVELOPMENT**

During 2008 we reconnoitered and installed 14 GPS benchmarks on and around the SAVC. Two of these sites were later abandon due to poor accessibility or poor sky view. The criteria for site selection were:

1. On the volcano close to the crater
2. Circumferentially at various levels
3. Span the fault zone
4. Cover the caldera
5. Clear sky view in 360°.
6. Elevation angle ~ 15°
7. Multi path free: absence of trees, bushes, fences or other obstacles
8. Solid ground or foundation with little obvious susceptibility to deformation caused by soil compaction, creep or erosion.
9. Accessibility and permission.

Using a hammer-drill, we drilled holes into the solid rock, rock walls or concrete slab and installed a custom-made steel pin and fixed it in place using epoxy anchor. The pins are roughly 16 x 1cm and have a 0.5mm dimple or pin hole on the top. Installing these pins flush with the host material is advantageous because they remain relatively discreet and unobtrusive which helps prevent them from becoming a target for theft or vandalism.



Drilling into rock. Using a hammer drill we perforate rock to install our benchmarks pins. Photo by author.



Anchoring the benchmark. Using Hilti epoxy we anchored the benchmark in the rock. Setting the pin flush with the surface discourages theft and vandalism. Photo by author.

## **APPENDIX B: FIELD MEASUREMENTS**

Campaigns style measurements took place once a month, usually during the last week of each month, from February 27 through September 28, 2009. Campaigns usually lasted several days due to the remote setting of some sites and logistical issues in reaching them. The climb up the volcano and occupation of the sites at the crater was always done with the accompaniment of colleagues from SNET. We would then return to San Salvador to rent a 4x4 truck to access the remaining 10 sites. Below is a typical campaign schedule:

- Day 1. CRSE and CRSW. These are the two sites located at the crater of Santa Ana.
- Day 2. FESP, ESCL and AGLA. These are the sites on the far side (north and east slopes) of Santa Ana and required several hours of travel time to reach. If weather and time permitted we would occupy MTBL and PDRF on this same day.
- Day 3. MLPA, LSPL, LAKE, FSEL, TSBL.
- Day 4 (if needed). MTBL and TSBL.

Initially we occupied all sites for 1-hour only. Starting in July we began to occupy sites FESP, ESCL, and AGLA for two hours. As AGLA and ESCL have baseline distance greater than 5km we knew that we should occupy them for longer duration. This should have also been the case with MLPA and MTBL, unfortunately, due to a logistical miscalculation the latter two sites were never measured for more than an hour.

For all but one differential occupation we employed the Trimble 5700 dual frequency receiver with a Zephyr Geodetic Choke Ring antenna. The exception occurred on April 30, 2009 when the two sites CRSE and CRSW were measured using a Trimble R7 dual frequency receiver. Data was always gathered at 30-second sample rate. The receiver was powered with either an internal battery or a 12v car battery depending on site accessibility.

We employed a fixed elevation spike-mount tripod. From point to bottom of antenna mount measured exactly 55cm. The tripod was designed so that precise leveling techniques could be employed. The tripod pin was placed into the pin-hole at each benchmark and then leveled to millimeter accuracy. These methods ensured that the antenna was placed in the exact same position during each campaign and reduced setup error to almost zero.



Tripod setup. A fixed elevation tripod with precise leveling can be assembled and by one person and practically eliminates setup error. Photo by author.

## **APPENDIX C: BASELINE PROCESSING**

For this survey we initially tried processing baselines using Trimble GPSurvey. We eventually switched to Trimble Geomatics Office (TGO) as it was more user-friendly and provided more processing options. Both baseline processing programs perform the interferometric differencing operations needed to solve the integer ambiguities, perform network adjustments and display baseline vectors and accuracy statistics. Both software packages also contained the Weighted Ambiguity Vector Estimator (WAVE) function.

### **C.1. Project Setup**

The following section describes the methodology used in this study for baseline processing with TGO.

1. Download raw data from the receiver to a desktop computer.
2. Convert data into a Receiver Independent Exchange format (RINEX).
3. Identify and name each data file based on its site identification code (e.g. FSEL)
4. Store each data file in a folder for that month's campaign.
5. Using TGO, develop a project template to maintain consistency with all baselines.
6. Create a new project for each station.
7. Download precise orbits (ephemerides) for the dates of observation.
8. Transfer all RINEX data, .dat-files and precise ephemerides into each projects individual "check-in" folder.
9. Open project and import base-station data followed by rover data (\*.obs, \*.met files) for all observations at each independent station. During importation ensure that all files have the proper name, antenna height and measurement criteria. For this project the four letter station code was input as name. Import settings were as follows:

Data import settings in TGO

<b>Name</b>	<b>Receiver</b>	<b>Antenna height</b>	<b>Measured to</b>
BASE	NetRS	0.00mm	Bottom of antenna mount
ROVER	5700	0.00mm	Bottom of antenna mount

10. Import precise ephemeris data \*.SP3 format.

11. Set processing style (we changed the following settings to force an L3 solution):

- a. elevation mask: 15°
- b. solution type: Fixed
- c. Global: frequency type - L2
- d. Iono:
  1. Ambiguity resolution pass – 10km
  2. Final pass – 0km

12. Process baselines

13. Fix base station with precise coordinates in WGS84

14. Perform network adjustment

15. Review baselines.

16. Make changes and reprocess questionable baselines.

Raw GPS data, which was taken from the receivers, was first converted into a Receiver Independent Exchange (RINEX) format. The raw data from the Trimble 5700 and the

NetRS was downloaded in \*.T00 binary format. Data was downloaded and converted after each campaign.

For this project we used the Metric template with default systems zones and WGS 1984 datum. When each station had a project file I placed all the \*.obs, \*.nav, \*.met, and \*.dat data from each campaign for that station into the “Check In” folder, which is found on under the TGO program files, sub-folder “projects.” The IGS precise ephemerides in \*.sp3 format for every day of each month’s campaign plus one day before and after the campaign’s start and finish dates began were imported to ensure that any overlap would be covered. Precise ephemerides are usually published within two weeks after the date.

Review all processed baselines for quality. A baseline will be identified by TGO as acceptable, flagged but acceptable, or unacceptable. TGO determines acceptable baseline solutions based on the quality control settings within the advanced settings of processing styles. For this study we used TGO’s default settings for dual frequency processing.

TGO baseline criteria.

These are the default settings in TGO for passing, flagging or failing a baseline solution.

Acceptance Criteria	Single Frequency		Dual Frequency	
	Flag	Fail	Flag	Fail
If RMS >	0.03	0.04	0.02	0.03
If Ratio <	3	1.5	3	1.5
If Reference Variance >	10	20	5	10

After running the WAVE baseline processor the baseline solution, or vector, is produced after differencing the carrier phase observations to solve the integer ambiguity. To force an “iono-free fixed” solution we changed the “Global” tab to L2 and in the “Iono” tab “Ambiguity resolution pass” is set to 10 km and “Final pass” is set to 0km. By applying these settings we are forcing a linear combination of the L1 and L2 frequencies that will eliminate the ionospheric delay and produce a fixed-integer baseline solution.

a. RMS is the quality factor that is used to determine which solution to use in a network adjustment. It is dependent on observation time and baseline length and is a measure (units of cycles or meters) of the data quality. A high RMS value is a good indicator of signal interference from the ionosphere, troposphere, multipath error, or other EMF interference.

b. Ratio or variance ratio, when acceptable, indicates that the ambiguities have been successfully resolved. It is the ratio of the lowest integer ambiguity solution to the next best solution.

c. Reference variance indicates the quality of the program's computed error compared with the estimated (apriori) error for a baseline. High values in reference variance indicate that the baseline data is below average.

## **C.2. L1 vs. Iono-Free Fixed**

An Ionospheric free fixed solutions, "iono-free" are produced using dual frequency, L1/L2 linear combination and can eliminate signal delay caused by the ionosphere. Fixed solutions indicate that the integer ambiguity has been solved sufficiently. While it is recommended to use L1-fixed solutions on baselines shorter than 50km as the iono-free solution may not cancel the error between stations through single differencing; we found that our baselines longer than 5km were producing "float" solutions in the L1 frequency. We therefore, set TGO to force an iono-free fixed solution for all baselines and compared the results to the L1-float solutions.

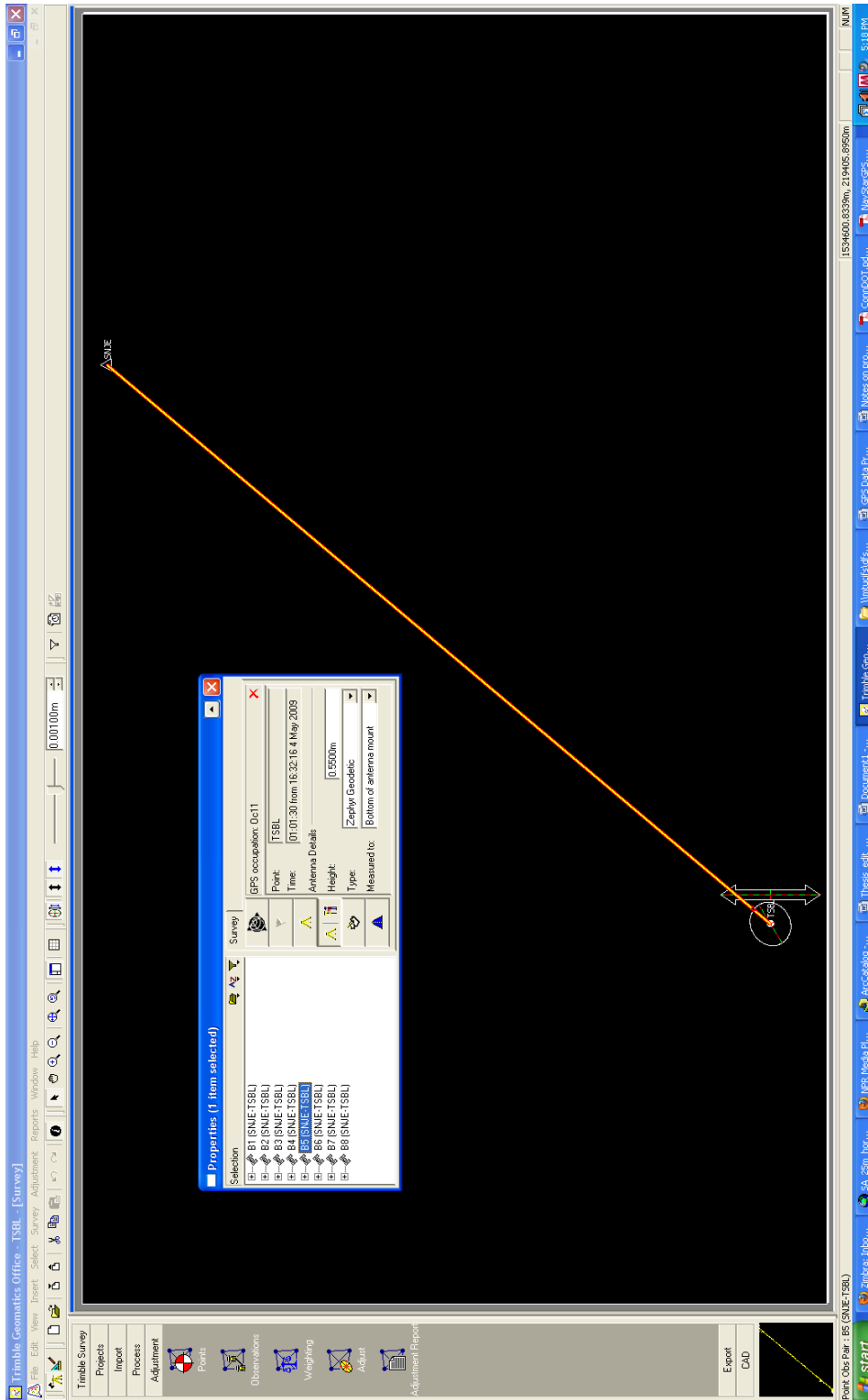


While the standard deviations for the L1-fixed solutions were generally better than those of the Iono-free fixed solutions, we discovered that the L3, linear combination produced more acceptable baselines whereas, L1 produced more flagged or failed baselines.

Each data file was identified and renamed with its unique station ID during download and conversion. The data was saved in a folder for that month's campaign. In TGO a project template was created that set the units and decimal places outputs as well as the coordinate system and datum.

Iono-free fixed versus L1.  
 This table shows the weighted standard deviations of the baseline solutions from all occupations from FSEL and AGLA.

<b>Station FSEL 1.8km baseline</b>		
<b>Iono Free Fixed</b>		
<b>North mm</b>	<b>East mm</b>	<b>Vertical mm</b>
3.260690929	2.564616416	7.571244635
<b>L1 Fixed</b>		
<b>North mm</b>	<b>East mm</b>	<b>Vertical mm</b>
2.971473542	1.33878136	4.2886436
<b>Station AGLA 9.7km baseline</b>		
<b>Iono Free Fixed</b>		
<b>North mm</b>	<b>East mm</b>	<b>Vertical mm</b>
3.831989206	4.304958735	39.597684
<b>L1 Fixed</b>		
<b>North mm</b>	<b>East mm</b>	<b>Vertical mm</b>
3.340486281	4.678766453	34.9417666



Processed baseline in TGO. The line represents the series of baselines from base-station SNJE to rover TSBL. A yellow line indicates that all baseline solutions were unacceptable. Had there been an unacceptable solution the line would be red and include a flag icon. In the upper left of the image is the baseline properties window.

# Baseline Processing Report

Project : *TSBL*

User name	hnlechne	Date & Time	9:35:51 AM 11/3/2010
Coordinate System	UTM	Zone	16 North
Project Datum	WGS 1984	Geoid Model	EGM96 (Global)
Vertical Datum			
Coordinate Units	Meters		
Distance Units	Meters		
Height Units	Meters		

## Processing Summary

ID	From	To	Baseline Length	Solution Type	Ratio	Reference Variance	RMS
<a href="#">B1</a>	SNJE	TSBL	4591.0009m	iono free fixed	10.5	1.215	0.012m
<a href="#">B2</a>	SNJE	TSBL	4591.0087m	iono free fixed	115.9	1.274	0.010m
<a href="#">B3</a>	SNJE	TSBL	4590.9954m	iono free fixed	70.5	1.095	0.014m
<a href="#">B4</a>	SNJE	TSBL	4591.0000m	iono free fixed	94.4	1.211	0.010m
<a href="#">B5</a>	SNJE	TSBL	4591.0085m	iono free fixed	3.2	1.895	0.015m
<a href="#">B6</a>	SNJE	TSBL	4591.0041m	iono free fixed	105.4	1.091	0.011m
<a href="#">B7</a>	SNJE	TSBL	4591.0076m	iono free fixed	16.2	2.436	0.020m
<a href="#">B8</a>	SNJE	TSBL	4591.0078m	iono free fixed	46.8	2.427	0.017m

Baseline processing report from Trimble Geomatics Office 1.6. This is the report from the baselines for station TSBL. It displays the basic information for each occupation in HTML format. The baseline IDs are hyperlinks for information on individual occupations.

Baseline report - Windows Internet Explorer

File Edit View Favorites Tools Help

X Convert Select

Baseline report

Hi:\Desktop\projects\_1\01\TSBL\Reports\Baseline\Frametbl.html

Live Search

9:43 AM

### Baseline Components (Mark to Mark)

From:	SNJE	Local	WGS 84
Grid			
Northing	1534685.0479m	13°52'05.68930"N	13°52'05.68930"N
Easting	218903.9564m	89°36'02.49129"W	89°36'02.49129"W
Elevation	1659.0236m	1660.1910m	1660.1910m

To:	TSBL	Local	WGS 84
Grid			
Northing	1531174.1933m	13°50'10.47539"N	13°50'10.47539"N
Easting	215950.9501m	89°37'39.49047"W	89°37'39.49047"W
Elevation	1868.9929m	1869.9222m	1869.9222m

Baseline:			
$\Delta$ Northing	-3510.8546m	NS Fwd Azimuth	219°26'40"
$\Delta$ Easting	-2953.0063m	Ell. Distance	4584.9346m
$\Delta$ Elevation	209.9693m	$\Delta$ Height	209.7312m
		$\Delta$ X	-2906.3997m
		$\Delta$ Y	-1071.2080m
		$\Delta$ Z	-3388.6050m

### Standard Errors

Baseline Errors:			
$\sigma$ $\Delta$ Northing	0.0008m	$\sigma$ NS Fwd Azimuth	0.045 seconds
$\sigma$ $\Delta$ Easting	0.0011m	$\sigma$ Ell.Distance	0.0009m
$\sigma$ $\Delta$ Elevation	0.0029m	$\sigma$ $\Delta$ Height	0.0029m
		$\sigma$ $\Delta$ X	0.0011m
		$\sigma$ $\Delta$ Y	0.0029m
		$\sigma$ $\Delta$ Z	0.0010m

[Back to Processing Summary](#)  
[Baseline Summary](#)  
[Baseline Components](#)  

- Standard Errors
- Covariance Matrix

[Occupations](#)  
[Tracking Summary](#)  
[Residuals](#)  
[Processing Style](#)  

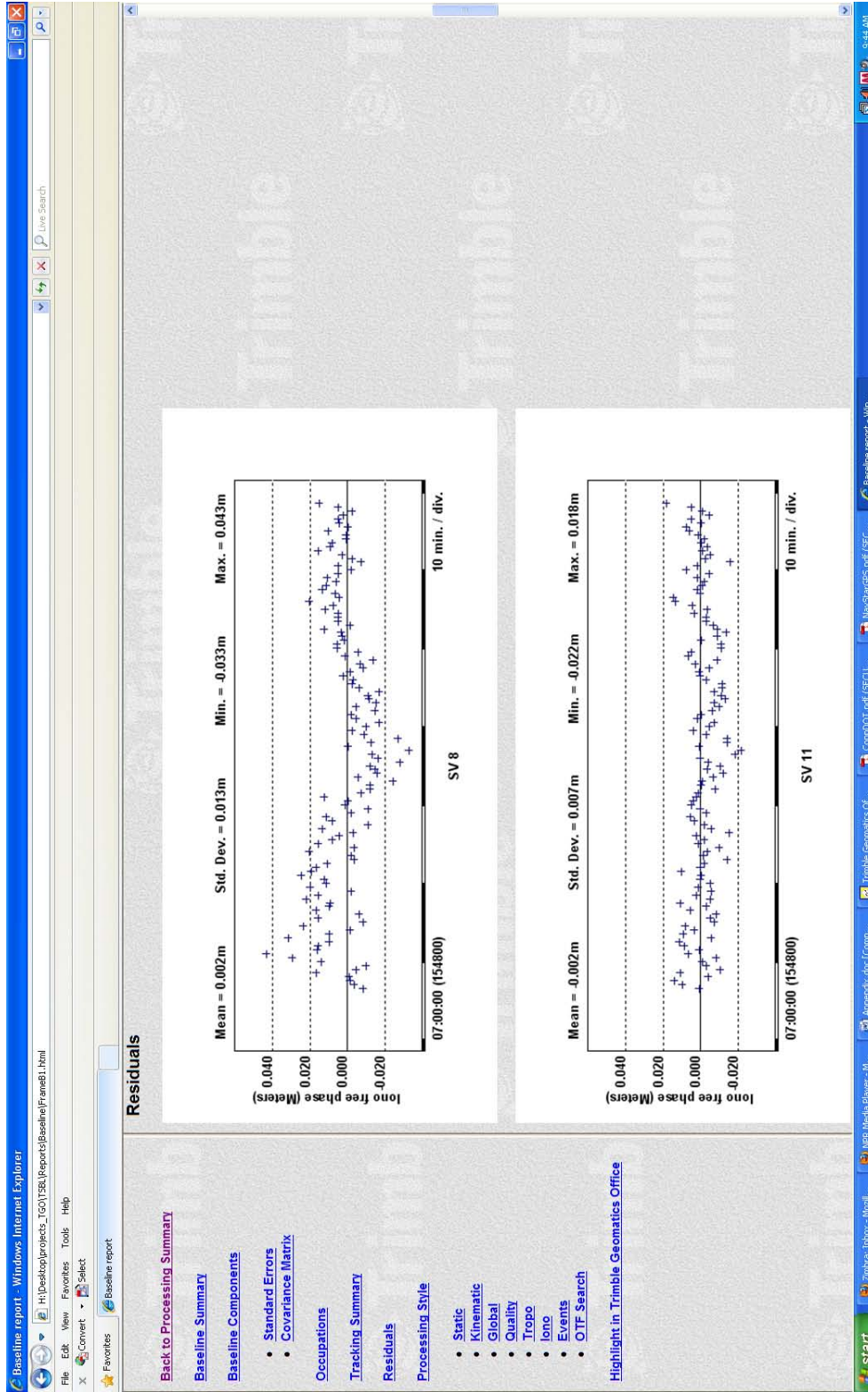
- Static
- Kinematic
- Global
- Quality
- Tropo
- Iono
- Events
- OTF
- Search

[Highlight in Trimble Camtasia](#)

[Z:\lib\stflbor\Proc...](#)  
[Hert NewsPlayer - Pl...](#)  
[Agenda.doc \[Comp...](#)  
[Trimble Geomatics of...](#)  
[Control.pdf \[SECU...](#)  
[No charges.pdf \[SEC...](#)  
[Baseline report - Win...](#)

Baseline summary from Trimble Geomatics Office for an individual occupation. This is the report from the baselines for station TSBL. This displays the directional components that were used in further statistical reduction.  $\Delta$ Northing  $\Delta$ Easting and  $\Delta$ Elevation are the positional differences between the base station.  $\sigma$  $\Delta$ Northing  $\sigma$  $\Delta$ Easting  $\sigma$  $\Delta$ Elevation are the standard errors produced by processing software.





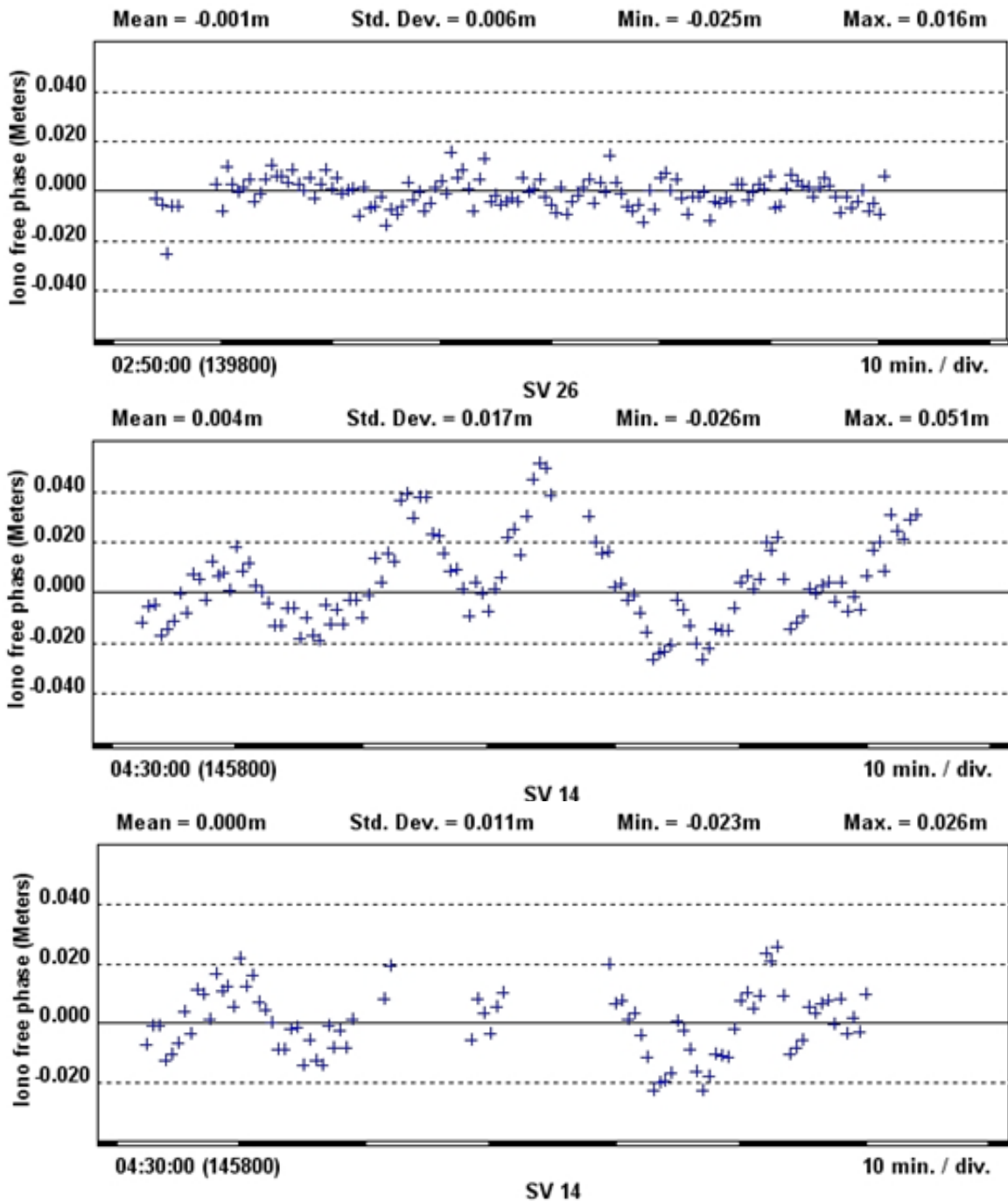
Satellite residuals. These are the plots of residuals for two satellites. 0.02 meters was our level of acceptable variance. When If the signal showed large time spans outside of this range efforts were made to disable that portion of the satellite.

### **C.3. Baseline Solution Improvements**

During the processing of the baselines in this study we employed two primary techniques to improve baseline solutions and remove flags. The majority of baseline solutions were improved to the point of acceptability. If we were unsuccessful at removing the flags the baselines were noted but not removed. While we did not encounter any failed baselines solutions in the Iono-free fixed that we were unable to resolve there were several in the L1 solution. However, as we did not use the L1 solutions for further statistical reduction those baselines were noted but not removed.

The first technique was the most simple and often improved baselines with unacceptable ratio or reference variance. When we encountered a poor, or flagged baseline solution due to ratio or variance our first step was to change the elevation mask from  $15^\circ$  to  $17^\circ$  and then reprocess the baseline. Often times that simple strategy would resolve most baseline solutions. If improvements were made but still not acceptable, we would change the elevation again to  $20^\circ$  and reprocess. We did not attempt to increase the elevation mask beyond  $20^\circ$ .

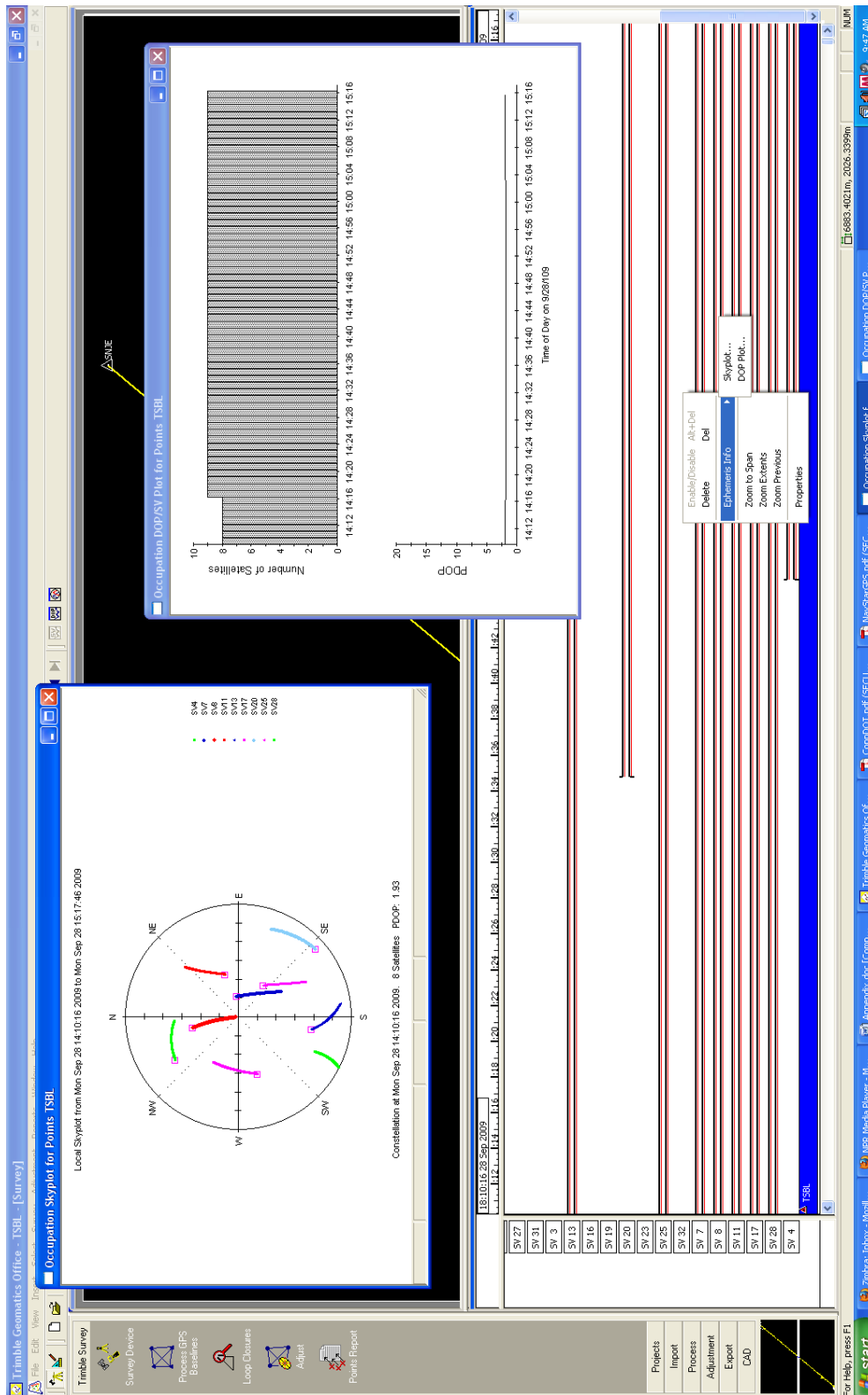
The second technique is more time consuming and complicated. An evaluation of the satellite residual plots, which are found on the baseline processing reports, show data quality of individual satellite signals. Satellites that have been chose by the processor for double differencing do not show residual plots in the baseline processing report. If there are gaps in the residual plot that indicates that the satellite was used for double differencing during that time period. Variance about the x-axis is an indication of noise for that particular satellite. For this study we chose 0.02 meters variance as a cutoff.



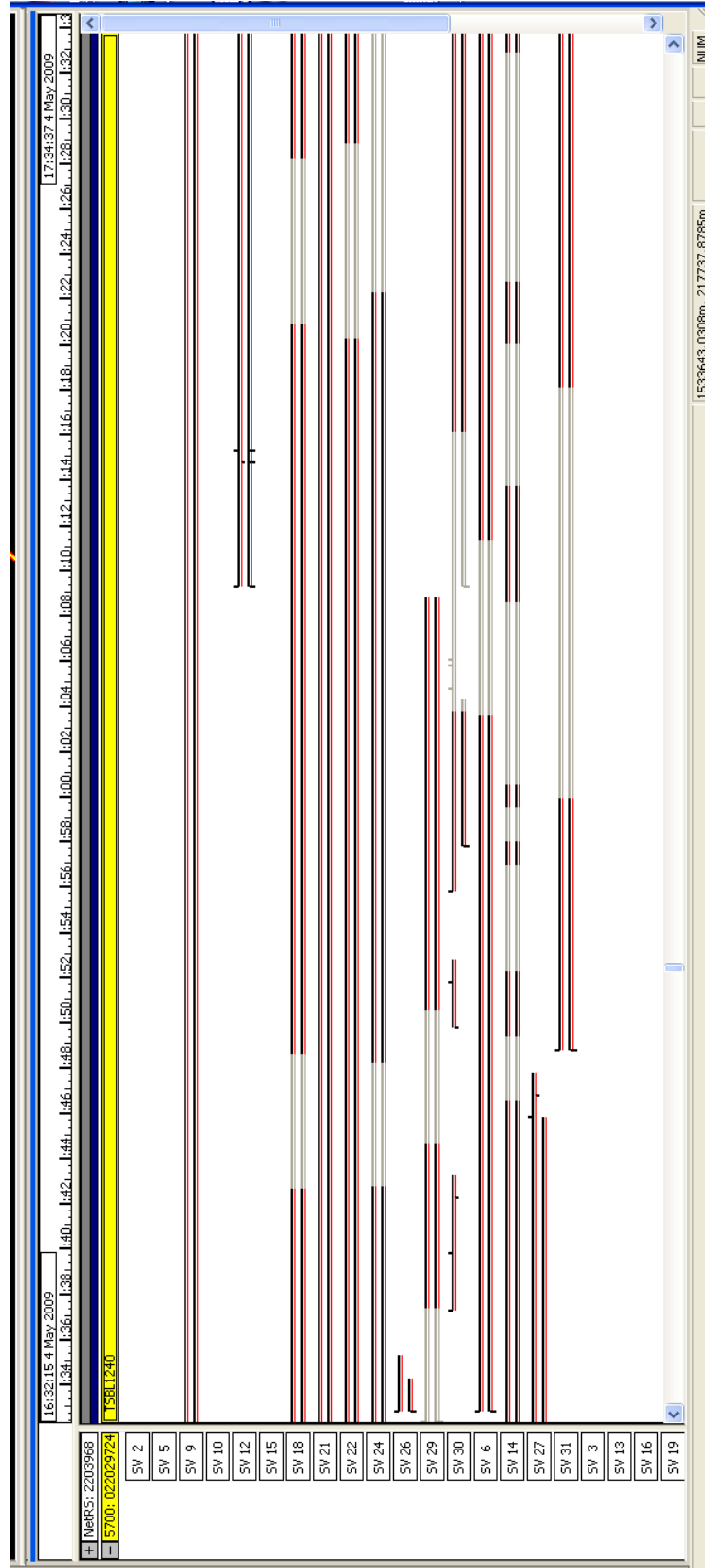
SV is the satellite vehicle. Black and white bars along the x-axis indicate time increments (10 minutes in this example). The number at the bottom left indicates the nearest to the start of observation. The residual plot on the top represents an almost ideal plot of the received satellite signal. The plot in the middle exhibits an SV that doesn't meet our acceptance criteria of 0.02 meters. The bottom plot shows the same satellite as after removing the majority of high residuals.



By examining the satellite residual plots we were able to determine the time when the variance of a particular satellite was beyond our established cutoff. From here we would return to the TGO project window and, using the timeline function, remove those sections of satellite signal that had unacceptable residuals. Occasionally, the entire time series for a particular satellite was outside our acceptance criteria, in which case we would disable the entire satellite. After this we would reprocess the one particular baseline that was problematic. We would repeat this process until we achieved an acceptable baseline solution. Occasionally as we approached an acceptable solution; we reached a certain threshold where any changes only made the solution's quality deteriorate. In this case we would go back to our last best solution and save that baseline. If a flag still remained it was noted but not removed.



Time line and sky plot. In the projects window of TGO we utilized the timeline function to eliminate sections of satellites that displayed poor signal quality. In the top left is the sky plot that displays the satellite geometry and PDOP during the observation. On the right is a variance of skyplot that shows the number of satellites in histogram.



Time line for an individual baseline. Here we utilized the timeline function to disable certain sections of satellites that displayed poor signal quality. The time can be determined by using the residual plot.

## APPENDIX D: STATISTICAL REDUCTION

After baseline processing was complete we took the 3-dimensional differential distances – north, east and vertical (NEV) – and the standard NEV error as well as the RMS, reference variance, ratio, and start and stop time from the baseline summaries produced by TGO. This data was put into an excel spread sheet in order to further reduce the positional error. Here we determined the weighted mean using

$$\bar{X} = \frac{\sum_{i=1}^n (X_i / \sigma_i^2)}{\sum_{i=1}^n (1 / \sigma_i^2)}$$

We then found the weighted standard deviation using

$$s = \left( \frac{1}{n-1} \sum_{i=1}^n (X_i - \bar{X})^2 \right)^{\frac{1}{2}}.$$

We then used built in MATLAB tools to determine a least squares linear regression for each directional component. The slope of this line was used as the velocity vector.

# Appendix D.1. Excel Statistics

## PDRF

		Baseline #		iono Free Fixed		dNorth #		dEast #		dVert #		Standard Error (m)	
segment	Solution type	Baseline Decimal	Baseline s/fo	Ratio	Ref. Variance RMS	d north	d east	d vertical	North	East	Vertical	start time	stop time
PDRF052	iono Free Fixed	0.5986	4408.5986	57	1.144	0.011	-4177.8766	1353.9132	0.0008	0.0008	0.0021	2/24/09 15:32	2/24/09 16:34
PDRF0811	iono Free Fixed	0.6064	4408.6064	51	0.973	0.012	-4177.8854	1353.9137	0.0009	0.0007	0.0018	3/22/09 16:31	3/22/09 17:32
PDRF1235	iono Free Fixed	0.6083	4408.6083	59.7	1.38	0.012	-4177.8893	1353.917	0.0009	0.0009	0.0037	5/3/09 22:53	5/3/09 23:58
PDRF1504	iono Free Fixed	0.5933	4408.5933	32.3	1.127	0.012	-4177.8749	1353.92	0.0009	0.0009	0.002	5/30/09 23:03	5/30/09 23:59
PDRF1801	iono Free Fixed	0.6108	4408.6108	20.4	0.923	0.011	-4177.8915	1353.9266	0.0009	0.0012	0.0025	6/29/09 15:42	6/29/09 16:43
PDRF2065	iono Free Fixed	0.615	4408.615	100.4	1.043	0.009	-4177.8954	1353.9249	0.0008	0.0009	0.0028	7/25/09 22:00	7/25/09 23:01
PDRF2441	iono Free Fixed	0.6088	4408.6088	85.8	0.897	0.01	-4177.8892	1353.9226	0.0008	0.0008	0.0019	9/1/09 16:50	9/1/09 17:50
PDRF2714	iono Free Fixed	0.5982	4408.5982	12.5	1.592	0.016	-4177.8753	1353.9238	0.001	0.0035	0.0035	9/28/09 22:17	9/28/09 23:20

4408.60493

## PDRF

		Baseline #		L1 Fixed		dNorth #		dEast #		dVert #		Standard Error (m)	
segment	Solution type	Baseline Decimal	Baseline s/fo	Ratio	Ref. Variance RMS	d north	d east	d vertical	North	East	Vertical	start time	stop time
PDRF052	L1 Fixed	0.5961	4408.5961	57	5.799	0.008	-4177.8752	1353.91	0.0006	0.0006	0.0015	2/24/09 15:32	2/24/09 16:34
PDRF0811	L1 Fixed	0.5968	4408.5968	51	5.215	0.009	-4177.8762	1353.9123	0.0007	0.0005	0.0013	3/22/09 16:31	3/22/09 17:32
PDRF1235	L1 Fixed	0.6041	4408.6041	59.7	8.684	0.01	-4177.8856	1353.9177	0.0007	0.0008	0.0029	5/3/09 22:53	5/3/09 23:58
PDRF1504	L1 Fixed	0.5846	4408.5846	32.3	5.556	0.008	-4177.8679	1353.9164	0.0006	0.0007	0.0014	5/30/09 23:03	5/30/09 23:59
PDRF1801	L1 Fixed	0.6054	4408.6054	20.4	6.848	0.011	-4177.8876	1353.9261	0.0008	0.001	0.0022	6/29/09 15:42	6/29/09 16:43
PDRF2065	L1 Fixed	0.6113	4408.6113	100.4	7.359	0.008	-4177.8909	1353.928	0.0006	0.0008	0.0023	7/25/09 22:00	7/25/09 23:01
PDRF2441	L1 Fixed	0.6042	4408.6042	85.8	5.208	0.008	-4177.8848	1353.9225	0.0006	0.0006	0.0014	9/1/09 16:50	9/1/09 17:50
PDRF2714	L1 Fixed	0.5938	4408.5938	12.5	8.116	0.011	-4177.8729	1353.92	0.0007	0.0007	0.0025	9/28/09 22:17	9/28/09 23:20

Excel spreadsheet page one. This is an example one of the spreadsheets that we used to further reduce the processed baseline data. It has both iono-free and L1 solutions. The data on this sheet was referenced on sheet two for further calculations.

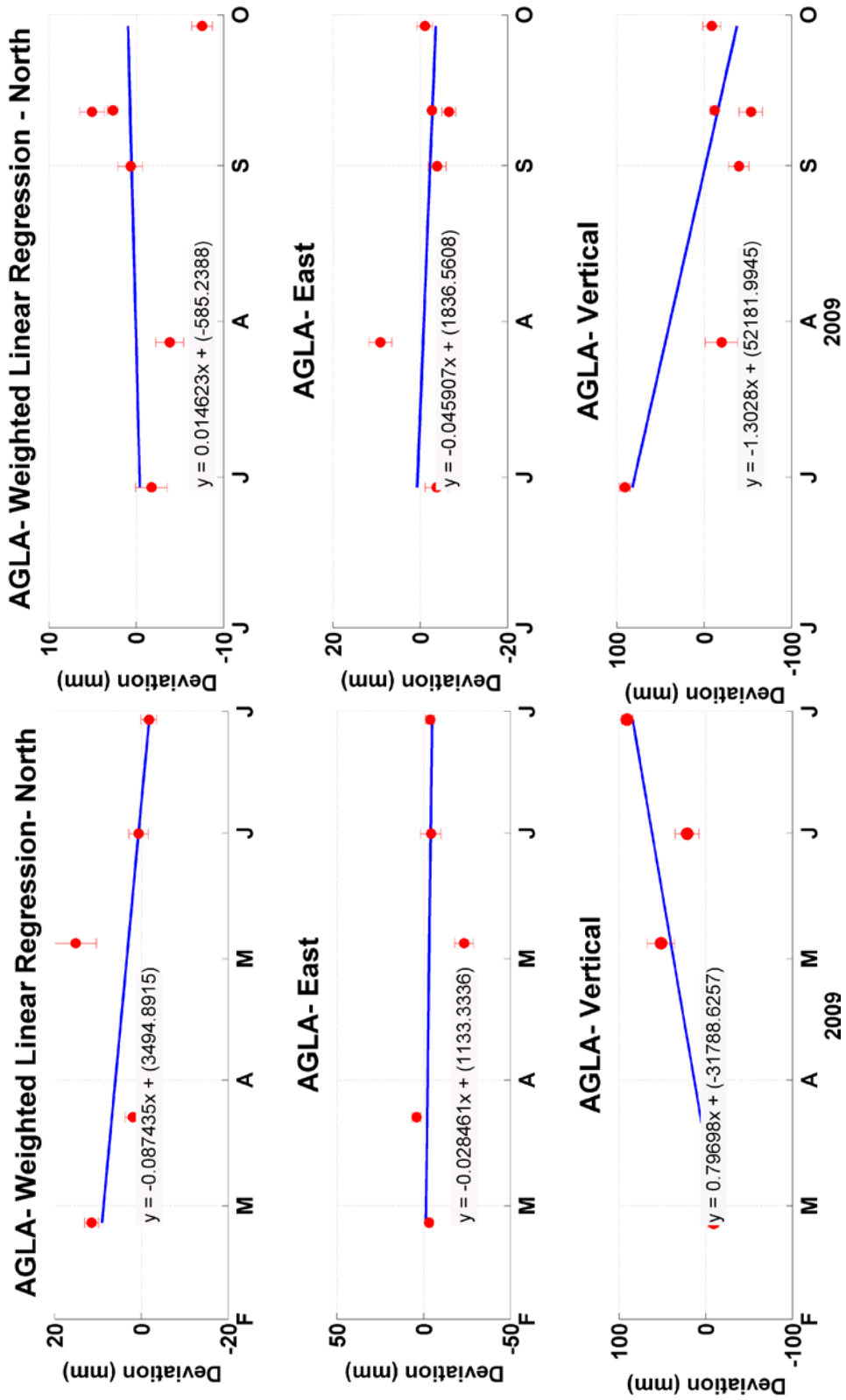
iono free fixed solution						
d North/ $\sigma^2$	1/ $\sigma^2$	d East/ $\sigma^2$	1/ $\sigma^2$	d Vert/ $\sigma^2$	1/ $\sigma^2$	
-6527932188	1562500	2115489375	1562500	-91016258.5	226757.3696	
-5157883210	1234567.901	2763089184	2040816.327	-123880617.3	308641.9753	
-5157888025	1234567.901	1671502469	1234567.901	-29316559.53	73046.01899	
-5157870247	1234567.901	1671506173	1234567.901	-100329400	250000	
-5157890741	1234567.901	940226805.6	694444.4444	-64210208	160000	
-6527961563	1562500	1671512222	1234567.901	-51189528.06	127551.0204	
-6527951875	1562500	2115504063	1562500	-111171772.9	277008.3102	
-4177875300	1000000	1353923800	1000000	-32763591.84	81632.65306	
$\Sigma$ dNorth/ $\sigma^2$	$\Sigma$ 1/ $\sigma^2$	$\Sigma$ dEast/ $\sigma^2$	$\Sigma$ 1/ $\sigma^2$	$\Sigma$ dVert/ $\sigma^2$	$\Sigma$ 1/ $\sigma^2$	
-44393253147	10625771.6	14302754091	10563964.47	-603877936.1	1504637.348	
<b>Baseline Length Av. M</b>						
4408.604925						
<b>North Av. M</b>						
-4177.8847						
<b>East Av. M</b>						
1353.920225						
<b>Elevation Av. M</b>						
-401.3425						
<b>Baseline Weighted Av.</b>						
-4177.885127						
<b>North Weighted Av.</b>						
1353.919177						
<b>East Weighted Av.</b>						
-401.344508						
<b>Vert. Weighted Av.</b>						
-401.344508						
<b>BL std. m</b>						
0.007415958						
<b>North std. m</b>						
0.008041322						
<b>East std. m</b>						
0.005117128						
<b>Elevation std. m</b>						
0.025314705						
<b>Residuals (m) = (d<sub>x</sub>) - x<sub>bar</sub></b>						
segment	start time (UTC)	Baseline Length	North	East	Elevation	
PDRF0552	2/24/2009	-0.006325	0.008526628	-0.005977332	-0.037191956	
PDRF0811	3/22/2009	0.001475	-0.000273372	-0.005477332	-0.028691956	
PDRF1235	5/3/2009	0.003375	-0.004173372	-0.002177332	0.000808044	
PDRF1504	5/30/2009	-0.011625	0.010226628	0.000822668	0.026908044	
PDRF1801	6/29/2009	0.005875	-0.006373372	0.007422668	0.030708044	
PDRF2065	7/25/2009	0.010075	-0.010273372	0.005722668	0.018608044	
PDRF2441	9/1/2009	0.003875	-0.004073372	0.003422668	0.014408044	
PDRF2714	9/28/2009	-0.006725	0.009826628	0.004622668	-0.009491956	

Standard Deviation of Weighted Residuals mm		
North	East	Vertical
8.058213207	5.148304156	28.08523709
Standard Deviation mm		
North std	East std	Vertical std
8.041321853	5.117128101	25.31470493
Residuals (mm)		
North (mm) IFF	East (mm) IFF	Vertical (mm) IFF
8.526628421	-5.977332474	-37.19195581
-0.273371579	-5.477332474	-28.69195581
-4.173371579	-2.177332475	0.808044186
10.22662842	0.822667526	26.90804419
-6.373371579	7.422667526	30.70804419
-10.27337158	5.722667526	18.60804419
-4.073371579	3.422667526	14.40804419
9.826628421	4.622667526	-9.491955814

Excel spreadsheet with the formula to determine the weighted mean of the positional components.

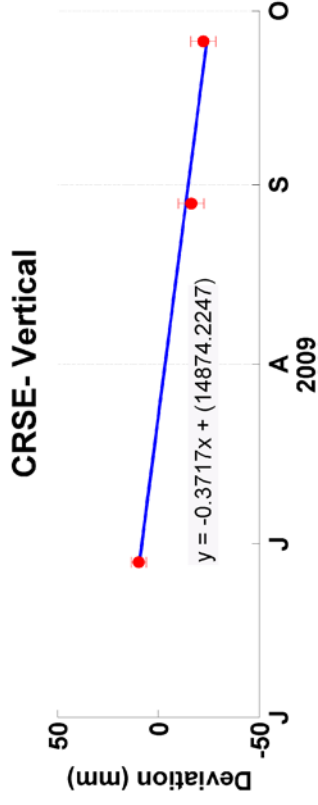
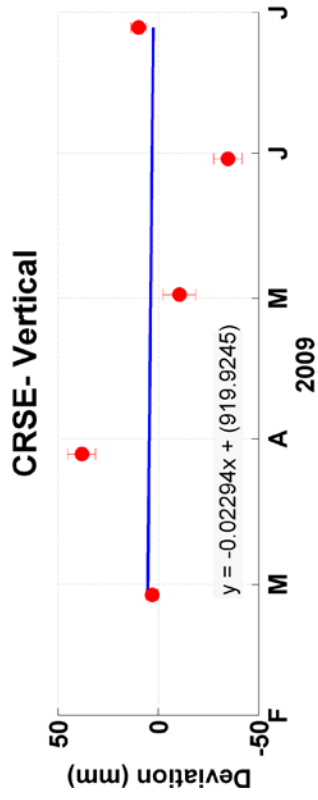
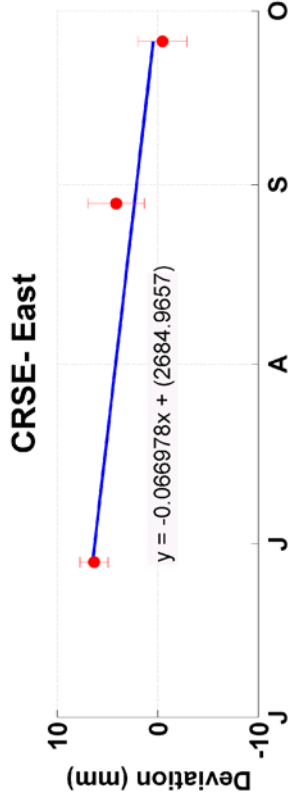
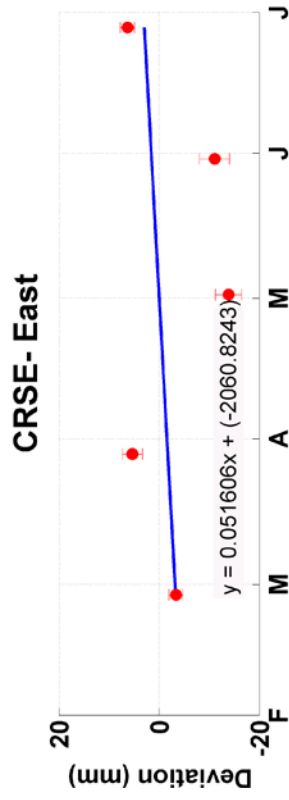
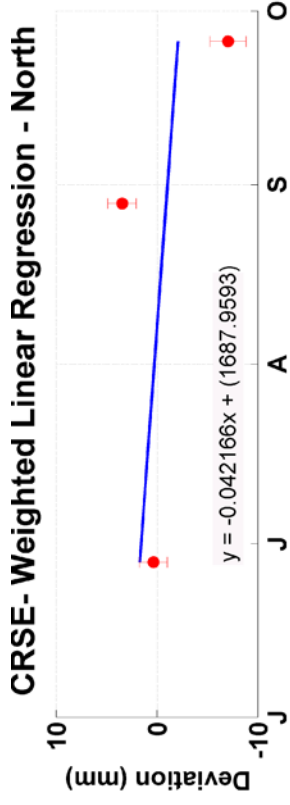
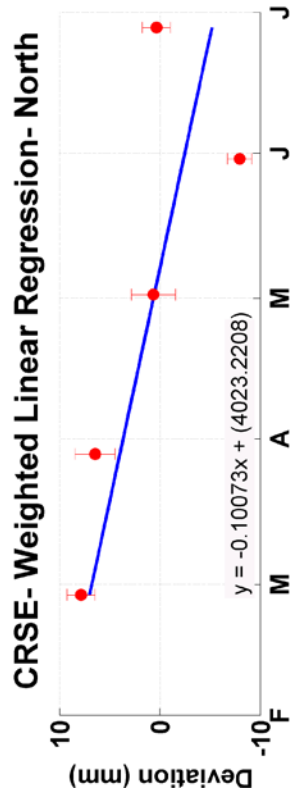


# APPENDIX E: REGRESSION PLOTS

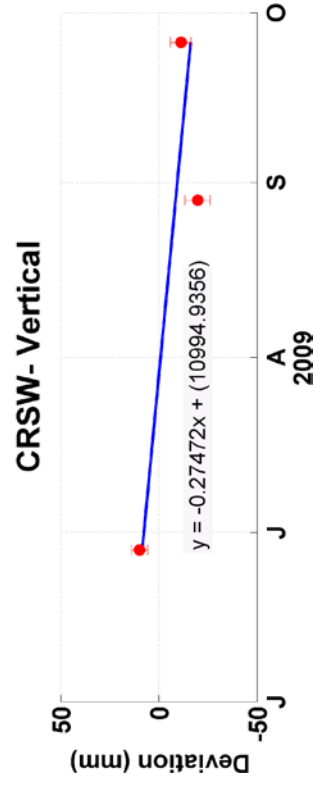
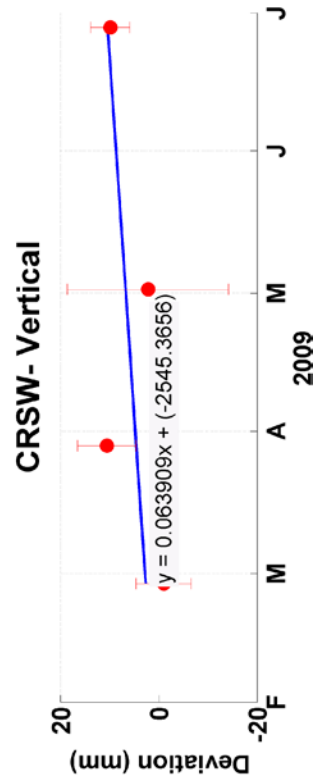
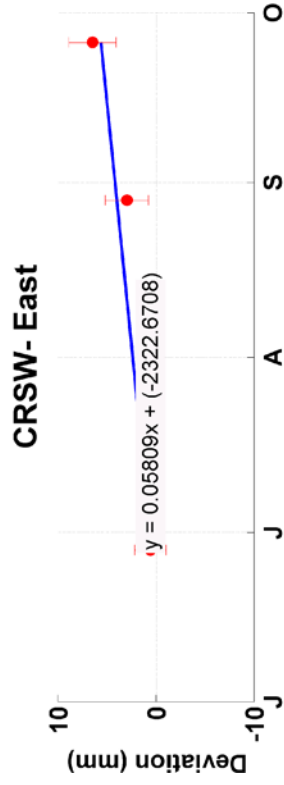
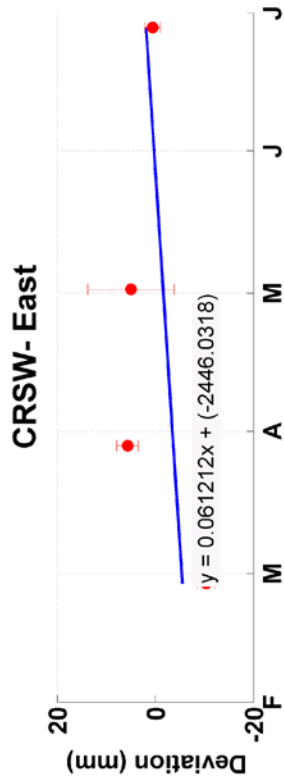
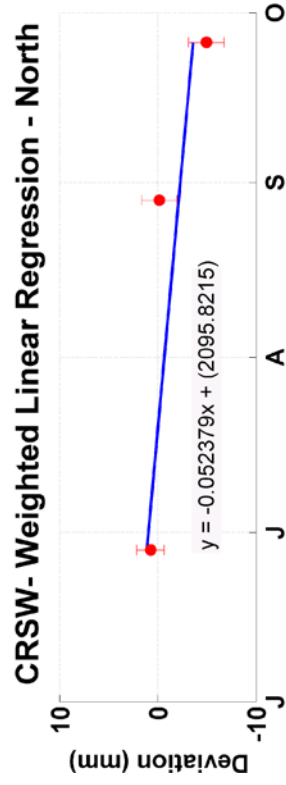
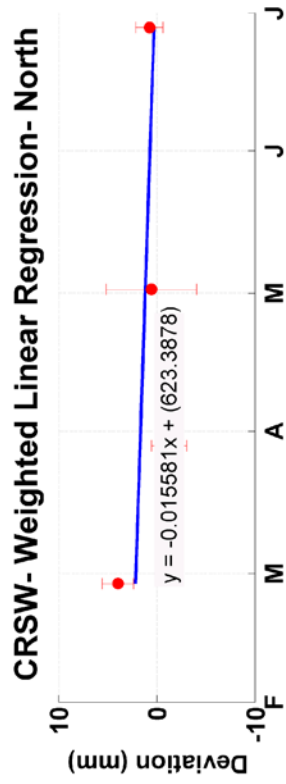


Weighted linear regression for the time period of inflation (left) and deflation (right). At station AGLA.

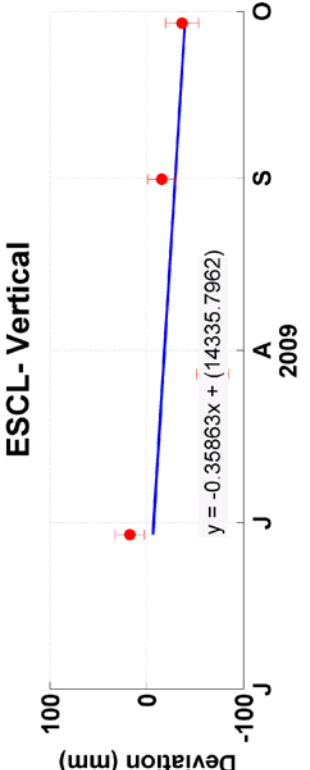
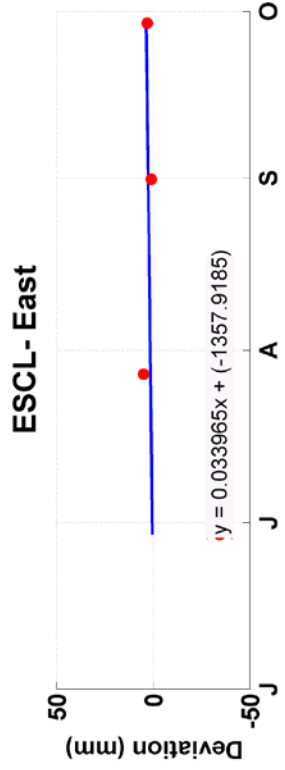
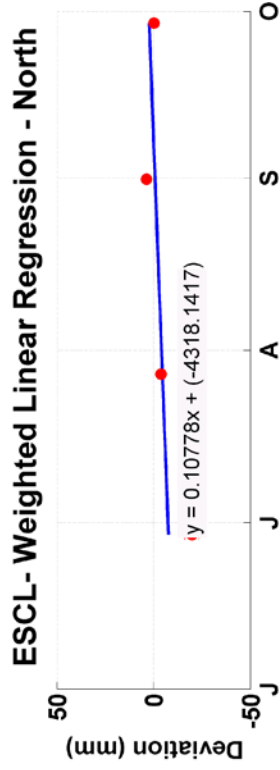
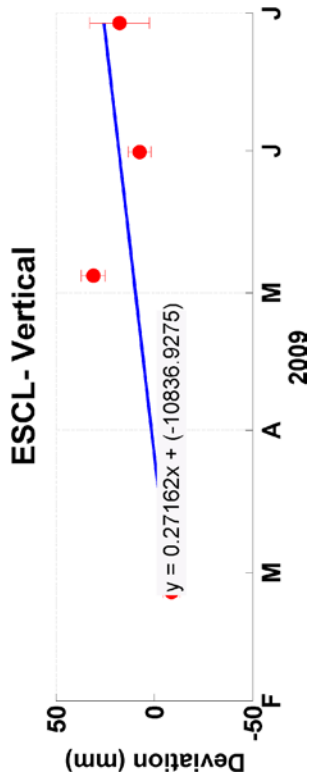
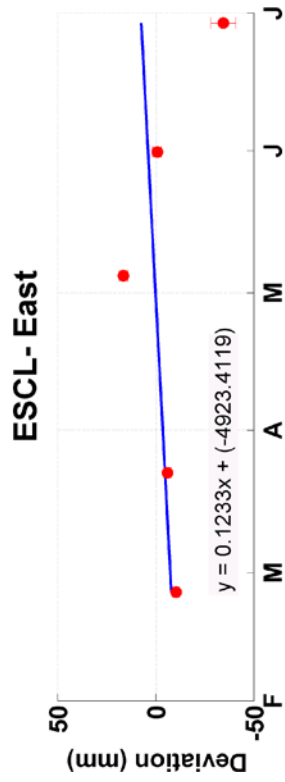
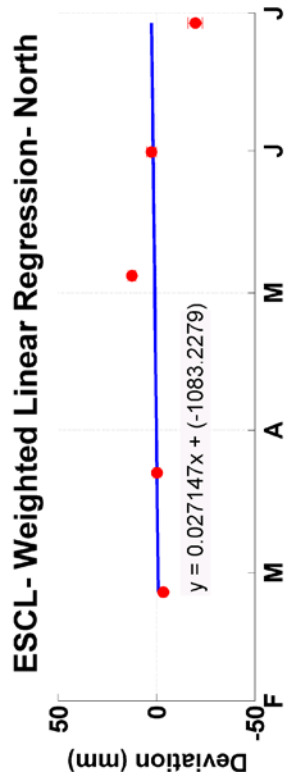




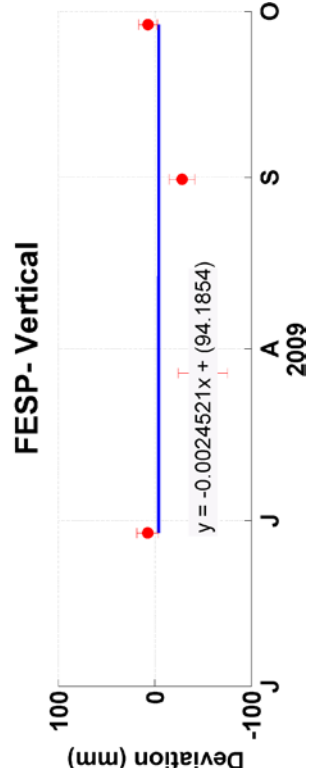
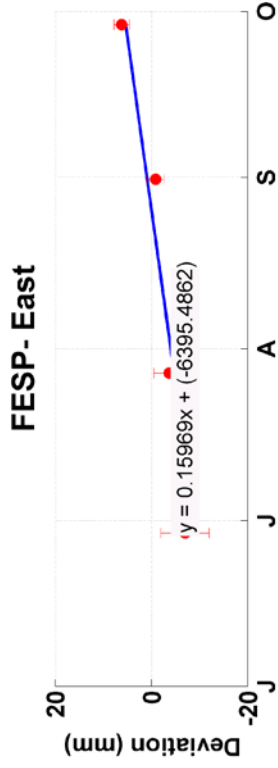
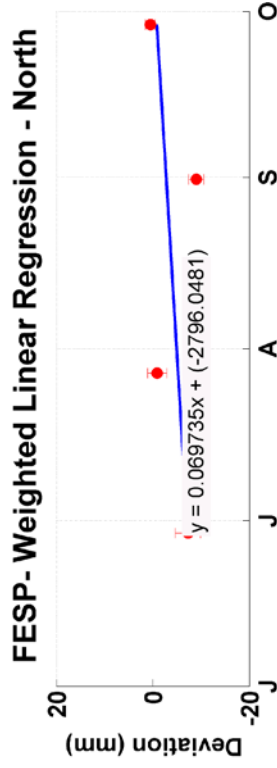
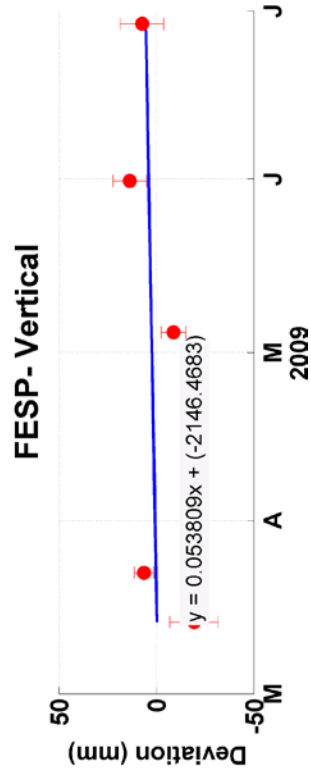
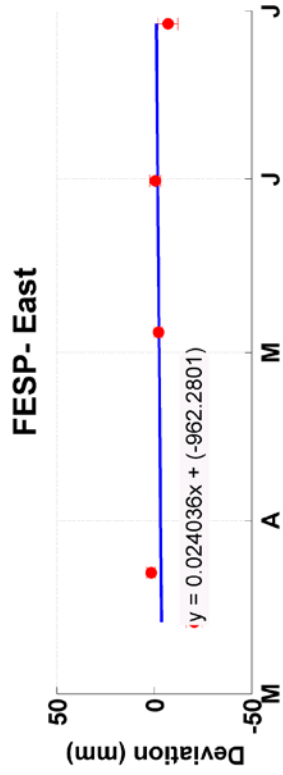
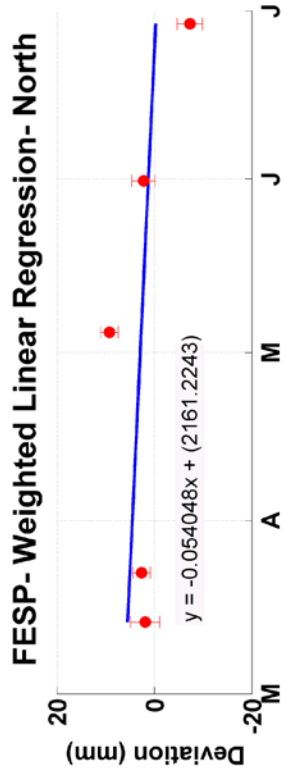
Weighted linear regression for the time period of inflation (left) and deflation (right). At station CRSE.



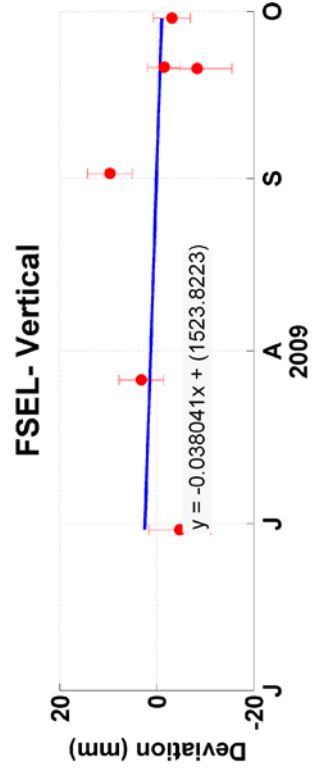
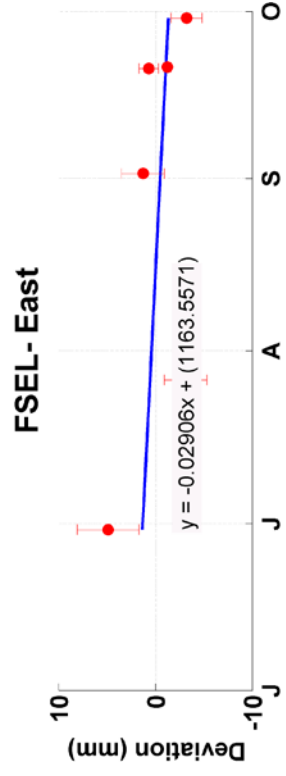
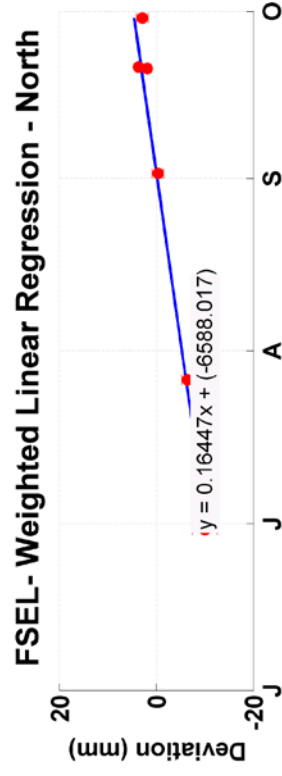
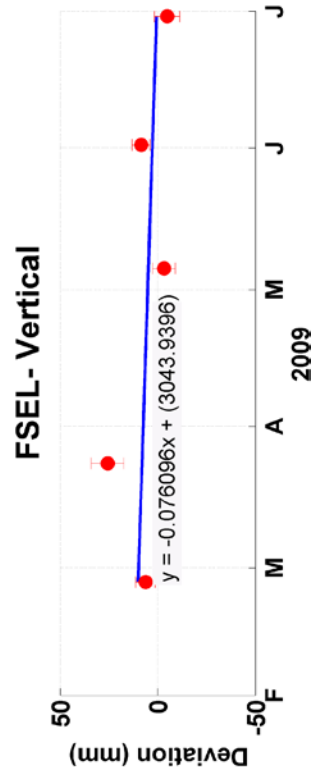
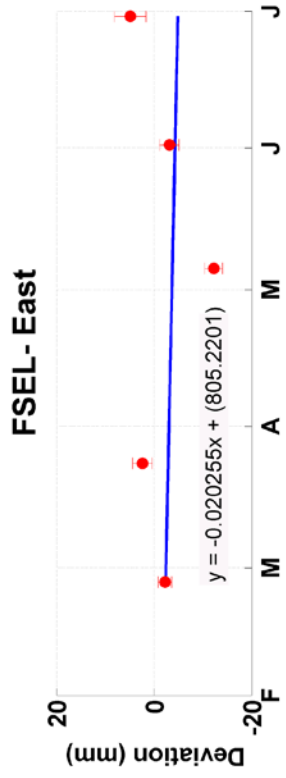
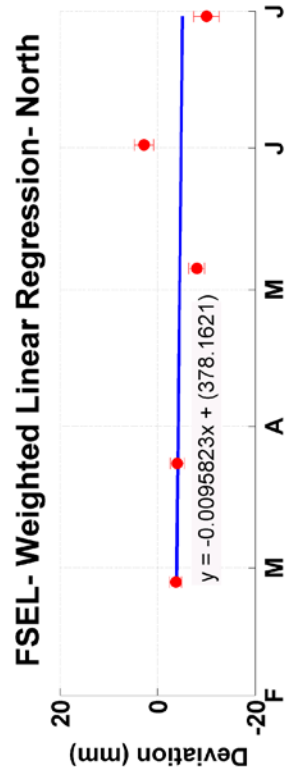
Weighted linear regression for the time period of inflation (left) and deflation (right). At station CRSW.



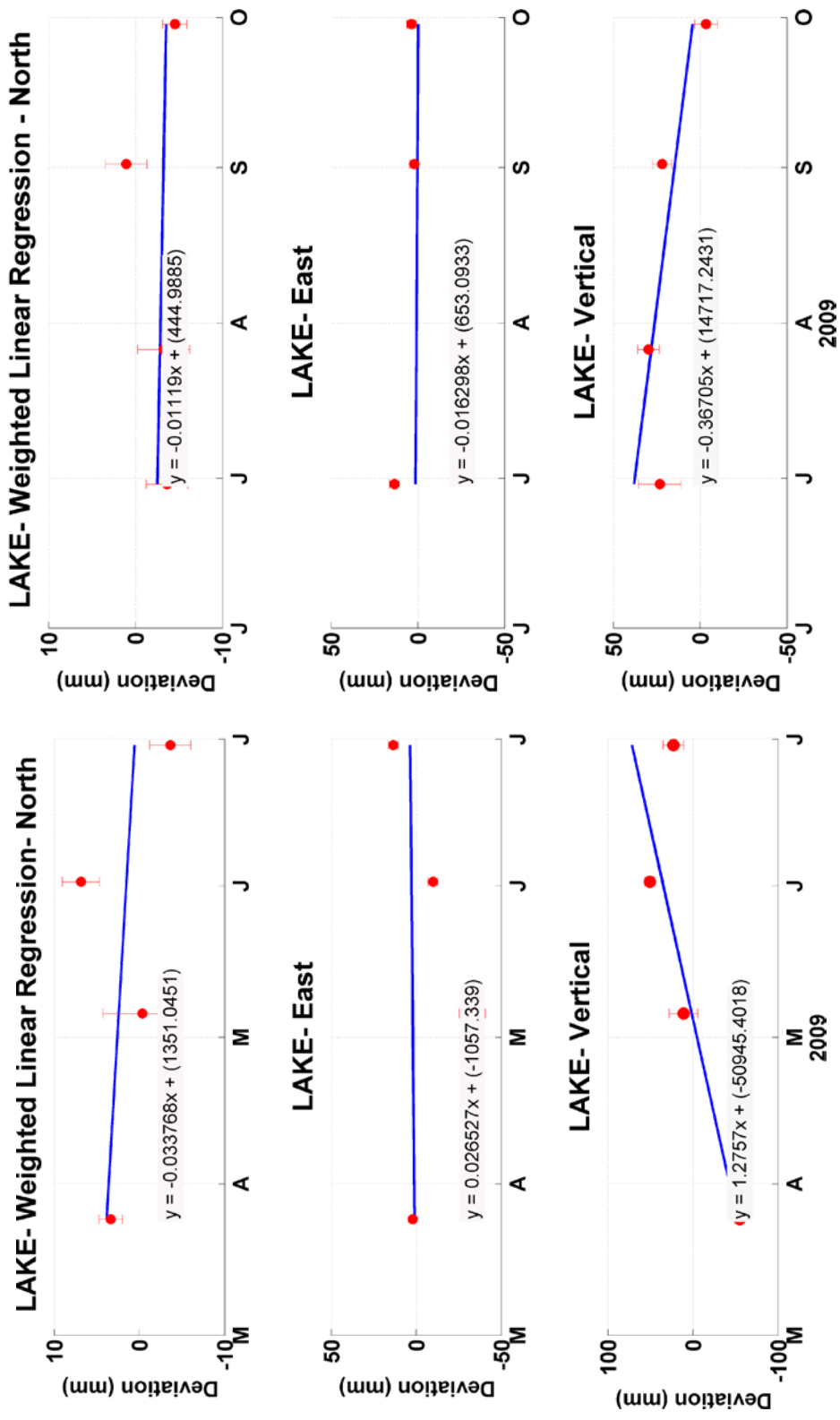
Weighted linear regression for the time period of inflation (left) and deflation (right). At station ESCL.



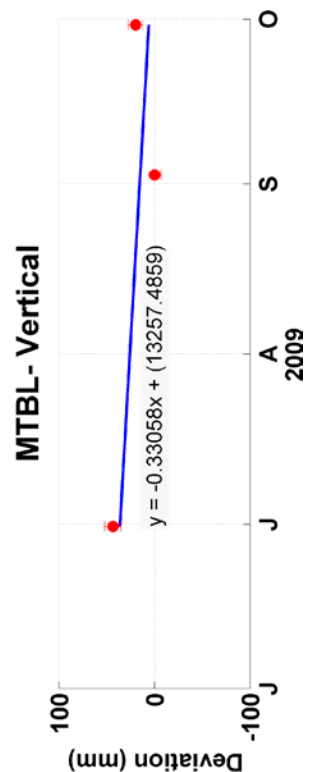
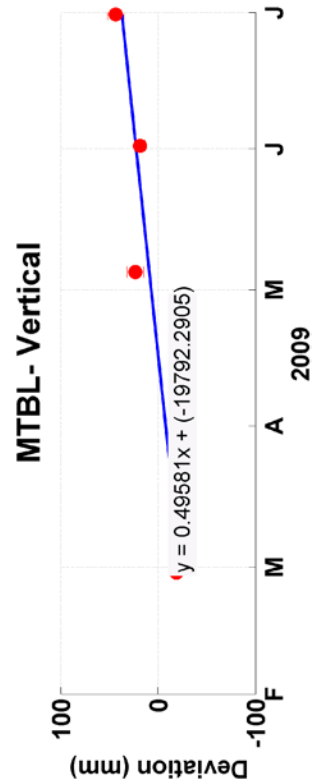
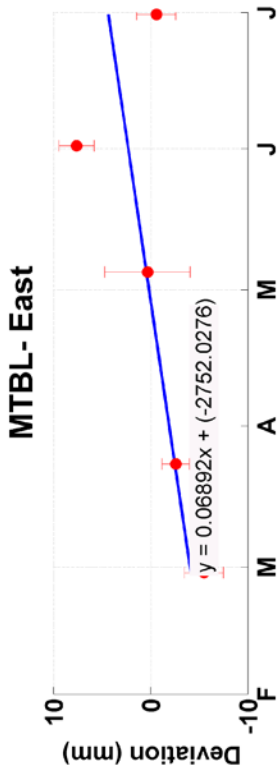
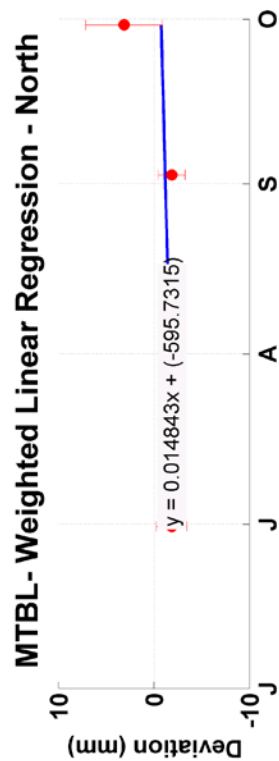
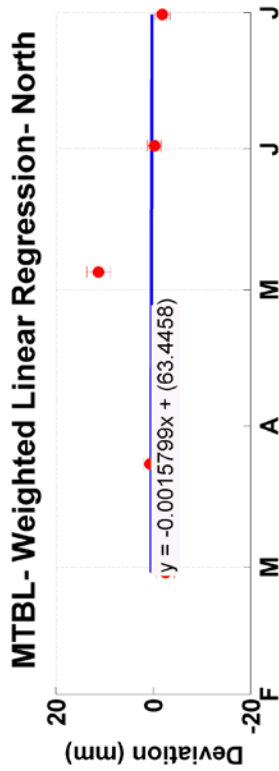
Weighted linear regression for the time period of inflation (left) and deflation (right). At station FESP.



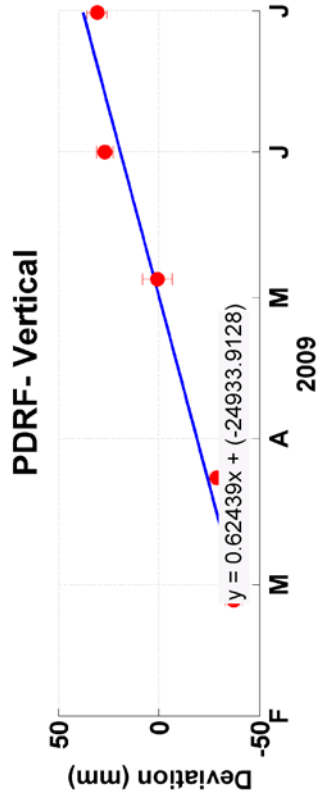
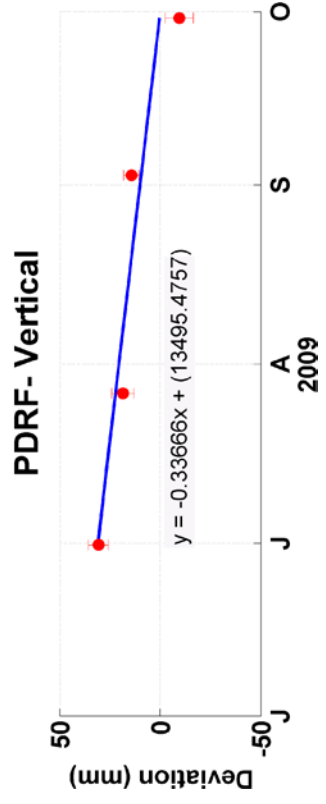
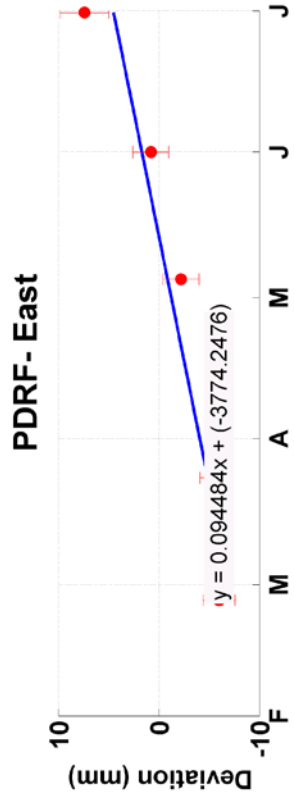
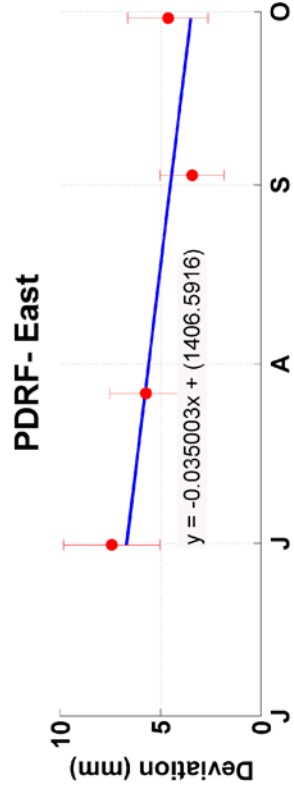
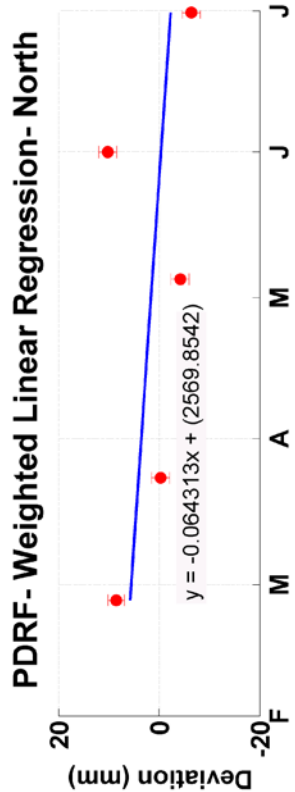
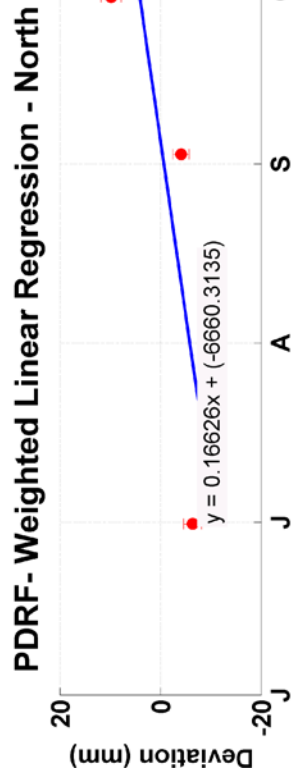
Weighted linear regression for the time period of inflation (left) and deflation (right). At station FSEL.



Weighted linear regression for the time period of inflation (left) and deflation (right). At station LAKE.

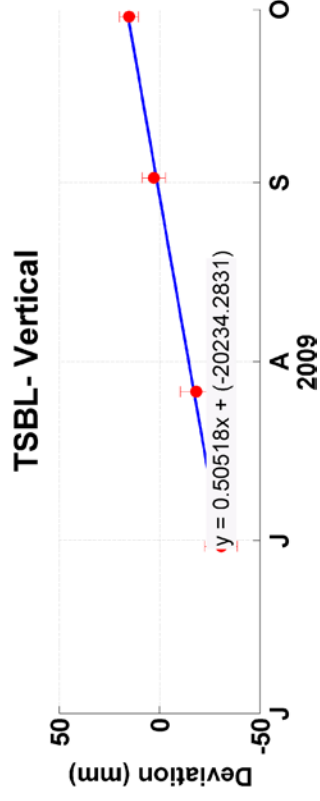
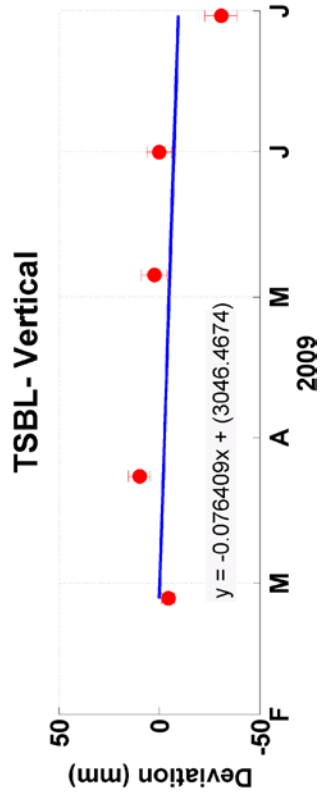
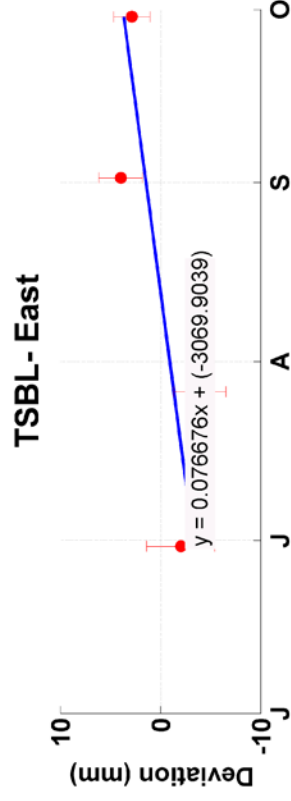
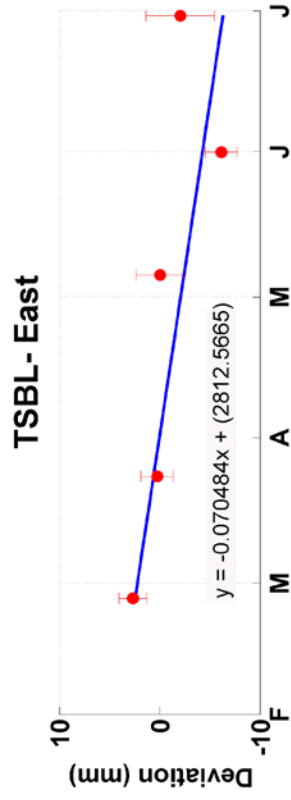
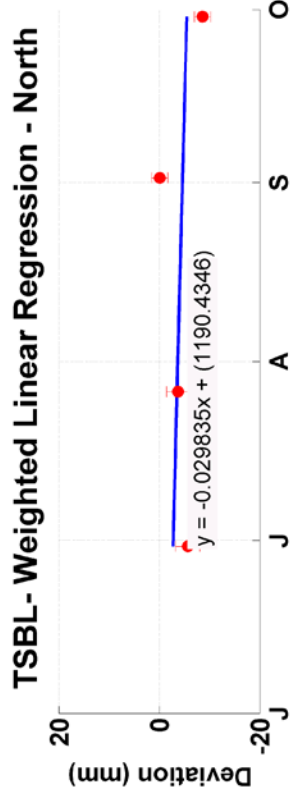
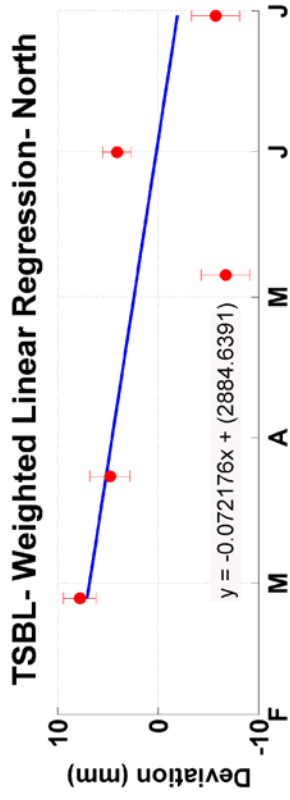


Weighted linear regression for the time period of inflation (left) and deflation (right). At station MTBL.

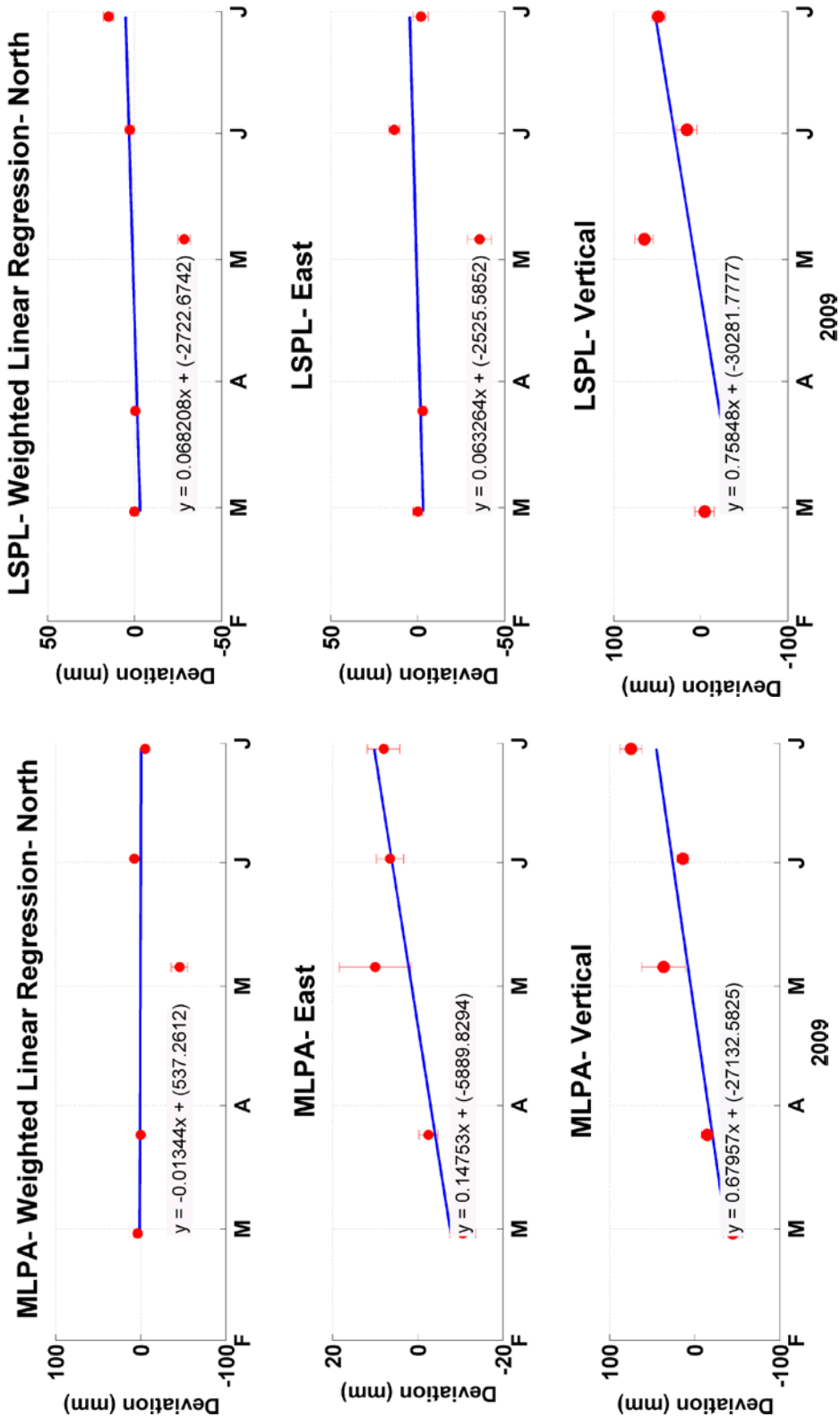


Weighted linear regression for the time period of inflation (left) and deflation (right). At station PDRF.



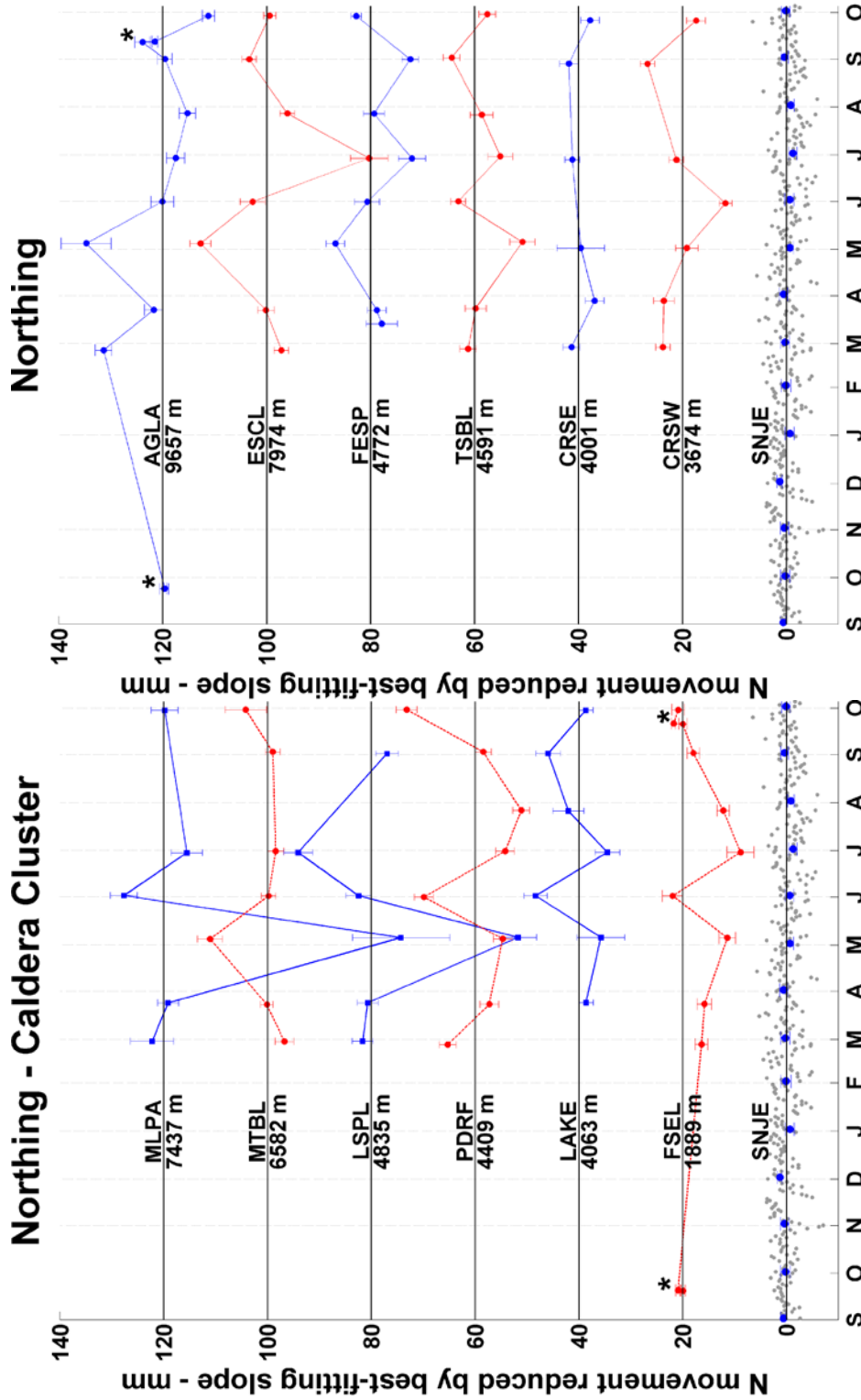


Weighted linear regression for the time period of inflation (left) and deflation (right). At station TSBL.

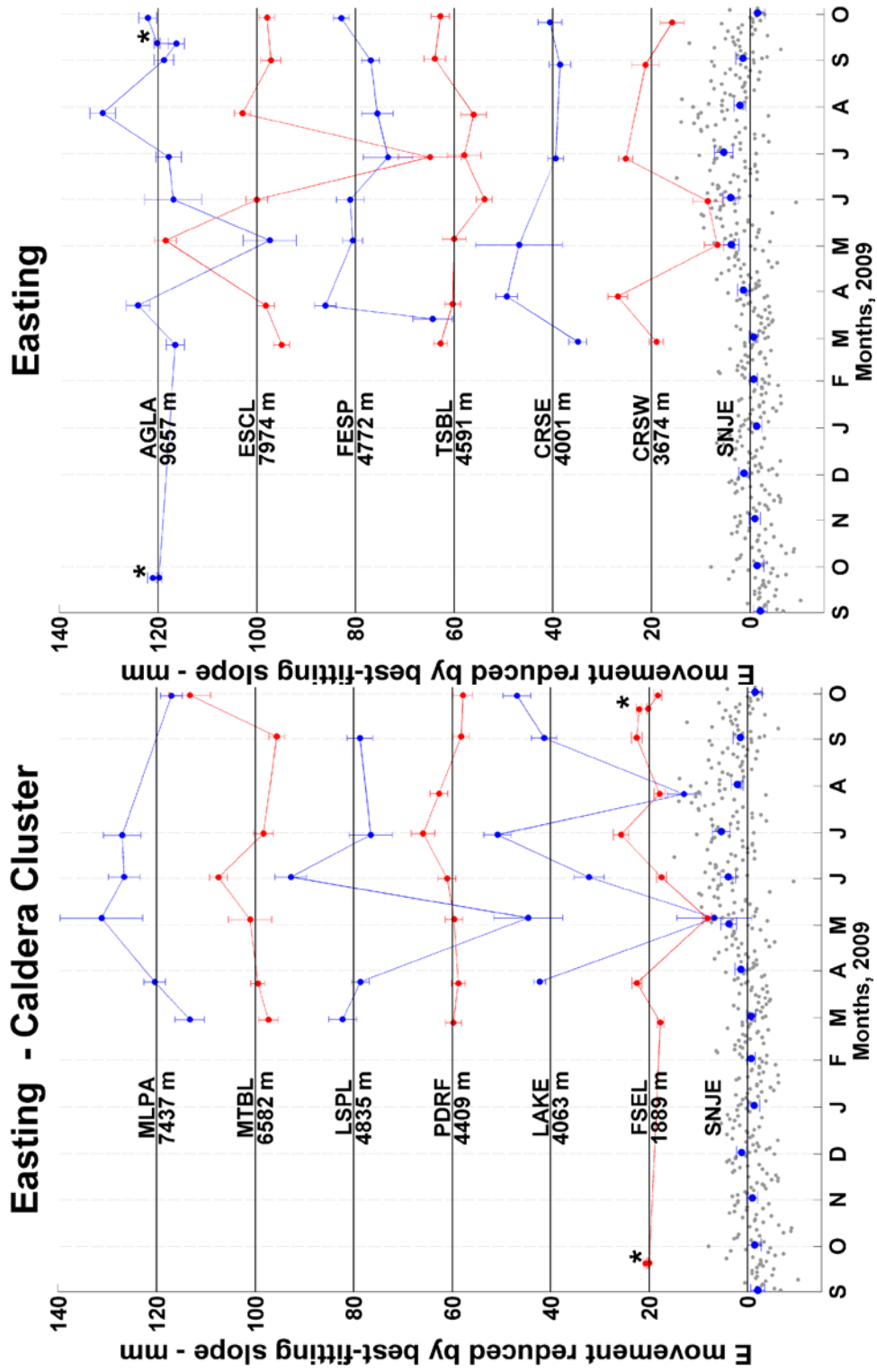


Weighted linear regression for the time period of inflation (left) at stations MLPA (left) and LSPL (right)

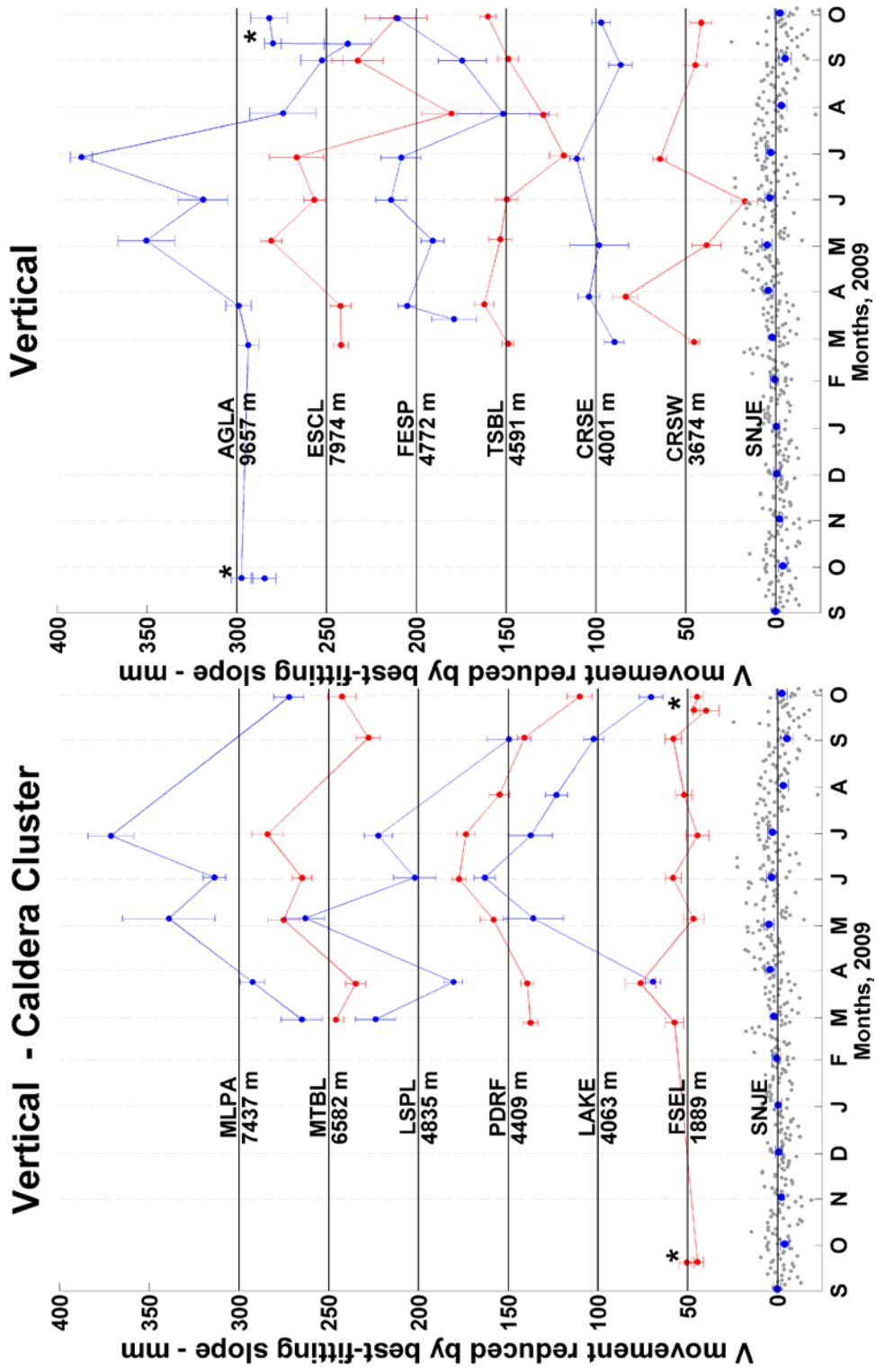
# APPENDIX F: BEST FIT RESIDUALS



North (a), east (b) and vertical (c) residuals from stations around the caldera and the volcano reduced by a weighted least squares linear regression. Error bars represent  $2\sigma$  error. Grey data points for the fixed base Station SNJE show the daily averages processed by GPSY relative to ITRF 95 and reduced by a best-fit line. Blue data points represent the monthly averages. Station identifications include distance from SNJE.



Residuals of the north component from stations around the caldera (left) and the sites around the volcano (right). The asterisk (\*) at FSEL and AGLA indicates 20-24 hour observations. Site IDs include baseline.



Residuals of the vertical component from stations around the caldera (left) and the sites around the volcano (right). The asterisk (\*) at FSEL and AGLA indicates 20-24 hour observations.